

MASTER

Timber reciprocal frame structures

Godthelp, T.S.

Award date:
2019

[Link to publication](#)

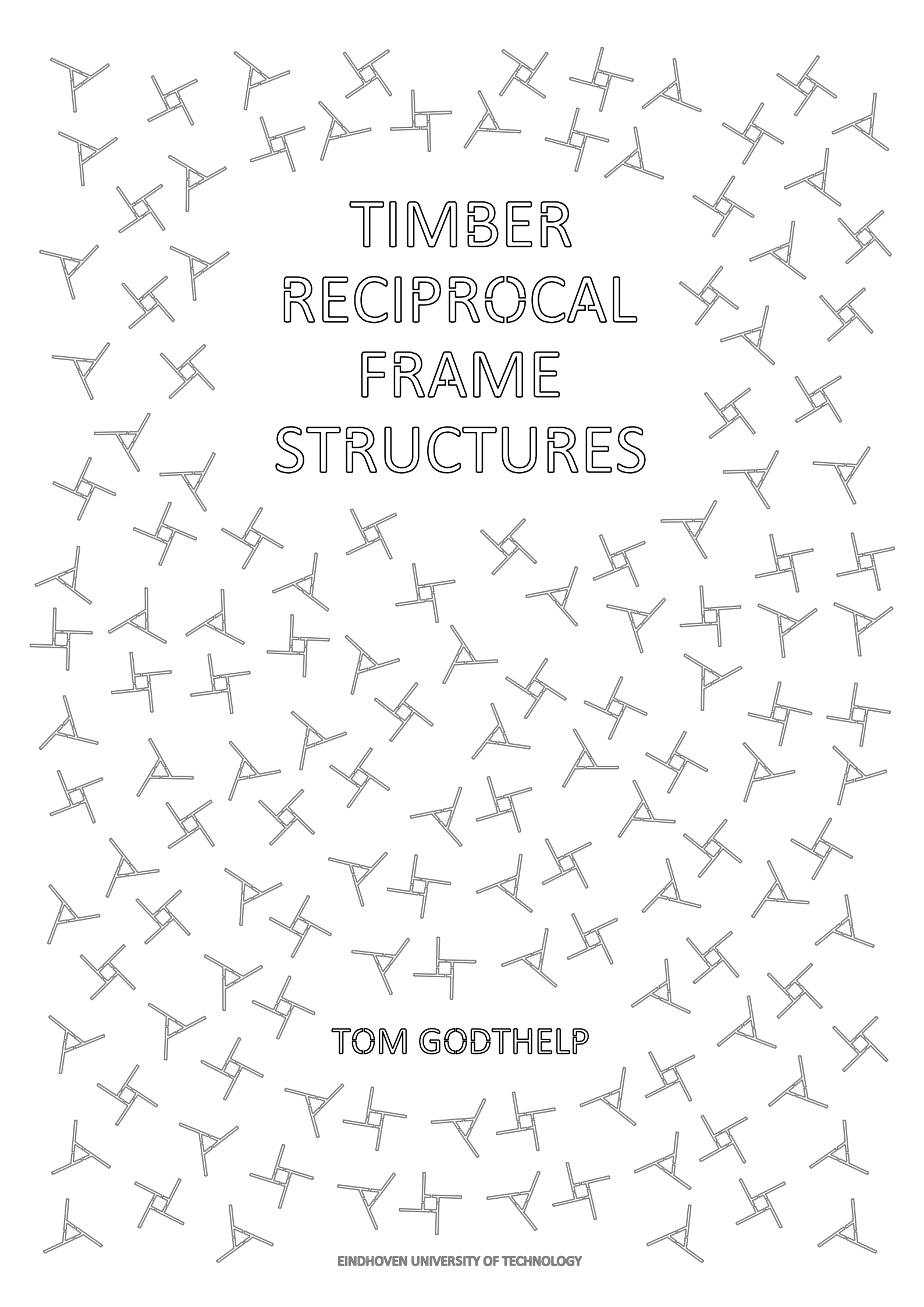
Disclaimer

This document contains a student thesis (bachelor's or master's), as authored by a student at Eindhoven University of Technology. Student theses are made available in the TU/e repository upon obtaining the required degree. The grade received is not published on the document as presented in the repository. The required complexity or quality of research of student theses may vary by program, and the required minimum study period may vary in duration.

General rights

Copyright and moral rights for the publications made accessible in the public portal are retained by the authors and/or other copyright owners and it is a condition of accessing publications that users recognise and abide by the legal requirements associated with these rights.

- Users may download and print one copy of any publication from the public portal for the purpose of private study or research.
- You may not further distribute the material or use it for any profit-making activity or commercial gain

The background of the entire page is a repeating pattern of two types of timber reciprocal frame joints. One joint is a simple A-frame with a horizontal base and two angled members meeting at a peak. The other is a more complex joint with four angled members meeting at a central point, forming a square-like shape. These joints are scattered across the page in a non-uniform, overlapping manner.

TIMBER RECIPROCAL FRAME STRUCTURES

TOM GODTHELP

TIMBER RECIPROCAL FRAME STRUCTURES

Graduation thesis

Version: Final - 5/27/2019
Thesis no. A-2018.250

Author: **T.S. (Tom) Godthelp**
0916277

🏠 NL Kossenland 13
1834 BJ Sint Pancras
☎ +31 (0)6 234 456 13
✉ t.s.godthelp@student.tue.nl
✉ tomgodthelp@gmail.com

Graduation committee: prof.dr.ir. A.J.M. (André) Jorissen (Chairman)
Professor Timber Structures

ir. A.P.H.W. (Arjan) Habraken
Assistant Professor Innovative Structural Design

R. (Rinus) Roelofs
Artist – Mathematical Morphology

Copyright © 2019 by **TU/e**

Eindhoven University of Technology (**TU/e**)
Department of the Built Environment
Master Architecture, Building and Planning
Specialization **Structural Design**

All rights reserved.

*No part of this publication may be reproduced,
distributed, or transmitted in any form or by any means
without the prior written permission of the author.*

*'A CAD model, by definition, is always
an abstraction of reality'* F. Scheurer



PREFACE

Ever since I was a small child I am making structures with wood as a hobby ranging from skate ramps to small and simple furniture. The master Structural Design has challenged me at a more advanced level by using state of the art technologies to create new wooden forms and structures. This has been inspiring me enormously.

My graduation project is the result of a research process that started during the lecture phase of the master Structural Design. Rinus Roelofs introduced me to the topic of Reciprocal Frames (RF) during a lecture series on adaptive structures. The subject inspired me enormously which resulted in my enthusiasm towards RF structures. I would like to thank Rinus for introducing me to the topic, for helping, and for inspiring me.

Almost every week meetings were conducted in student groups to discuss the progress of each graduation project. Here, I got inspired and motivated by other students to present my work in an understandable way. Elaborating my progress was sometimes challenging in which I have learned a lot. Therefore, I thank my colleague students of the project group FAMO (Fabrication and Material Optimization) and Arthur van Lier from the computational timber group for their feedback during these meetings.

The timber meetings were guided by André Jorissen and the FAMO meetings were guided by Arjan Habraken. They gave me the freedom and time to do whatever I suggested, helped me to understand the relation between form and structure, contacted me with people from industry, practicalized, and directed my study towards an end. I am very grateful for their guidance, knowledge and encouragement throughout the development of my research. I realize that this is not all obvious and am grateful for that.

The design to production process of this study would not have been possible without timber industry partner Heko Spanten and PhD. student Zeeshan Ahmed. I would like to thank Lambert van den Bosch and Aart Houweling from Heko for the provided manufacturing facilities, materials, and knowledge to transfer the developed Reciprocal Frame Designer to practice. I believe that it made my research much more valuable and your enthusiasm, spurred by a 'everything is possible' mentality, motivated me enormously. Zeeshan, thanks for letting me learn and use your Ultimaker 3D printer to manufacture many scale models. It helped me to test the RFD on small scale and to understand the subject.

Finally, I would like to thank my family and friends for their unconditional support throughout my study and for helping me maintaining balance between study and leisure. Although, the project sometimes was a bumpy ride, I really enjoyed it and hope that this research will encourage new structural applications and contributes to a next generation of sustainable timber structures. Low carbon construction does not have to be boring.

Tom Goolthelp, Eindhoven 5/27/2019



ABSTRACT

The definition 'Reciprocal Frame' (RF) applies to structures that are feasible by means of circulating compression or tension interactions between their constituent members. This relation indicates that beam depths and connections correlate to an RFs' structural geometry. Until now, a combination of RF form finding that regards both beam depths and structural design of connections has not yet been developed. Although researchers developed computational form finding methods to create geometrical solutions and described the global structural design, computational complexity may have prevented a direct inclusion of detailing in the overall design.

In this context, the following research goal is established:

'The goal of this research is to develop a computational design to production tool for vaulted timber reciprocal frame structures using an optimized connection typology and a sustainable timber-based material'

The completion of this goal could:

- **Offer** A scientific basis for analysis and design;
- **Make** RF design more accessible to the designers pallet;
- **Create** New and practical structural applications;
- **Contribute** To a next generation of sustainable timber structures.

These mentions are implemented in the final product of this research that present a new and direct RF form finding method including the structural design of beam dimensions and detailing based on the polygon 'center to center' modification method. A parametric model -to be referred to as 'The Timber Reciprocal Frame Designer' (RFD)- is developed to design three- and four-member RF assemblies from any arbitrary NURBS surface. Eccentricities between members that may result or are generated from this surface correlate to detailing and beam depth causing the need to be controlled. Therefore, a method has been established that allows this control and results in direct geometrical solutions. Among geometrical equations, fictional beam stiffnesses in combination with initial strains are used to derive the geometrical shape.

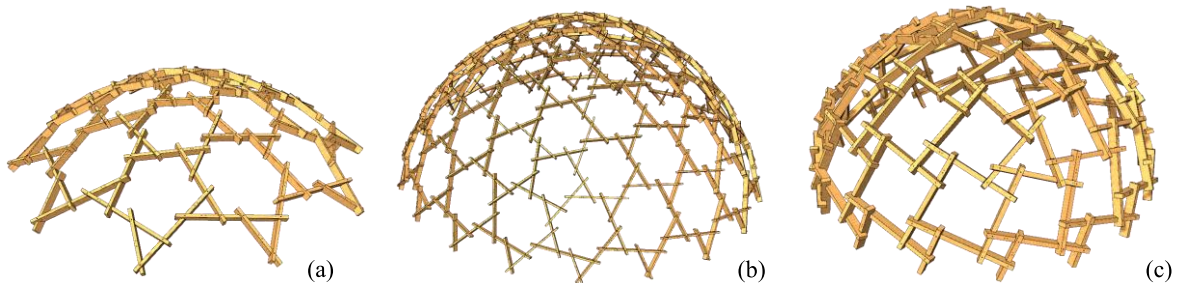


Figure 12.1: RFD results covering the same span using geodesic icosahedra (a,b) and cubes (c) as basic geometry

A geometrical shape is supplemented in the RFD with standardized detailing and beam dimensions that are checked, and if necessary adjusted to satisfy stress and deformation regulations. In conclusion, the RFD provides a tool in which designs can be produced by using industry standard machines stimulating structural designers to add RFs to their design pallet. An experimental validation of the design to production process is made by means of a full-scale model, built in cooperation with the timber industry. Three resulting RF designs made with the RFD are displayed above (Figure 12.1).

The developed RFD is the product of a literature and form-finding study. To be able to understand design choices and designations, the chronically ordered chapters are written upon the theory of its predecessor (Figure 12.2).

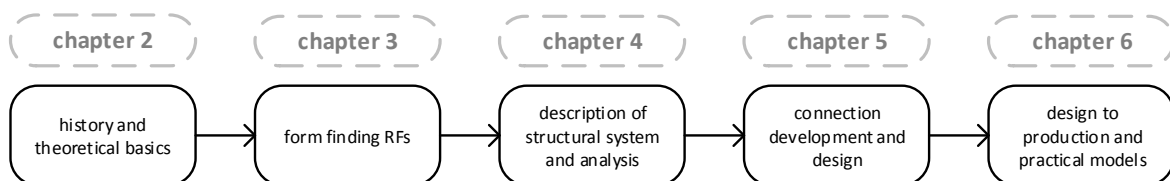


Figure 12.2: Chapter order with associated subjects



TABLE OF CONTENTS

| | | |
|------------------|--|-------------------|
| <u>1</u> | <u>THEORETICAL INTRODUCTION</u> | <u>12</u> |
| <u>2</u> | <u>RECIPROCAL FRAME STRUCTURES</u> | <u>16</u> |
| 2.2 | HISTORY | 17 |
| 2.3 | GEOMETRY | 22 |
| 2.4 | EXTENSIVE GEOMETRY | 25 |
| 2.5 | COMPUTATIONAL MODELING | 27 |
| 2.6 | CONCLUSION AND DISCUSSION | 32 |
| <u>3</u> | <u>FORM FINDING</u> | <u>36</u> |
| 3.1 | HOW TO DESIGN A BASIC RF - MODEL 1 | 36 |
| 3.2 | HOW TO DESIGN AN EXACT RF - MODEL 2 | 37 |
| 3.3 | HOW TO DESIGN A WIDE VARIETY OF RFS - MODEL 3 | 38 |
| 3.4 | CONCLUSION | 42 |
| <u>4</u> | <u>STRUCTURAL BEHAVIOR</u> | <u>48</u> |
| 4.2 | MECHANICAL SCHEMATIZATION | 49 |
| 4.3 | STRUCTURAL BEHAVIOR | 53 |
| 4.4 | THE INFLUENCE OF CHANGING PARAMETERS | 55 |
| 4.5 | CONCLUSION AND DISCUSSION | 58 |
| <u>5</u> | <u>DETAILING</u> | <u>62</u> |
| 5.1 | CONCEPT | 62 |
| 5.2 | STRUCTURAL DESIGN | 66 |
| 5.3 | CONCLUSION | 69 |
| <u>6</u> | <u>DESIGN TO PRODUCTION</u> | <u>72</u> |
| 6.1 | FIRST MODELS | 72 |
| 6.2 | COMPLETE 3D PRINTED RF MODEL | 73 |
| 6.3 | TRANSFERRING THE RFD TO PRACTICE | 74 |
| 6.4 | CONCLUSION | 77 |
| <u>7</u> | <u>SUMMARIZING CONCLUSIONS AND RECOMMENDATIONS</u> | <u>80</u> |
| 7.1 | CONCLUSIONS | 80 |
| 7.2 | RECOMMENDATIONS | 82 |
| <u>8</u> | <u>BIBLIOGRAPHY</u> | <u>84</u> |
| 8.1 | REFERENCES | 84 |
| 8.2 | FIGURES | 85 |
| <u>9</u> | <u>ANNEX 1 : COMPARISON STRUCTURAL DIMENSIONS RF3, RF4 CONFORM EUROCODE 5</u> | <u>88</u> |
| <u>10</u> | <u>ANNEX 2: EXPLANATION CALCULATION OF BEAM DIMENSIONS AND DETAILING CONFORM EUROCODE 5</u> | <u>96</u> |
| <u>11</u> | <u>APPENDIX 1: HOW TO USE THE RECIPROCAL FRAME DESIGNER</u> | <u>113</u> |
| <u>12</u> | <u>APPENDIX 2: IMPLEMENTATION OF THE RFD IN AN ACTUAL PROJECT</u> | <u>114</u> |

1 THEORETICAL INTRODUCTION

This page introduces the graduation subject ‘Timber reciprocal frame structures’ by clarifying its aim, principle and terms.

The reciprocal frame (RF) structure is a comprising definition for several structural systems that are feasible by means of compression or tension interactions between their constituent elements. This type of structure could be used to create spectacular structures.

The individual elements in RFs are all mutual supported by their adjacent elements which is necessary to ensure global and local stability and to ensure the functionality of the complete system: the adjacent element in an RF always acts as support setting specific requirements for the connections (Figure 1.1). In other words, the connections are a whole with the individual elements and determine the structural behavior and geometrical design of the whole structure. When individual elements mutually support each other without for instance notches, the connections create a slope. Consequently, detailing cannot be separated from the structural RF design.

The structural principle of RFs allows to span greater distances or areas than the length of the individual elements itself. This is demonstrated by history that shows that the principle of reciprocal frame structures was adopted in timber structures in times when the availability of timber was scarce. However, the shortage of material has not always been the prime reason to choose for RFs – it often has been the fascination for its aesthetical beauty. Furthermore, the fact that the individual elements in RFs can be similar or even identical and the length can be adopted to enable easy transport without heavy equipment shows the systems’ potential.

The RF principle can be used to construct bridges, roofs, floors, and even to span large hall roofs in which timber often is the preferred material. This is thus emphasized by historic RF applications^[1].

The choose for timber in RFs has economic and implementation arguments for the building industry: short lengths, inferior scrap wood, slender and buckling sensitive sheet materials, recycled wood, locally grown wood species, can all be used in RF structures and are often less sought after. It shows that the RF principle lends itself for using residual flows from industrial timber production.

Furthermore, wood is a renewable and carbon storing material approving its use in an ecological and sustainable sense with the advent of climate change. It makes wood one of the most promising building materials which has been shown by numerous contemporary studies^[2]. These studies cover innovations and resulting technologies that are mainly driven by advances in computation technologies.

Computation could bridge the gap between the physical and digital world by acting as an interface. The advances in computational design are not only optimizing the traditional way of structurally designing timber structures, but in addition, enables the design of geometrically more complex structures such as RFs.

From designing RFs to the choice of the main material, this introduction discusses the literature study topics. Moreover, it results in the aim of this graduation project which is to develop a computational RF structural design tool using an optimal jointing system and a sustainable timber-based material. This could lead to the creation of a sustainable timber RF structure. The following study provides the theoretical knowledge to achieve this aim.



Figure 1.1: The structural principle of a reciprocal frame (RF) assembly portrayed by numerous people



RF THEORY

This chapter introduces and evaluates the theory behind timber reciprocal frame structures by assessing contemporary research. The conclusions based on the abridged theory result in the approach method of this research.

-

2 RECIPROCAL FRAME STRUCTURES

Reciprocal frames (referred to as RF) are structures in which a combination of balanced structural elements create a span greater than their own length. This balance and equilibrium is established at intermediate supports where the elements mutually support each other in a cyclic manner. To be able to create a force equilibrium between these elements, the minimum number of elements in an RF assembly (unit) is three.

The inner supports in an RF assembly have the characteristic that they do not meet each other at the longitudinal extension of the elements - the extremities - but somewhere along the length of the supporting element creating a distinctive appearance in which a structural morphology could not be clearly identified.

This lack of clear structural morphology has been resulting in a scarce of complicated RF applications. However, simpler RFs have been applied for centuries by for instance the native Americans to construct tepees and by other civilizations to construct roofs. A main reason seems to be that the RF technique offers the chance for fast and simple construction. The past decades however, have been showing an increased interest in RF structures that is mainly explainable by advances in computational design technologies.

This can be seen in the next chapters that briefly describe the morphology and history of RFs to create an understanding of the RF system and to identify current trends in research.

2.1.1 ADVANTAGES

The force equilibrium between members in an RF assembly offers the possibility to use straight members to create curved geometries. These straight members can be joined together using simple and low-tech techniques making the system perfectly suitable for temporary structures, and structures that can be rapidly assembled. Furthermore, the RF system has proven its

applicability in times when the availability of materials, especially timber, was scarce.

2.1.2 MORPHOLOGY

The simplest RF assemblies consist of one unit or fan that are made with three or more members. When multiplying the number of units, complex, multi-unit RF assemblies can be made by which it becomes possible to span large distances by using relatively small individual members lengths.

One can vary the connection topology i.e. style between the members by using concentric or eccentric connections to be able to design curved geometries. However, when using concentric joints, the detail design often requires additional measures such as steel connectors. Two simple RF assemblies with eccentric joints and consisting of one unit but multiple members are showed below (Figure 2.1). In these examples, eccentric elements form a closed circuit by means a stable equilibrium of forces: the reciprocal frame.

2.1.3 DESIGNATION

The term reciprocal derives from the Latin word *reciprocus* which means back and forth referring to a mutual action or relationship. Other descriptions for this type of structure that often can be found in literature are *nexorade*, *mutually supporting* or *interlocking elements*, *Leonardo grid*, *Lamella*, *Mandala*, or in German '*Hebelstabwerk*'. However, this report uses the '*reciprocal frame*' (RF) since it is the most frequently used term in recent research^[1].

The term '*reciprocal frame*' was first adopted by Graham Brown in 1989 who developed a patent for a 3D closed circuit of sticks^[3]. His patent led to the formation of the first academic research group and associated publications. It has been inspiring and stimulating research from around the world and has been leading to numerous practical applications. However, the first RF applications already existed thousands of years earlier.



Figure 2.1: The structural principle of a three- and four-member single unit reciprocal frame



2.2 HISTORY

History shows that for thousands of years mankind has been able to span distances greater than the lengths of the materials available by using RF assemblies and with that fulfilling different needs and purposes. Figure 2.3 shows the full RF timeline referring to all history discussed below.

In history, the first applications of RFs can already be found in the Neolithic civilization (< 2000 BC). Here, simple RFs were used in a tipi type configuration to create habitats where one could live protected from the weather. The permanent and legged RFs were tied together at the top and covered with wood or mud.

Presumable around this same period, Indigenous Americans used approximately the same type of structure, originally covered with hides, as rapid to assemble and temporary structure, perfectly suiting their nomadic lifestyle. Lodgepole pine and red cedar were used as structural poles in these tipi's.

2.2.1 BRIDGING

Not for living, but for a complete other reason was the construction of Julius Caesar's bridge over the Rhine during the Roman empire. This bridge was constructed to decrease the drowning risk during river crossing and was the first bridge to span the Rhine (Figure 2.3). The interlocking reciprocal connection between the columns and beams of this bridge naturally provided a solid inclined connection making a bridge capable to support large troop weights and enable safe transportation.

A similar interlocking type of reciprocal connection that was used for Caesar's Rhine bridge can be found in the construction of bridges made during the Ming Dynasty in China. One surviving court painting by Zhang Zeduan shows a reciprocal bridge that spanned approximately 19 meters. These arched bridges were widely used and

made using straight and relatively small timber elements. Today, there are unfortunately no known surviving examples of these bridges. However, the technique, originally founded around 1033 AD, was rediscovered and redeveloped in the 1970s resulting in existing and relative modern examples of the Rainbow bridge (Figure 2.3).

2.2.2 LEONARDO DA VINCI

The old designs of the Rainbow bridges could have inspired Leonardo da Vinci during the renaissance in the fifteenth century. In fact, Leonardo proposed a bridge design similar to the design of the Rainbow bridges^[1].

This military bridge design was proposed as temporary construction to be used in emergency situations to cross for example rivers. Locally found timber weaved together by means of the reciprocal ideology should shape the bridge. Today, this typical bridge design is still being described as the Leonardo bridge.

Furthermore, da Vinci engaged in other RF designs and was the first who tackled the geometric challenges of RFs analytically^[1]. In his famous works 'Codex Atlanticus' and 'Codex Madrid' several RF patterns were drawn. These sketches were accompanied by descriptions that discussed geometry, structural design, clothing, and construction processes. For instance, the geometrical design was described in ratio between height and span.

In addition, the use of standard elements, the materialization, and the fact that loading near supports on members increases was discussed which was highly advanced for that time. The geometrical RF patterns show an advanced perspective on the design which is emphasized by the fact that of some of his patterns still cannot be found in practical RF examples today.

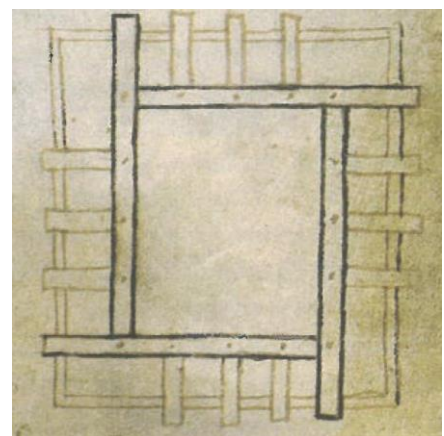


Figure 2.2: Early RF designs by Leonardo da Vinci - approx. 1235 AD (Left) and Villard de Honnecourt - approx. 1225 AD (right)



2.2.3 FLOORS AND ROOFS

Villard de Honnecourt is sometimes mentioned as the Leonardo da Vinci of the Middle Ages. His surviving sketches describe construction techniques - including an RF pattern - and mechanical devices. He described reciprocal structures as follows:

*IN THIS WAY YOU CAN EVEN WORK ON A HOUSE OR A
TOWER USING TIMBER THAT IS TOO SHORT - VILLARD DE
HONNECOURT, 1235 A.D.^[1]*

The RF technique was very valuable in the middle ages since there were large timber shortages due to considerable population growth. Therefore, it may be expected that the RF technique was widely used in that time (Figure 2.2).

A remarkable reciprocal example from this time can be found in the 13th century Lincoln Cathedral, England. The timber frame used in this cathedral spanned 21 meter which then was a record-breaking span. Unfortunately, the RF lost its function during a renovation in 1760 by the addition of a column (Figure 2.3).

Other historical reciprocals of that time that still can be found in practice are rare. However, recent renovations have been exposing English RFs in for instance Kalmscott Manor and The Wollaton hall of which Sebastian Serlio proposed a similar structure in 1537 (Figure 2.3).

These RFs were purely functional as their structural patterns were unexposed. The main reason for using RFs seemed to be a scarcity of available timber in the desired length. Esthetical examples, however, can also be found. The Esthetical and four intertwined letters 'P' represent -by four interlocking reciprocal beams- the name Pius Papa Piccolomineus Pientinus. A papal who's residence was based in the Palazzo Piccolomini in Pienza, Toscana Italy (Figure 2.3). Another beautiful example of an esthetic application can be found in the Casa Negre designed by Josep Maria Jujol -an associate of Antoni Gaudi- in Barcelona.

2.2.4 FIRST UNDERSTANDINGS OF STRUCTURAL BEHAVIOR

Leonardo da Vinci analytically described the structural RF behavior briefly alongside his sketches. It however took until the 17th century till the mathematician John Wallis first described a method on how to calculate the forces acting on the members in an RF by using the law of lever. This rule simply relies on mechanical equilibrium between the elements.

Wallis not only developed a calculation method. To be able to calculate the forces, he transformed the member arrangements into line models and made physical models, that helped to define, and understand the

structural behavior. Furthermore, he was the first to multiply single unit RF systems too multiple unit RF systems (Figure 2.3), suggested construction sequences, and proposed connection designs.

In addition to this first scientific approach from Wallis, the French military engineer Émy proposed in 1837 numerous RF proposals. This 'Traité' de l'art de la charpenterie' became one of the bases of modern timber engineering^[1].

2.2.5 OTHER MATERIALS

Till now, all the discussed reciprocal history focused on using wood as primarily building material. However, the reciprocal technique can be applied using other materials.

This was described by Émy who showed in his works that by shaping stones in a specific form, an interlocking flat stone vault can be made. The structural behavior of these vaults rest in the transformation of bending forces -throughout interlocking shear connections- to the supports according to the principle of stereotomy^[1].

By using this technique, the individual stones -that can have the same shape- support each other at their edges causing that bricks must be laid crossways and must have angled edges. It results in no need to use connectors or mortar between the bricks. The angled brick edges enable shear transferring that is mainly caused by the self-weight of the bricks. Regarding flat vaults, this technique results in exceptional high forces at the center bricks in the vault.

Joseph Abeille was the first to describe this technique in 1699 by means of a patent. Later, this patent was studied by Frézier in 1737 which resulted in numerous brick designs and a design rule noting that the angle between the bricks should not exceed 45°. The technique resulted in a few practical applications among which namely cathedrals. Today, researchers still investigate this technique - primarily as application in domes - in which the main described material is rock; however, cast concrete can also be used^[4].

With the rising use of cast concrete in the twentieth century, the need to use RF systems because of scarce available timber lengths, became less necessary. The technique however did not get out of favor. One special aesthetic and functional twenty century application can be found in the Independence hall in Philadelphia, designed by Louis Kahn. He designed a concrete reciprocal consisting four members spanning a staggering 13 meter (Figure 2.3).

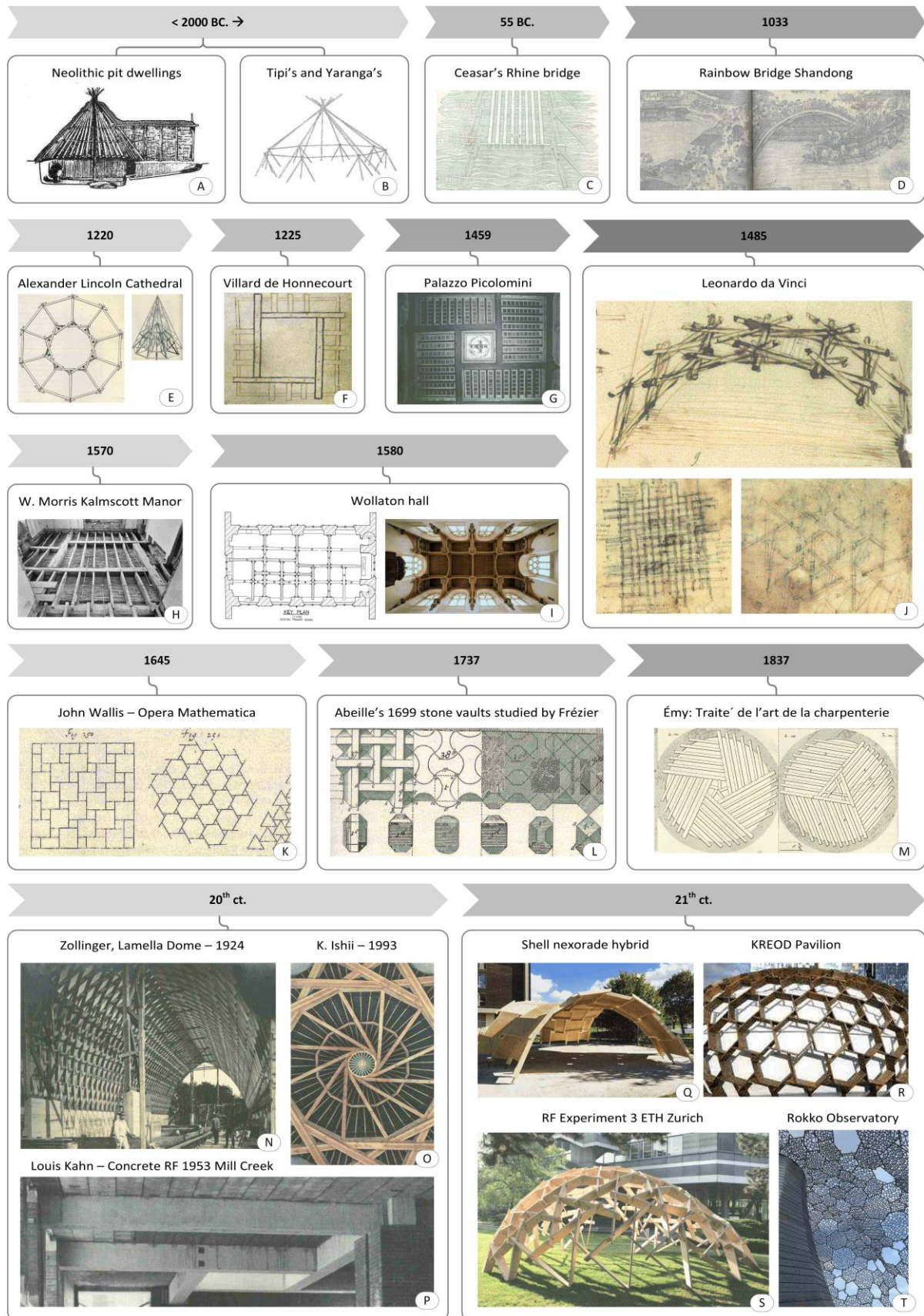


Figure 2.3: Reciprocal frame history timeline. Years may be approximations



2.2.6 TWENTIETH CENTURY

In search for a cost effective, and material efficient roof structure, the German engineer Friedrich Zollinger developed a new technique based on RF jointing. However, this so-called Lamella or Zollinger roof system uses in plane jointing instead of overlapping jointing and requires a great number of steel fasteners. Zollinger however, stated that his technique resulted in 60 percent less wood and 40 percent less labor in comparison to standard roof structures for that time (1924). This proved to be a big advantage for post WW1 Germany. One big disadvantage of the system was the un-stiff bolting connection that resulted in a relative large overall sagging^[1].

A small deformation in one Zollinger connection result in large overall deformation by the great number of connections. This fact also needs to be considered in other RF designs. Nevertheless, the Zollinger frames where widely used in housing developments in Europe^[1]. Probably mainly explainable by the need for housing and fast inexpensive construction.

Other twentieth century RF examples of can primarily be found in Japan. A special example in which the design was spiritually inspired by Buddhist temples and shrines built in Nara, is the Bunraku Puppet Theatre in Seiwa designed by Kazuhiro Ishii. Its roofs where all built using the RF technique (Figure 2.3).

Here, a multiple unit RF using short sturdy beams covers the auditorium. A single unit and spiraled RF - using 12 beams - is applied in the exhibition room. The RF principle of Leonardo's bridge is applied to connect the buildings by means of an open gallery. By using anchors and notches in the beams of the auditorium, a planar structure could be created. By using steel, it became possible to allow bending in the timber joints. The built took completely place using hand drawings which is remarkable considering the complex geometry.

Less complex RF geometries started to be used in the late twentieth century when single unit low impact or eco-friendly homes started to be built from rough timber logs. These houses have been often built by self-builders who spread their knowledge on how to build these low impact houses and even started communities. The initiator of these houses seems to be Graham Brown who built around 30 RF houses himself, patented an RF technique, and sees building RFs as a spiritual activity^[5].

Inspired by the patent by Graham Brown, John Chilton started an academic research group in RF design. Here Olga Popovic Larsen later completed the first PhD research about RFs in 1996 leading to numerous publications, and an indication of widespread curiosity.

2.2.7 TWENTY-FIRST CENTURY

The last few decades, RF research has been an increasing topic for academics primarily driven by advances in computational design technologies and by a fascination for aesthetical beauty. It has been leading to many form finding techniques of which some are applied in practical applications.

To date, one of the most advanced RF applications is the Mount Rokko Observatory in Japan that was completed in 2010. This aesthetical RF does not have a structural function except bearing its own weight.

The main RF structure of the Mount Rokko Observatory is made by 50-millimeter welded eccentric stainless-steel tubes in which, at some locations, reciprocals made by Japanese cypress create an infill (Figure 2.3). In winter, icing can collect on the tubes and during the summer the structure provides shading. The design procedure used a guiding mesh was used based on Voronoi diagrams (see 2.5.4).

The largest RF roof till this date, spanning 44 meters, has also been made in Japan. This roof uses an RF technique similar to the Leonardo bridges and was designed by Tetsuro Kurokawa who build several RFs in Japan. For this example, the structural members are made from locally grown cypress wood that earlier was regarded as unusable. By using this wood, Kurokawa tried to stimulate local wood use and decrease the wood import. Japan is world's largest wood importer^[1].

In Europe, recent built RFs have been preliminary pavilions resulting from RF research. The KREOD pavilion is no exception and is built as showcase pavilion for the London Olympics (Figure 2.3). Since it is demountable, the joints where designed using a principle normally solely applied in furniture: no screws or glue could be used. Furthermore, by using a constant curvature, the pavilion could be made from equal and standardized timber elements. The designers developed a tailored parametric algorithm to construct the pavilion.

Many pavilions have been made to explore the capabilities of RF design tools. At the ETH Zurich a revolutionary RF design tool resulted in at least four pavilions (Figure 2.3).

The connections between the individual members in these RFs primarily where made using joinery milling either by hand. In some of their self-called experiments, notches where used whereas in another the jointing solely was restricted to bolts.



The shell nexorade hybrid pavilion by the Ecole des Ponts in France used solely robotics in the jointing manufacturing^[6]. Their new approach to RFs combines structural cladding and members in the form finding to form one mechanical structural scheme. The paneling in this system distributes loads to the members and ensures stability simultaneously (Figure 2.3).

It seems that in this century the ongoing research in RFs led to more pavilions than actual practical examples. The architectural potential of more complicated RFs still needs to be explored. However, the applications of RFs are not primarily reserved for architectural purposes.

2.2.8 ART AND OTHER APPLICATIONS

Renowned architect, and famous from his timber architecture, Pritzker Prize winner Shigeru Ban designed a reciprocal art sculpture too. This project, built at the University of Houston, was made from laminated *bamboo strips* using a multiple unit RF supported by interlocking steel columns. By using both negative and positive arranged RF unit styles, a convex and concave curved grid was created (Figure 2.4).

IN CHINA, BAMBOO STRIPS HAVE BEEN USED FOR THOUSANDS OF YEARS TO CREATE RECIPROCALLY WEAVED BASKETS^[7].

FOR A SIMILAR DESIGN, SEE THE SPORTS BALL USED IN SEPAK TAKRAW BELOW.



The RF principle is not limited to static structures, by creating joints with a certain degree of freedom, RFs allow to create kinetic structures. This was first explored by Emilio Perez Piñero who patented a foldable RF roof structure in 1965. This tridimensional grid was deployable by means of a 'scissor' mechanism that was stabilized by interlocking RF joints^[8].

The interlocking RF principle was also used in furniture by Pino Pizzigoni who designed a reciprocal table and chair^[3]. These designs can be counted as art furniture and show that by using the RF principle, vertical structures can be made. In the field of RF art, inspiration can be found in the work of M.C. Escher and mathematical artist Rinus Roelofs who experimented with RFs and corresponding geometric entities. By means of full-scale physical models and by constructing numerous geometrical patterns, Roelofs has been showing the aesthetical and structural potential of his so called 'Leonardo da Vinci Bar Grids'.

2.2.9 REMARK

RF structures seem to have references in both Western and Eastern cultures. Unfortunately, historical surviving RF references are rare. Furthermore, these have not been linearly distributed over history but fragmented in which the last centuries show an increased interest, complexity, and practical applications. The applications however, demonstrate that the architectural adoption still needs to be explored. This research aims to contribute to this. For a complete overview of RF history and patents see^{[1][3]}. The next chapter discusses the RF design basics.

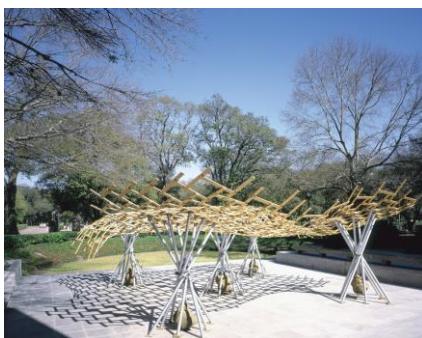
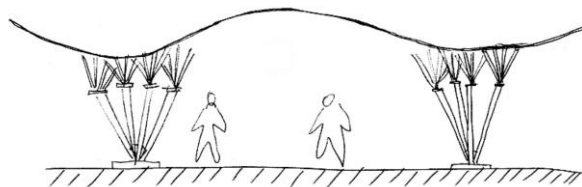


Figure 2.4: Reciprocal art structure made with laminated bamboo strips, designed by Shigeru Ban



2.3 GEOMETRY

To understand, study, and visualize structures, designs must be made. Where regular structures can be easily designed and drawn by hand or computer aided design (CAD), it should be underlined that this feature does not completely apply to RFs. Especially when looking at three-dimensional RF grids with eccentric jointing, a manual (CAD) design can be problematic without the use of design methods.

An elementary design method can be established by considering a two- or three-dimensional grid structure that is made from series of intersecting members. Here the members meet each other at their extremities.

In elementary geometry, polygons share this property since their sides are shaped by finite chains of linear line segments that can be identified as structural members.

It contrasts with RFs where the beams do not meet at their extremities, but somewhere along the length of the beam. This geometrical property can be achieved by modifying the geometry of basic polygons. The design of RFs is very challenging to be accomplished without the use of polygons.

The following four polygon modifying methods can be used to construct an RF:

- Rotation;
- Translation;
- Rotation and translation;
- Center to center and offset.

All methods are briefly described below (Figure 2.5) and in the coming chapters by considering single unit and planar systems.

2.3.1 ROTATION

To create an RF by means of rotation, one must first consider any arbitrary convex polygon and determine for every side its middle point or end/start point. Second, all polygon sides are rotated around their normal vector at the found point by a predefined angle α . Third, the intersection points at every adjacent linear line must be joined with the rotated lines. The resulting joints can always be made in planar systems.

In non-planar systems however, eccentricities between the lines occur resulting in the need to apply other connecting methods. This geometrical method will be valid for all modifications and will be discussed in 2.3.5.

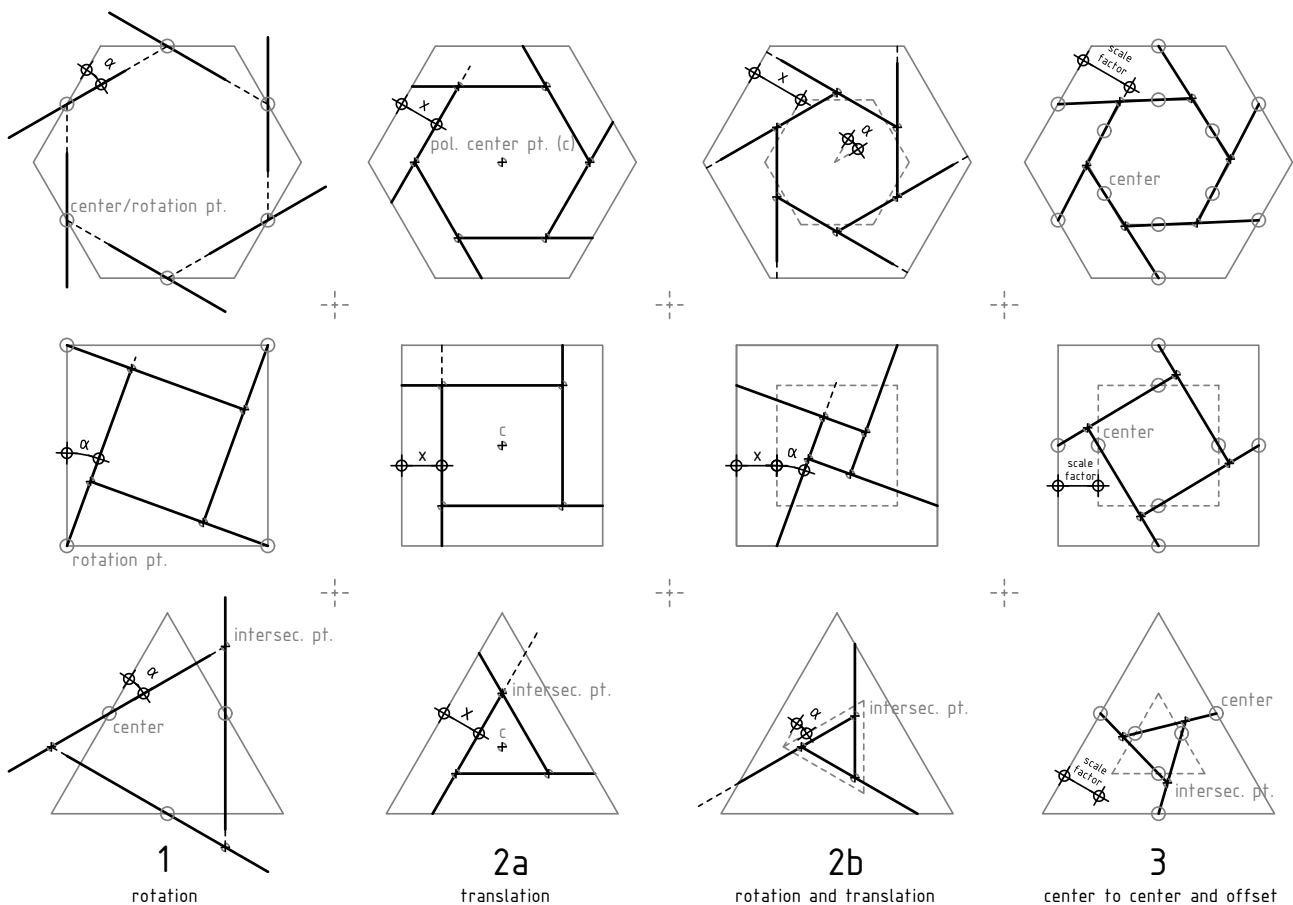


Figure 2.5: Geometrical RF design methods applied at three different polygonal shapes: triangle, quadrilateral, hexagon



2.3.2 TRANSLATION

Modification by means of translation modifies the base polygon by translating its sides in perpendicular direction towards the polygon center point. An important remark here is that the translating distance should not exceed the distance between the base polygon edge line and its center point.

2.3.3 ROTATION AND TRANSLATION

An RF assembly can also be achieved when combining the rotation and translation method described above. This method however, does not seem to contribute to the overall polygon transformation methods since it does not add extra freedom of form with respect to solely rotation. Furthermore, the complexity to create an evenly divided or regular grid is increased. It makes the transition between the polygons not arbitrary but difficult to determine using simple geometric rules. This research aims to use relatively simple geometrical rules to determine an RF assembly. Consequently, the combination of rotation and translation will not be studied further.

2.3.4 CENTER TO CENTER AND OFFSET

The center to center method naturally creates a regular divided grid when using multiple basic polygons. First, by scaling any arbitrary convex polygon towards its center point, a smaller duplicate is created. Second, the midpoints at each side of the basic and scaled polygon must be determined. Third, the midpoints of the basic polygon relate to the midpoint of the neighboring side of the scaled polygon and can be jointed with a linear line. Fourth, the created lines must be enlarged to the intersection points that can easily be found since the lines share the same plane.

The resulting RF is thus determined using scaling. The scaling factor S_v is the same in all directions and linear transforms the basic polygon with a factor $0 < S_v < 1$. Furthermore, by creating the RF lines with the polygon center points and considering multiple polygons or RF units, member intersections are naturally created.

2.3.5 PARAMETERS

The methods listed above determines the design of an RF. In addition, when regarding an RF with eccentric jointing, the global form depends on the following parameters^[1]:

- *Style* of the fans or units;
- *Number n* of members per unit;
- *Engagement length a* of a member;
- *Eccentricity e* between the members;
- *Overall length l* of one member;
- *Configuration* of members in the structure.

These designations will be used throughout this report.

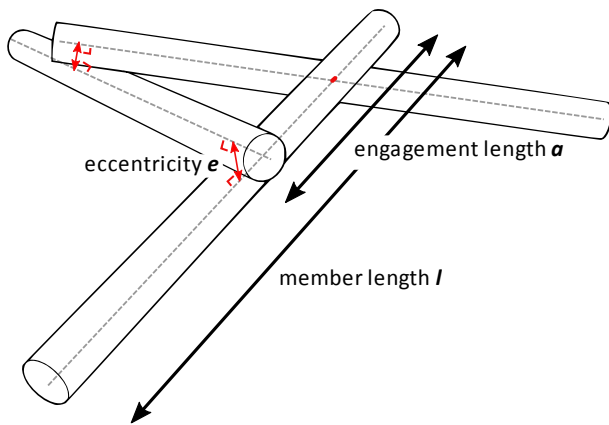


Figure 2.6: Parameters in an RF with eccentric jointing and three members

The desired curvature of an RF is to a large extent determined by the style of the RF unit i.e. connection typology. The figure above shows the most common style that could be structurally stable when using friction or notching at the joints between the members. This structural equilibrium does not account for every reciprocal style. Of the four possible styles considering three members and one unit, two could be structurally

stable by itself. The other two are unstable without using additional connectors between the members.

The eccentricity is independent of the unit style and is defined as the shortest distance between two members. This shortest eccentricity line is unique and is characterized by being exact perpendicular to the axes. Through a mathematical determination of the lines' linear vector equations, and by using the perpendicular property, the intersection points can be determined. Eccentricity distances do not need to be dependent of the member height. However, when using an eccentricity that is smaller than the member depth, additional connection measurements need to be taken.

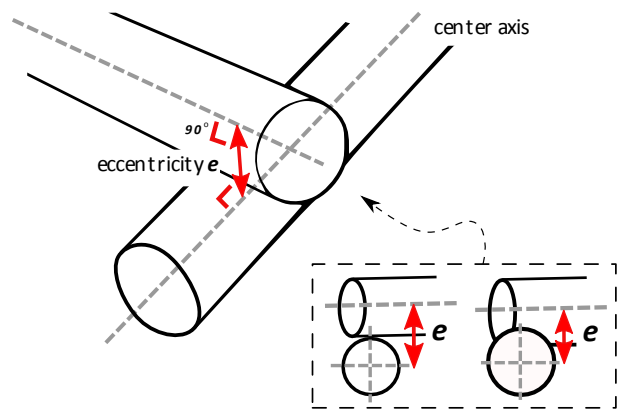


Figure 2.7: The visualization of eccentricity and its influence on the member depth

The combination of multiple styles or the use of one style is determined by the configuration. It also covers the variation in number of elements, engagement length, and overall length. One can make an RF design by modifying all these parameters; however, using all these parameters in a multiple unit RF design may result in design problems. Therefore, design choices are made which are discussed in chapter 3.

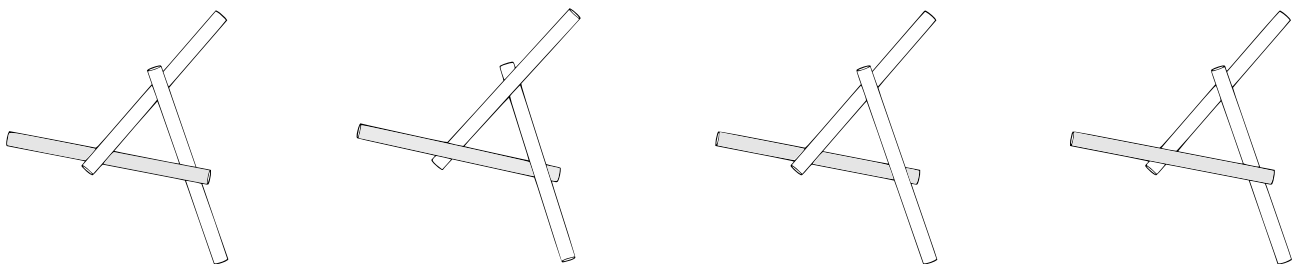


Figure 2.8: The four possible RF styles for three-member single unit assembly's (first and second unit are stable, the third and fourth not without additional measurements – FLTR)



2.4 EXTENSIVE GEOMETRY

The described transformation methods can be used to create planar RF structures. Whether it is possible to apply them to multiple unit RF systems and elevated systems remains unclear. This chapter therefore describes the extensive geometry meaning elevated and multiple unit RF grid ea. systems with more than one connection group.

2.4.1 ECCENTRIC SYSTEMS

An elevated and single-unit RF grid can be created by transforming the intersection points over the normal vector of the basic polygon. This creates an eccentricity between the lines or members. Hence, an eccentric jointing system is created. When applying this transformation to the described polygon transformation methods, a multiple unit RF system can be constructed. The proposed four methods all have (dis)advantages.

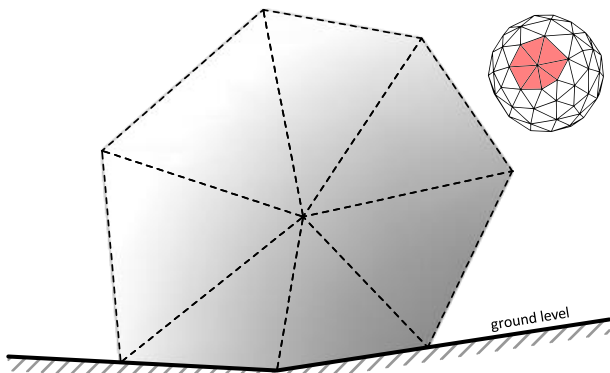


Figure 2.9: Example tessellated surface

Figure 2.9 shows an arbitrary double-curved surface tessellated by seven irregular triangular panels. This surface is used to discuss the different polygon transformation methods that are being applied to this system. The striped gray bottom-line represents ground level. All triangles have one common edge and are noncoplanar i.e. have different normal vectors.

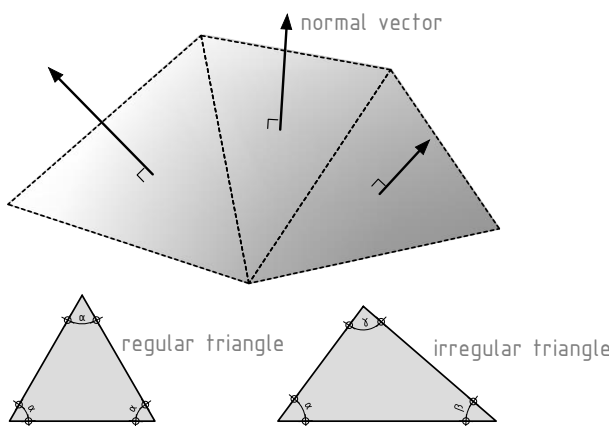


Figure 2.10: the visualization of a normal vector of three adjacent surfaces and polygon regularity

The normal vector of a surface is the vector that is perpendicular to the surface plane. Its origin is in general located at the surface center point but, can be located at any arbitrary location at the surface. Adjacent surfaces are noncoplanar when they have different normal vectors. These surfaces together shape a tessellated surface i.e. a surface that is subdivided by means of tiling. The example spherical surface is tessellated by triangular polygons (see 2.5.4).

ROTATION

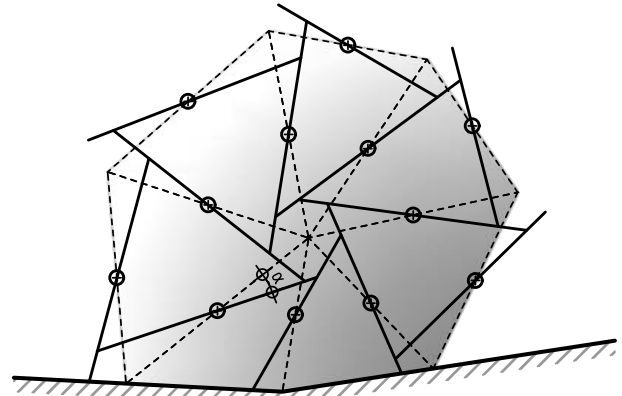


Figure 2.11: Rotation method

The rotation method creates an RF grid by changing the angle α between the basic polygon edge and the new edge. The resulting RF is irregular when the basic triangular polygons are irregular.

By changing the rotation point to the start/end points at ground level, support locations do not change; however, this results in an even more irregular RF grid (Figure 2.12). This is also the case when using regular polygons as basic geometry requiring the use of different rotation angles therewith complicating form finding procedures. In case of planar tessellated systems, more regular geometries can be created. Eccentricities between the members could then be applied by means of geometrical methods as shown by Thönissen et al.^[1].

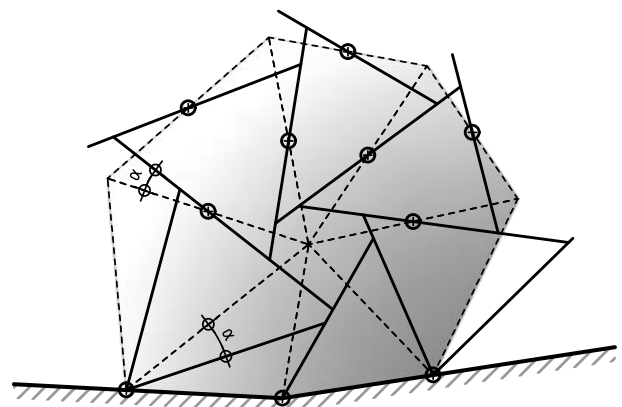


Figure 2.12: Rotation method different at supports

TRANSLATION

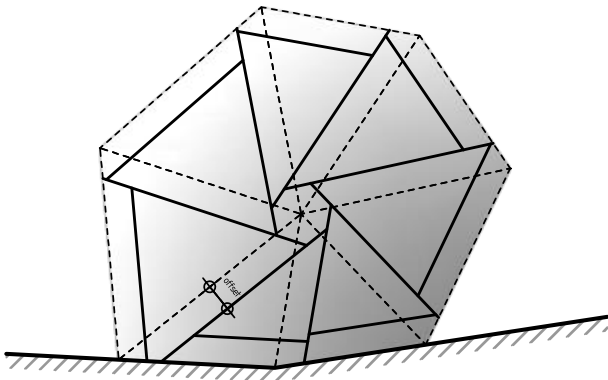


Figure 2.13: Translation method

The translation method creates a regular RF grid with irregular basic polygons; however, the support positions change when applying this method. When applying a rotation transformation next to translation, the method does not add extra freedom of form with respect to solely rotation.

The transformation shown above proves that the number of members is dependent on the number of polygon edges. This is shared by all other transformation methods; however, when examine the RF unit in the middle where seven members meet, it is apparent that this method results in a great number of connections. Especially when using a surface built from triangles the number of connections is large in comparison to a surface built from rectangles. Given this fact, that applies for the rotation method too, and although the supports change during the RF generation. The center to center method may prove to be superior.

CENTER TO CENTER

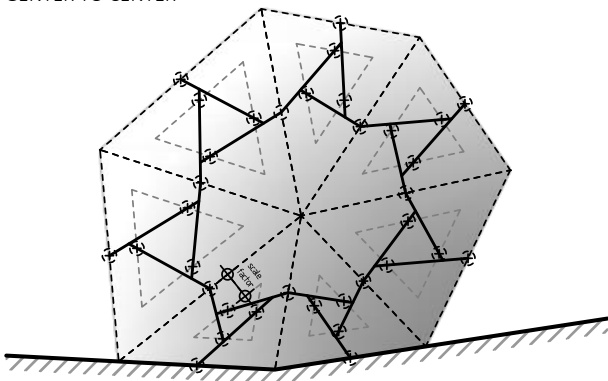
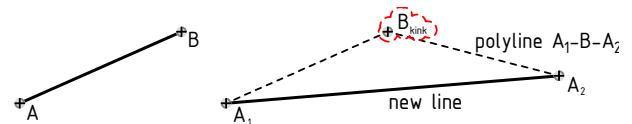


Figure 2.14: Center to center

The center to center method^[9] is different from the other transformation methods because it depends on scaling whereas the other methods depend on basic polygon transformation. Although, the method uses the basic geometrical properties to draw new RF lines.

Figure 2.14 shows that kinks occur at the transitions between the different RF units. These kinks are nonpreferable because they require complex joints or kinked members. Furthermore, the planar triangular panels result in planar RFs. This can be preferable, but the disadvantages are not. Therefore, the kinked lines need to be transformed into linear ones.


Figure 2.15: Transforming a kinked line into a linear line_(A-B)

The two lines that are kinked at their intersection point can be joined into one polyline ($A_1 - B - A_2$).

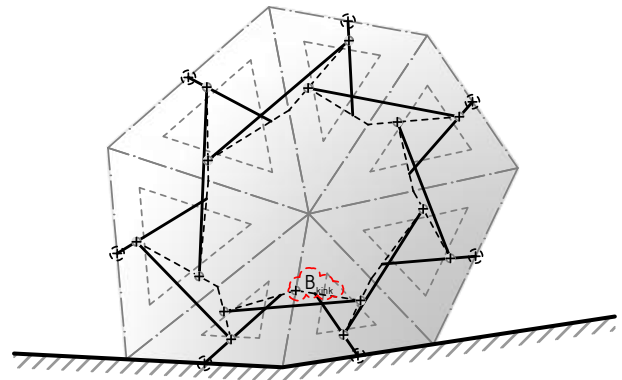


Figure 2.16: Polyline transformation method

Hereafter the new start and endpoint (A_1, A_2) of this polyline can be used to construct a new linear line (line A-B). When it is applied at the doubly-curved surface, it naturally creates eccentricities in a reciprocal manner. Furthermore, by changing the scale factor per RF unit, the engagement length can be changed individually.

Nevertheless, the RF can be established with a uniform scaling factor. The resulting multiple unit RF is thus depended on the basic shape of the polygon, and the figure (Figure 2.16) shows that the resulting RF lines still need a modulation after transforming the kinked lines into linear ones.

Furthermore, when the basic polygons are noncoplanar, eccentricities between the lines will be naturally created after the transformation. When applying the translation method these eccentricities could change in a linear fashion and planar panels can be used as infill between the members according to Douthe et al.^[6] It still needs investigation whether this accounts for the center to center method. Nevertheless, the eccentricities and the modulations will be thoroughly discussed in chapter 3.



2.5 COMPUTATIONAL MODELING

The reviewed design methods of last chapter can be used to geometrically create an RF design.

Nevertheless, an RF design remains extremely difficult to control manually requiring the use of a precise algorithmic definition. The reason is that predictability of a manual design is limited since the parameters cannot be predefined and automatically adjusted to fulfill for example the structural need. Especially when constructing multiple unit RF designs, it seems inevitable to employ computational aid to:

- Allow for structural (FE) analysis;
- Design detailing i.e. enable CAM;
- Predict geometrical configurations;
- Predict dimensions.

Commercially available computer aided design (CAD) software to control the RF design has not yet been widely available. However, the last few decades have been showing an increased interest in computational RF design among researchers which has been resulting in numerous published design methods. These design methods can be subdivided into three main approximation methods all of which responding to one or more specific problems:

- *Analytic approaches* i.e. exact determination;
- *Bottom-up approaches* i.e. self-generating;
- *Top-down approaches* i.e. optimization strategies.

Within these approaches, several independent form finding methods have been developed that will be briefly discussed below. To understand these methods, the first section presents the definition of form finding.

2.5.1 FORM FINDING

The earliest definitions of form finding comprise the idea to find an optimal shape of a structure by using form follows force aiming to allow efficient use of materials. RF structures are however distinguished by this since its structural ideology of 'reciprocally supporting' is leading in the design. By using this ideology, one can find a structure that is in a state of static equilibrium^[10].

Form finding methods that regard mechanical equilibrium - can be referred to as classical form finding - is thus subordinate in the RF design procedure; but, when adjusted can be used. Therefore, this report uses a broadened definition of form finding that has been implemented in the past decade.

FORM FINDING IS FINDING AN APPROPRIATE
ARCHITECTURAL AND STRUCTURAL SHAPE^[10]

Classic form finding is relevant to structures that transfer their loads primarily through axial or in-plane forces. This is in contrast with RF structures that transfers forces primarily through shear and bending as discussed in chapter 3.

Applied examples of classic form finding can already be found in the late seventeenth and eighteenth century in catenary or funicular arches of St. Paul's Cathedral and the St. Pieter in Rome. Later, in the late 19th and 20th century, the famous hanging chain models were used by Antoni Gaudi and extended in studies on physical models by Heinz Isler and Frei Otto^[10].

The computational age however has been making the construction of physical models less essential. It is in contrast with RF assemblies where some researchers claim that the construction of physical models still is the most diffused method to design RFs in architecture^[3]. To overcome this, numerous methods have been developed - some based on classic form finding - which are briefly described below.

2.5.2 ANALYTIC APPROACH

The analytic design approach has been developed to be able to manually determine and control the parameters listed in 2.3.5. A reason for this development can be found in the need to control the RF design without using algorithms that depend on for instance optimization strategies.

By using an analytic approach, one specifies the RF design by using geometrical equations.

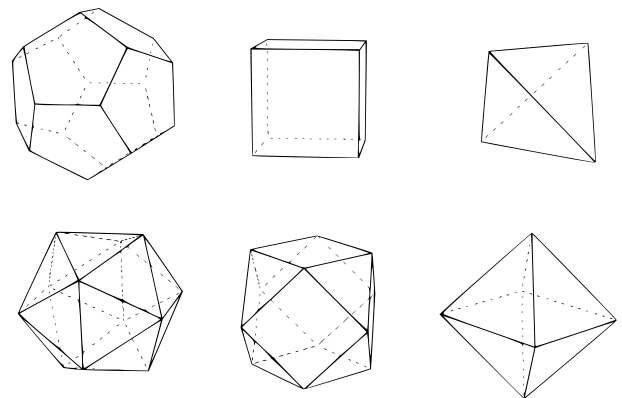


Figure 2.17: Six Platonic solids. FLTR: Dodecahedron, cube (Hexahedron), Tetrahedron, Icosahedron, Hexahedron, Octahedron

One method that has been presented in 2011 by Sénéchal et al.^[11] uses geometrical equations to deform regular polyhedrons into RF assembly's by rotating the polygon edges over their normal vector as described in 2.3.1. A similar and simplified approach is presented by Rizzuto in 2014^[12]. Here an RF structure is created by controlling an initial parameter. When choosing the transformation angle α as initial parameter, one can obtain the simplest equations. In addition, the presented equations enable the eccentricity as initial parameter which can be beneficial in structural design.

The option to manually control the eccentricity is a great advantage since it can depend on member depth. Nevertheless, analytic approaches have been restricted to be used for regular quadrilateral and tri-hex polygons. It cannot be applied to free-form structures and is restricted to the original shape of the often referred to as Platonic solid or polygon (regular). This does not apply for the bottom-up approach.

2.5.3 BOTTOM-UP APPROACH

A bottom-up approach is applicable to design any arbitrary RF and is inspired by self-generating forms found in nature. In principal, the technique is based on adding sets of new RF units to a starting single unit RF assembly in a preferred growth direction. These so-called iterative additions rely on choosing an elementary unit style (see 2.3.5) that is then distributed over the preferred direction. A final RF design is created by connecting the different unit styles and by optimizing its transitions as showed by Gherardini and Leali in 2017^[13].

The final RF design does not necessarily have to rely on a guiding surface design or geometries since it purely relies on the choose of unit style. As the final design depends on decisions at local RF unit level, it is difficult to adapt the design to preliminary design requirements. Changes at local RF level result in large overall design changes. Therefore, it could be difficult to apply this method to situations where geometrical restrictions apply. It seems that this method is applicable to form studies; but, difficult to apply for practical situations.

When comparing the bottom-up approach and the study of RF assembly's by means of physical models, the bottom-up approach may prove to be well usable since it allows to modify parameters per RF unit. The connections between the different units however, must always be considered.

This can become a problem when one prefers to individually control them since, in a multi-unit RF, parameters depend on each other. The algorithm that enables the iterative additions must be adapted to this.

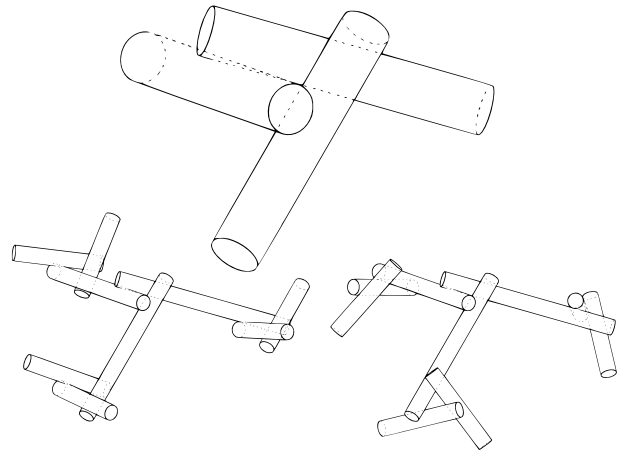


Figure 2.18: Example of the Bottom-up approach

Figure 2.18 shows a simple single unit RF consisting of three members at the top and two resulting configurations that were made by the bottom-up approach. By means of iteratively adding extra units to the system in the three growth directions, a multi-unit RF is created. The results show that the RF unit style is the leading form generator. It is in contrast with a top-down approach in which tessellated surface is mainly used as basis to generate an RF thus followed by optimization algorithms.

2.5.4 TOP-DOWN APPROACH

An optimization algorithm depends on spatial ordering or transformations of a basic reciprocal shape by using predefined strategies. This is the most widely used method in RF form finding since it allows to take preliminary design requirements into account. To date numerous strategies have been developed - some of which evolved from classic form finding - that are discussed below described by means of optimization method.

TESSELLATION FUNDAMENTALS

In general, the RF design processes - regarding the top-down approach - starts by creating RF geometries by means of translation methods. These translation methods can be applied to tessellated two- or three-dimensional surfaces or geometries. Tessellation regarding RF assembly's is tiling of a basic geometry with a defined geometrical polygonal shape. This tiling operation often depends on mathematical rules.

The first step in a tessellation operation is to generate a grid of points on the basic geometry. These points can be generated automatically or manually. Thereafter, techniques such as Delaunay triangulation^[1], Voronoi diagrams, or manual drawing can be applied to generate the polygons whom later to be transformed into RFs.

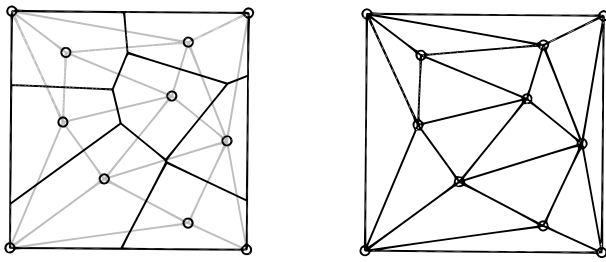


Figure 2.19: Voronoi diagram in black (left) and Delaunay triangles (right) based on the same point grid

Voronoi diagrams and Delaunay triangulation share that a Voronoi diagram can be created using Delaunay triangles by connecting the triangle center points. In practice, this is the most convenient procedure to construct Voronoi's. Additionally, Voronoi diagrams can be constructed by means of radially growing circles with defined points as centers. As soon as the edges of the growing circles collide, intersection lines are created that shape the Voronoi diagram. Thus, the point to line distance is a maximum.

Delaunay triangulation is a mathematical triangulation joining nearest points in a point group regarding the rule that no duplicate points are inside the circumcircle of any triangle. These circles are constructed by intersecting tree discontinuous triangular points at the polygon edges.

The mathematical methods Voronoi and Delaunay can be implemented in an algorithm but, are not the only approaches to create tessellations. Other methods depend on geometric organization of points where after these points can be connected using for instance polylines. Nevertheless, the points can always be joined manually to create a desired polygonal subdivision yet, this requires much work, creates a greater risk of errors, and does not allow previewing the RF design. All methods require basic point grids

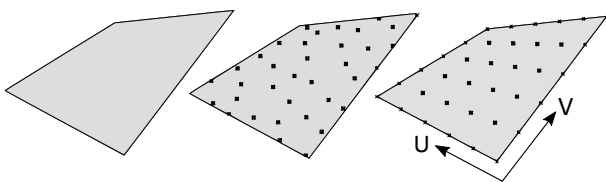


Figure 2.20: Random and curvature based (UV) surface subdivision of an arbitrary doubly curved surface



Figure 2.21: Two identical curves subdivided by parametric curvature (left) and by equal point distance (right)

These grids can be constructed by numerous algorithmic methods using for instance geometric curvature or by means of other constraints in a so-called subdivision determination or parametrization.

Surfaces divided by points in parametric space or by computing the relative distance between points are most commonly adapted (Figure 2.20). The parametric space contains the parameters or distributions that are needed and used to construct a surface.

This can be abstracted by the mathematical representation of Non-Uniform Rational B-Splines (NURBS). NURBS surfaces are defined by control point that are constructed by mapping the functions of two parameters in 3D space.

Point grids constructed by means of parameter space do not necessarily translate into equal point distances in 3D space. The higher the curvature revolution, the higher the concentration of control points resulting in unequally divided points. The project type and desired RF assembly decide which point grid should be used.

Finally, the point grid can be connected using the methods listed above to create a tessellated geometry consisting of regular polygons. These polygons are the basis in an RF transformation.

OPTIMIZING STRATEGIES

Eccentricities between the members in an RF are the product of noncoplanar polygons as discussed in chapter 2.4. The polygons define the basic shape of the RF and correspondingly eccentricities. These eccentricities and engagement lengths, cannot always be controlled directly i.e. in the first step or analytically as discussed in 2.5.2. Modification of one of these parameters affects the complete RF design.

A direct control of these parameters could be preferable since eccentricities determine connectivity of members and could have an influence on the member depth depending on detailing. Furthermore, structural behavior and ease of fabrication could be affected. Therefore, several methods have been developed to optimize eccentricities, engagement length, and other RF parameters following the top-down approach i.e. define an optimization strategy.

The following optimization strategies have been developed by researchers over past two decades:

- Iterative solvers;
- Dynamic relaxation;
- Mapping.

ITERATIVE SOLVERS

Iterative solvers iteratively compute the best geometrical solution of an RF assembly by selecting the best fitting element from a set of alternatives. This set can be created by changing geometrical parameters and is in general not determined by computing arbitrary solutions but, by evolving towards better solutions.

The best solution can be found by optimizing towards a predefined problem that in the simplest case consists of minimizing or maximizing a fitness function. Regarding RF structures, an illustrative problem can be defined as follows in which the eccentricity e between the elements can be optimized as:

$$\arg \min f(e) = e_{old} - e_{new} \geq 0 \quad (2.1)$$

In which e_{old} is defined as the length of the 'old' eccentricity line before the optimization procedure whereas e_{new} can be predefined as the preferred 'new' eccentricity length. By changing e_{old} towards e_{new} one can create a new RF structure. However, this optimization requires geometrical rules as being able to deform the member length l . The orientation and shape e.g. ideology of the RF assembly must be remained.

This has been shown and Song et al.^[14] who proposed a method to keep the RF design relatively close to the basic surface during the optimization procedure. In addition, Parigi^[15] et al. proposed a method to optimize towards both engagement length and eccentricity by means of both a genetic algorithm and a gradient based solver to reduce computational calculation time. Thönissen et al.^[1] developed a vector translation based iterative algorithm that uses a standard optimization algorithm as an extended study to Bavarel^[16].

Preliminary work has been using the following mathematical optimization procedures in RF design:

- *Genetic algorithms*^{[15][16]} are stochastic and based on the in nature occurring survival of the fittest principle. Explores the entire design space;
- *Gradient based solvers*^[15] are stochastic and evolve towards a solution by following the gradient of the fitness function;
- *Least squares methods*^[14] uses predefined and randomly generated solutions to approximate the geometrical solution;
- *Newton-Rapson method* uses numerical iteration to find (a) solution(s) of (a) predefined differentiable formula.

The Newton Rapson method was used to optimize the eccentricities between the stainless-steel members of the Rokko Observatory (Figure 2.3).

In general, iterative solvers do not allow the RF designer to preview the final design instantly. Therefore, it is difficult to predict the influences of parameters and to verify whether the design satisfies to for instance geometrical requirements. Furthermore, there is no guarantee of finding a geometrically possible solution. This led to the development of using dynamic relaxation - commonly used in regular form finding - to be used in RF design.

DYNAMIC RELAXATION

Form finding by means of dynamic relaxation is not limited to RF structures. In fact, it has been evolving from regular grid and cable structure form finding. Douthe and Bavarel where the first to suggest a method on how to apply dynamic relaxation to RFs for which they developed an algorithm^[17].

In contrast to the other discussed iterative solvers (except Newton-Rapson), the dynamic relaxation method is not fully deterministic. This means that no randomness is involved in the development of the RF design. In short, dynamic relaxation uses fictional bending forces applied at an undeformed regular grid structure forcing it to transform into an RF where after it finds static balance by means of kinetic energy dissipation. Furthermore, the described geometrical RF transformations can be used followed by dynamic relaxation of fictional line forces to optimize for instance eccentricities.

When the fictional bending forces are applied to transform the grid structure into an RF or to optimize eccentricities, stresses are induced of which the kinetic energy needs to be dissipated to be able to reach a static balance. This static balance can thus take predefined parameters into account such as the eccentricity between the elements. To be able to dissipate the kinetic energy, fictitious damping must be applied^[17] at all joints. The forces and dampers are fictitious because they have no physical representation. By using numerous iterations, a dynamic relaxation algorithm converges towards its solution.

The number of needed iterations to convert towards a design solution can differ per situation and depends on the complexity of the optimization procedure. The optimization procedure of dynamic relaxation is nonlinear making it perfectly suited to coop with large deformations. Furthermore, an advantage is that it allows to use the same model for form finding and for structural analysis^[17].



Dynamic relaxation belongs to the category of dynamic equilibrium form finding methods that includes the particle spring method. The particle spring method evolved from the graphic industry - where it has been used to solve problems such as cloth simulations - towards the building industry. The method is perfectly suitable to design for instance hanging chain models and to solve for other geometric optimization problems. Since this research does not focus on particle spring systems, the author references for a comprehensive and concise elaboration to Kilian and Ochsendorf^[18]. The authors' definition can be found below.

PARTICLE SPRING SYSTEMS CONSIST OF PARTICLES (LUMPED MASSES) AND MECHANICALLY DEFINED LINEAR ELASTIC SPRINGS; THAT, WHEN EXPOSED TO FORCES AT THE PARTICLES, FIND ONE EQUILIBRIUM POSITION BASED ON THEIR MECHANICAL PROPERTIES.

EXPLORATION OF DYNAMIC RELAXATION

Form finding by means of the particle spring system allows real-time analysis and discovery of the structural design^[18]. Therefore, it has been included in the 2014 Kangaroo physics plug-in for the NURBS based 3D CAD software Rhinoceros and Grasshopper^[19]. Kangaroo is a collection of algorithms including an RF design and eccentricity optimization tool.

The RF design tool is based on the rotation of basic mesh segments along their normal vector conform 2.3.1. Hereafter the eccentricities can be optimized using the eccentricity optimization tool that depends on dynamic relaxation. Figure 2.22 shows how the tool was explored by designing three examples based on basic and relative regular meshes.

These explored RF examples did not always converge towards an optimal solution. It seems that regular RF structures are very difficult to produce by using the tool since it is almost impossible to completely impose the desired form. Furthermore, not all parameters such as engagement length and eccentricity could be defined precisely resulting in the need to review other described methods.

MAPPING

One of these methods is the mapping method that involves the transformation of a two-dimensional RF grid to a three-dimensional surface. The mapping operation results in linear or curved reciprocal lines depending on the mapped surface.

To achieve usable results, the flat representation of the mapped surface needs to be as large as the two-dimensional reciprocal geometry used for the projection.

Furthermore, reciprocal edges need to represent the edges of the mapped surface. The resulting reciprocal geometries depend on the curvature of the mapped surface which however could result in geometries that do not satisfy uniformity as can be seen (Figure 2.23).

This could be avoided by using different projecting densities i.e. a non-uniform projection geometry which adds extra complexity. Furthermore, to be able to implement eccentricities, the curved lines need to be transformed into linear lines. This transformation corresponds to the described polyline transformation (Figure 2.15). The eccentricities can be iteratively optimized using different projecting densities.

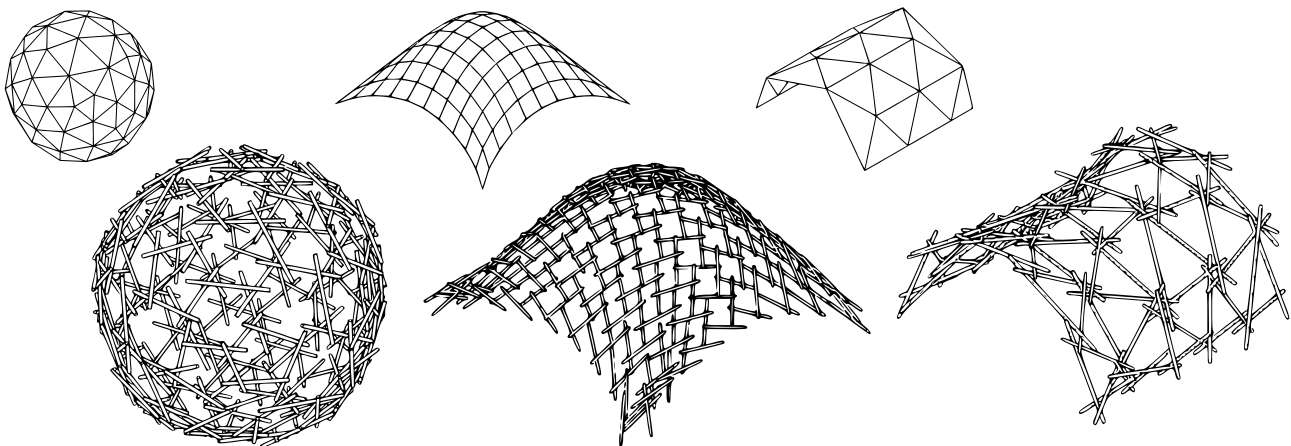


Figure 2.22: Three RF assemblies constructed with Kangaroo's RF design tool using dynamic relaxation as eccentricity optimization. Displayed above, their basic meshes before rotation of mesh segment

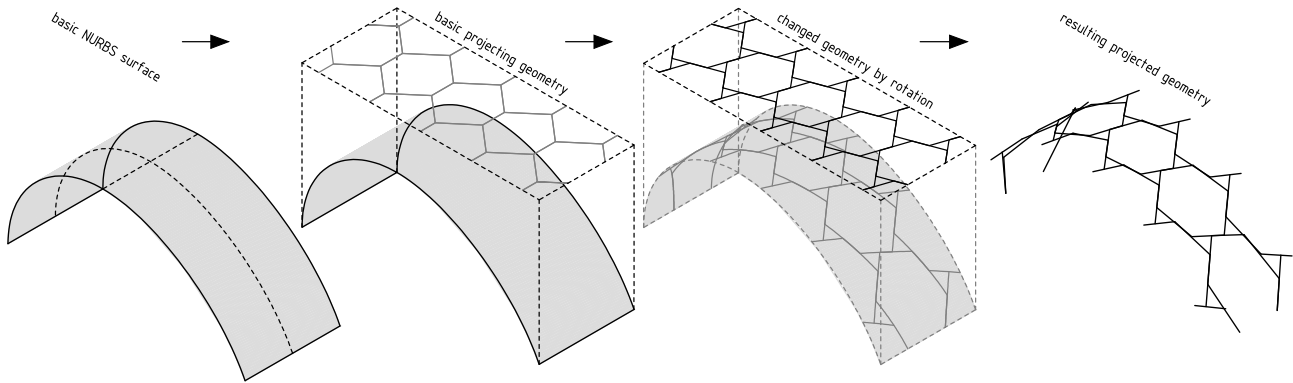


Figure 2.23: An example of the mapping method FLTR with an mapped RF geometry

2.6 CONCLUSION AND DISCUSSION

The mapping method is a possible top-down design approach. In total, the discussed history, ideas, techniques, and design methods in this chapter are the basis of RF engineering and are used to support the conclusions below. An attempt has been made to cluster the best of this below to justify the choices on which the rest of this report is based.

2.6.1 CONCLUSION

RF structures can create curved geometries by using straight members, can span longer distances than the individual element length, can be joined using low tech techniques, and have proven their applicability in times when the availability of materials, especially timber, was scarce.

HISTORY

The non-linear history of RFs shows that the technique fragmented has been applied over time proven by all practical references; some of which still exist today, and by surviving literature. In contrast with the thousands of years that have been showing a non-linear history, the amount of research and interest in RFs over the past decade seems to have been growing exponentially. This naturally resulted in sophisticated RF design methods.

DESIGN

The polygon modification methods rotation, translation, this combined, and the center to center method evolved from recent research. When regarding single unit RF designs, the methods do not differ much and do not result in major design discrepancy. However, when regarding multi-unit RFs, the methods do differ and result in great design discrepancy. The center to center method results in an RF grid that uses the simplest geometric rules. The other methods rely on angles or distances to transform a polygon. This transformation data could have to vary much depending on the geometrical variety of the basic geometry. The scaling factor, used in the center to center method, covers this

variation naturally. Furthermore, this method results in the least connections when considering triangular basic meshes or surfaces, creates regular RF geometries, and does not require changing the location of structural supports. Therefore, it will be used in the development of new RF design tools that are discussed in chapter 3.

COMPUTATIONAL

The complex nature of RFs requires computational need in which for instance the center to center method can be applied. When regarding a computational design, a basic mesh or surface can be divided, or can consist of more than one polygon. Eccentricities between the reciprocal members will thus be created after the polygonal RF transformation if the individual normal vectors of the planes differ. An important notice here is that the number of members depends on the number of polygon edges and the chosen transformation method. The resulting multi-unit RF is thus depended on the basic polygonal shape and their mutual relation. This relation determines the eccentricity distances which can be optimized using three main approximation methods.

These three methods cannot all be applied in free form design. The top-down approach however, seems to be an exception to this since this approach allows to take predefined design requirements into account that is desired for the final research. Within this method, the numerous optimization procedures do not all allow interactive user control i.e. to preview the design instantly. When using for instance genetic algorithms this is not possible but, it is preferable. Design changes at local RF level result in global design changes.

EXPLORATIONS

The explored RF design tool is the only accessible digital design tool. This tool optimizes the eccentricities of RFs by means of dynamic relaxation but, is not suitable to converge to an optimal geometrical solution (Figure 2.22).



This additionally accounts for the mapping solution that requires geometric and eccentricity optimization. Other tools developed by RF researchers are mainly kept within the walls of universities and all have their downsides as described in 2.5. It seems therefore unavoidable to design a free form RF tool for this research that allows direct user control. This enables structural (FE) analysis, detail design (CAM), prediction of geometrical configurations, and enables the dimensions prediction. In conclusion, to find the appropriate architectural and structural shape called form finding.

2.6.2 DISCUSSION AND FUTURE WORK

From the RF designs of Leonardo Da Vinci to the design of the complex Rokko Observatory, from bridge applications to canopy's, kinetic structures, art; and from the use of timber to stone. It indicates that the variety in RF applications and materials is great despite geometric challenges.

Where the practical RF applications in historical examples seemed to be induced by material shortages, complex examples of today have an investigative and aesthetic function. With the advent of climate change and as cutting-edge timber engineering finds more and more practical applications, these functions can be supplemented with others, hopefully resulting in reciprocal timber architecture.

The described theory could cover the design of reciprocals and is practically applied in the next chapter in the development of three RF design tools. By starting with single-unit RFs, the complexity is built up step by step for each tool by using the gained knowledge of its predecessor. The third tool for example, features a parametrized connection design and is suitable for almost any arbitrary design. Two questionable connection designs of recent RF projects are displayed below and could be an inspiration

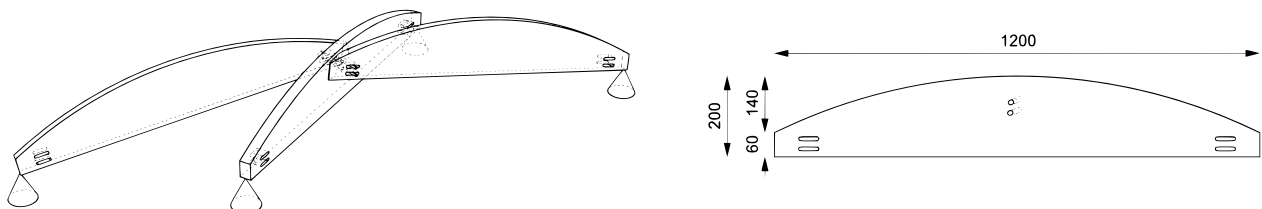


Figure 2.24: Zollinger reciprocal connection in sawn timber applied in the Hale County Animal Shelter by Rural Studio

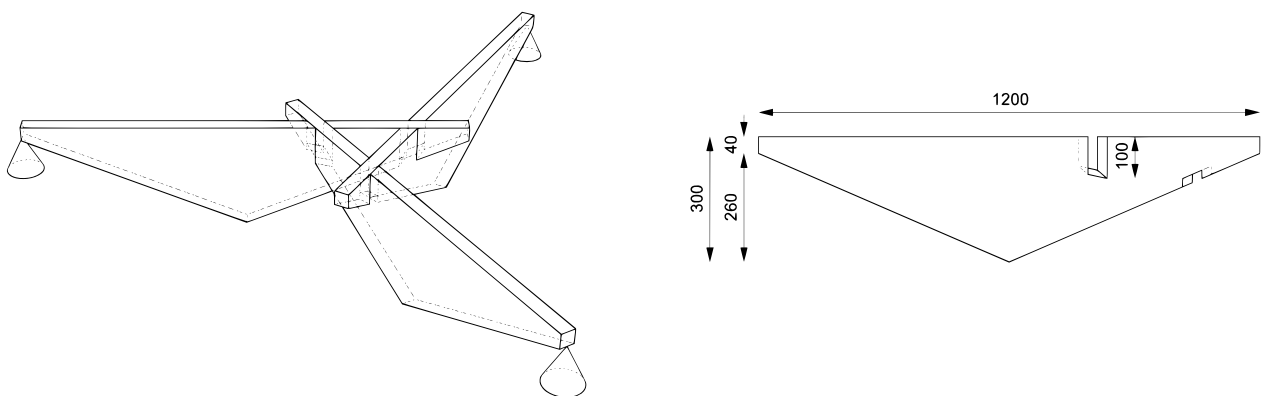


Figure 2.25: Reciprocal connection in glulam timber applied in the modular pavilion Kyushu Geibunkan by Kengo Kuma

The background of the page is a light gray color. Overlaid on this background are numerous white, three-dimensional geometric shapes. These shapes are primarily rectangular prisms and triangular prisms, some of which are tilted at various angles. They are arranged in a way that creates a sense of depth and architectural structure, resembling a complex, abstract framework or a series of interconnected beams. The lines of these shapes are clean and sharp, contrasting with the soft gray background.

FORM FINDING RECIPROCAL FRAMES

This chapter discusses three developed RF design tools. The first tool is suitable for single-unit RF systems whereas the others are suitable for multi-unit RF systems. The third described tool can be used to design almost any arbitrary RF.

-



3 FORM FINDING

Form finding is finding an appropriate architectural and structural shape. This chapter describes the form finding procedure to design multi-unit RFs by gradually increasing complexity. The first tool to be described is suitable for designing single-unit RFs whereas the second tool is suitable for ten-unit RFs. Finally, the third tool is suitable for almost any arbitrary RF design using three- or four-member units.

3.1 HOW TO DESIGN A BASIC RF - MODEL 1

As described before, the design of RFs cannot be accomplished without the use of geometrical rules. The center to center method naturally creates a regular divided grid when using multiple basic polygons. Because of this, and others described reasons in chapter 2.3, this method is used in the development of all the described RF form finding methods.

3.1.1 FROM GEOMETRY TO DIGITALIZATION

The center to center method can be programmed into the Rhinoceros/Grasshopper CAD environment to control the RFs' design parametrically. It was chosen to use this environment because of the following reasons:

- *Feasibility with NURBS surfaces:* Derived from flexible wood strips for drawing curves by hand, Rhino's NURBS engine enables to easily draw mathematically exact geometries;
- *Fast iteration:* Possible by means of generative algorithms in Rhino's visual programming environment Grasshopper (GH);
- *Open source Plug-in community:* Developers and researchers from all over the world create new and often free GH applications.

With GH, the center to center method can be easily programmed by using its geometrical rules. First, by scaling a polygon towards its center point a smaller duplicate is created. Second, the midpoints at each side of the basic and scaled polygon must be determined. Third, the polygon midpoints relate to the midpoint of the neighboring side of the scaled polygon and can be jointed with a linear line towards its vector intersection point. Single-unit RFs with eccentric jointing can now be created by moving these intersection points over a polygons normal or z-vector (Figure 3.2). Figure 3.1 shows the visualization of this proces to create a single-unit concentric RF in GH.

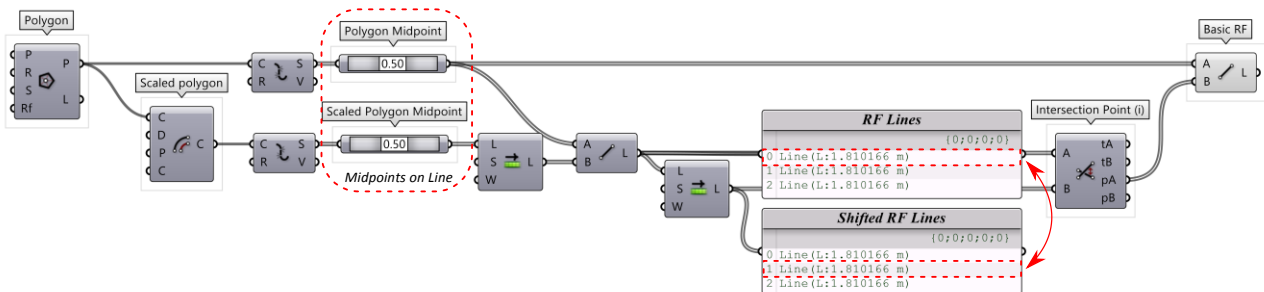


Figure 3.1 Basic GH components needed to create a single-unit concentric RF. The data requires shifting (method in red) to create an RF and to find the intersection points between adjacent lines

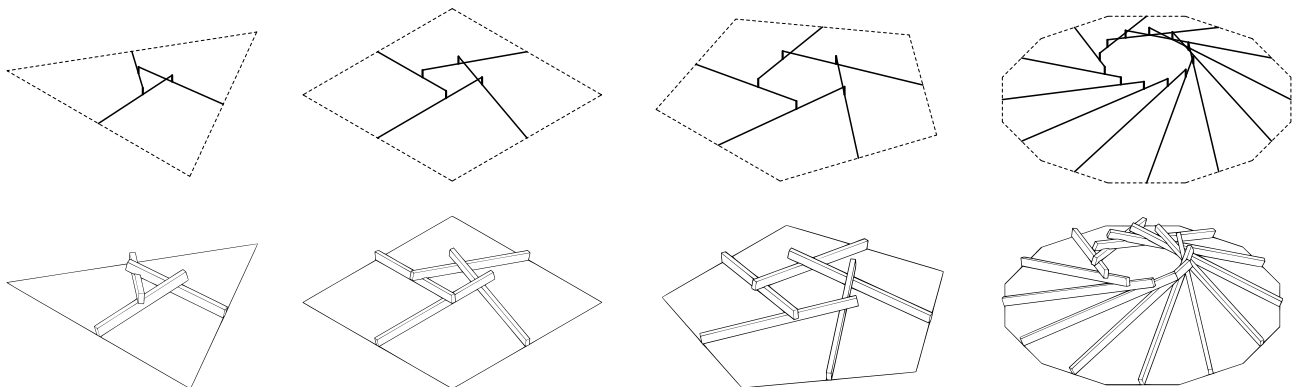


Figure 3.2: By increasing the number of polygon edges and by moving the intersection points over the polygons' vertical axis or plane normal vector eccentric single-unit RFs are created. The beam height is determined by the scaling factor and point height



3.2 HOW TO DESIGN AN EXACT RF - MODEL 2

The method on how to create a single-unit eccentric RF that is described above can be used as basis in the creation of a multi-unit RF. This chapter examines the required geometrical transformations and its limitations when employing the method to an exact determination of a multi-unit RF. Among the bottom-up and top-down approach, this is one of three possible RF form finding approaches. The tool was developed to explore freedom of form by using solely geometrical translations.

3.2.1 ORIGAMI

As a single unit RF is created by moving the intersection points, found at the center to center method over the plane vertical axis, the required transformation to model possible neighboring RFs can be determined. This method is in a way comparable to origami since it depends on geometrical folding or translations.

First, consider a single unit triangular RF. The input parameters that determine its shape are the total height, scale factor and polygon dimension. These

parameters determine the total and final span of the complete multi-unit RF. With this shape, the angle α_2 can be determined that is used to determine the first rotation angle that is (Figure 3.3):

$$\alpha_{transform} = \alpha_2 + 180^\circ \quad (3.1)$$

Second, by applying this angle to copy and rotate the basic triangular single-unit RF, a four-unit RF is created. Third, the same angle is used for the second rotation creating a ten-unit RF. This is the maximum number of rotations to be able to create a connecting RF. Further transformations result in deviating triangular shapes that cannot be dissolved by changing the parameters.

One of these deviating triangles can be seen below appointed as *dt* in the lowest section. These three triangles are dissolvable by changing the input parameters height and/or scale factor. When changing these towards each other, a platonic solid icosahedron partly is created. Thus, this is the only complete multi-unit design that can be created with this method.

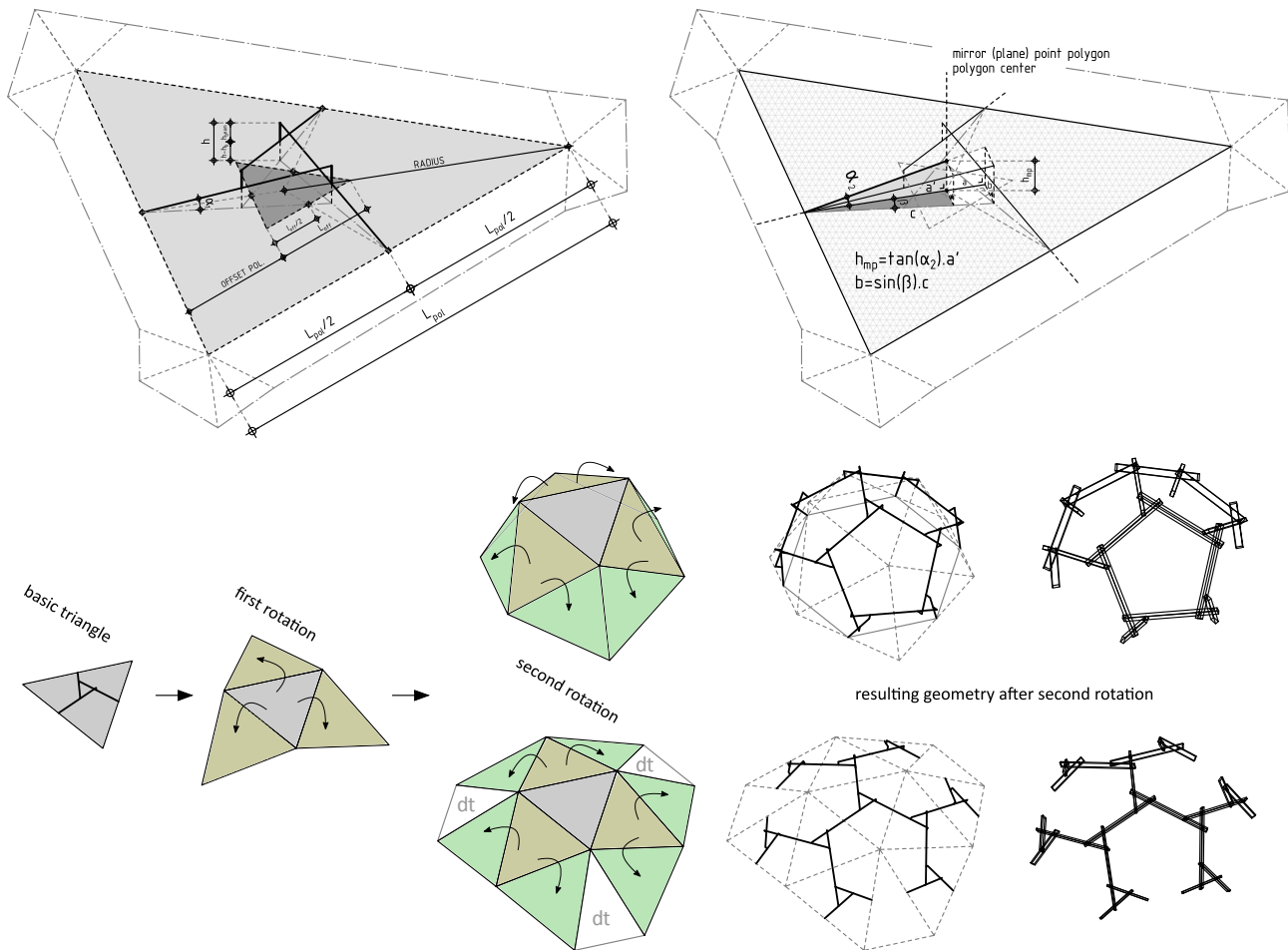


Figure 3.3: Design procedure of an exact mathematical determination of an RF

3.2.2 LIMITATIONS

In addition to the limited design freedom, the analytic transformation method cannot be applied to other polygonal shapes. When using other basic polygonal shapes, the polygon edges do not connect. Consequently, and just as described in chapter one, the possibility to take preliminary design requirements, such as span dimensions, is limited with this exact approach.

A genetic algorithm can be implemented to try to reach a span by changing the scale factor and polygon dimensions towards a preferable parameter. This increases computational complexity and disables the possibility to directly control parameters. Therefore, the Reciprocal Frame Designer (RFD) has been developed.

3.3 HOW TO DESIGN A WIDE VARIETY OF RFs - MODEL 3

The RFD is an RF form finding tool developed to design three- and four-member RF assemblies from any arbitrary NURBS surface. It has been completely designed within the Rhinoceros/Grasshopper environment and is based on a top-down approach. It was decided that this is the best suited form finding approach for this research because it has been assumed that in practice, designers would create a certain design where after it should be suited for an RF structure.

The RFD uses several geometric optimization strategies after the application of the center to center method to a with triangles or rectangles subdivided NURBS surface or mesh (Figure 3.4).

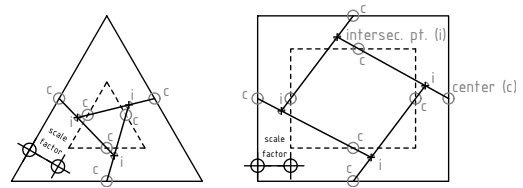


Figure 3.4: Center to center method

3.3.1 CREATING A BASIC RF GEOMETRY

Surfaces can be subdivided in UV-direction by using parametric curvature or equal point distance where after geometric rules must be applied to create panels (Figure 3.6). Meshes often consist already of triangular or quadrangular panels but may require equalization or smoothing before application in the RFD (Figure 3.5).

SURFACE SUBDIVISIONS AND MESHES

Triangular meshes are always planar whereas quadrangular meshes are not always planar. This does not matter for the scaling method since it depends on surface scaling from their area centers where after the edge midpoints at (scaled) surfaces are determined. A subdivision conversion is only possible by using untrimmed surfaces. Trimmed surfaces do not allow preserving surface boundaries. Untrimmed surfaces need to be created using primitives as extrusions, sweeps and revolving surfaces. Meshes however, can be used to create more complex shapes and can be prepared for use in the RFD by means of 'inflating' a planar mesh with Kangaroo's particle spring system^[19].

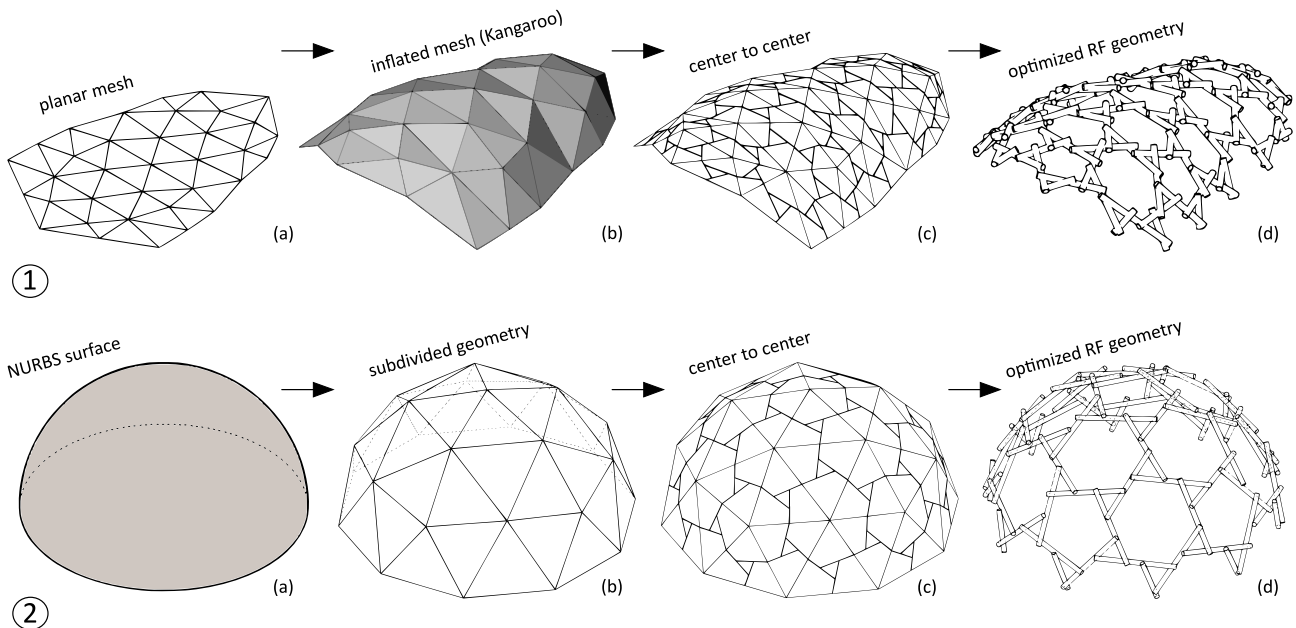


Figure 3.5: Two methods on how to design an RF with step (b) to (d) being the same for both methods. Method 1 starts with inflating a mesh. Method 2 start with an NURBS surface that is subdivided by means of geodesic polyhedron

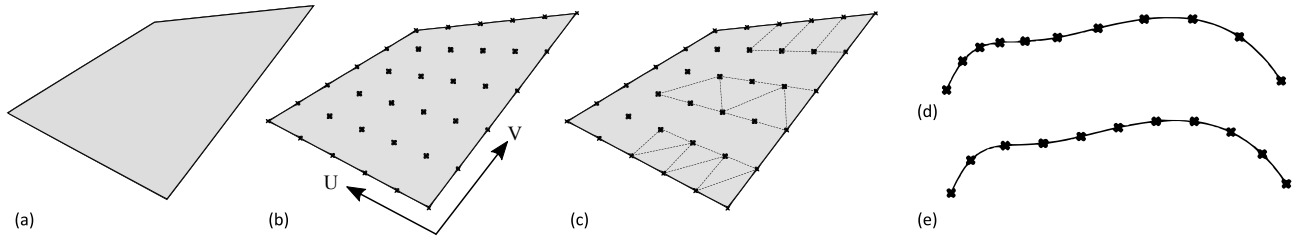


Figure 3.6: NURBS surface (a) subdivided in UV direction by points (b) by means of parametric curvature (d) or equal point distance (e) where after these can be panelized (c) by geometrical rules

APPLYING THE CENTER TO CENTER METHOD

By using the center to center method, the number of members in an RF unit depend on the number of surface or mesh edges. Triangles create three-member RFs and rectangles create four-member RFs. At all common surface edges, RF members naturally meet each other because the starting point of an RF line lies at the center of a surface edge. In this situation, eccentricities between the elements are not yet created since each RF unit is still considered as planar single-unit. This is changed by joining two individual members -in this respect considered as lines- with communal starting points, into a single polyline (Figure 3.7). Hereafter, the end points of this polyline can be used to create a new linear line that is defined by endpoint A and B (line A-B). This method has also been earlier described by Anastas *et al.*^[9] but is not enough to create a basic RF geometry for any arbitrary NURBS surface. Figure 3.7 shows the geometric RF transformation applied to a subdivided single curved surface. It shows that a 'kinked' polyline is only created when the neighboring surfaces are noncoplanar.

Consequently, additional measurements are taken to be able to create eccentricity by means of geometric transformations.

First, the new lines that are created between all end points of polylines are moved towards the initial RF starting points at the polygon centers. This is the 'kink' in the polyline. The transformation is thus determined by evaluating the mean length of the two-line parts L_s that exist between intersecting RF lines.

Hereafter, the eccentricity e_g is determined by the average lengths and angles of both triangles according to:

$$e_g = \frac{L_{s,mean} \sin(\alpha_{mean})}{2} \quad (3.2)$$

Second, lines that lie between coplanar planes and are thus already linear, are moved over a distance smaller than two times the length of e_g creating a basic RF geometry with eccentric jointing.

$$e_{g,2} < e_g \rightarrow e_{g,2} = e_g / 2 \quad (3.3)$$

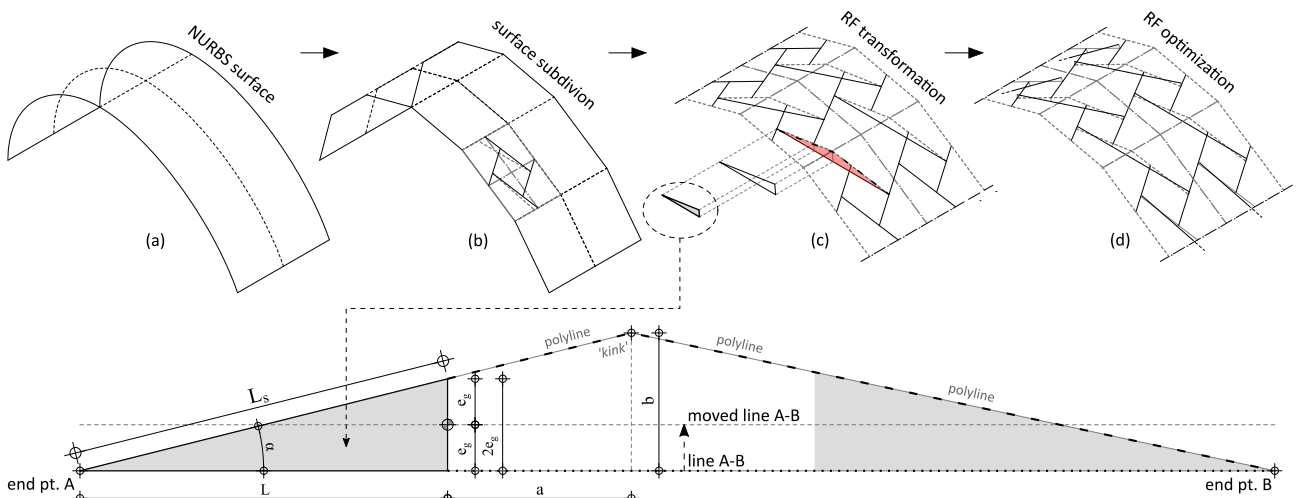


Figure 3.7: Basic geometrical design procedure that has been applied in the RFD

3.3.2 ECCENTRICITY OPTIMIZATION

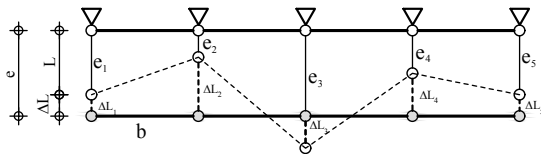
Despite the geometric optimization procedure described above, eccentricities between members depend on the basic geometry and surface subdivision (Figure 3.9). This is not preferable in structural design since all members then should have different sizes, connections should be able to cover a variety of slack, or the mechanical force distribution would be dependent on the initial geometric shape.

Therefore, an optimization method is developed that enables manual eccentricity control. With this method, each individual line is optimized towards the preferred eccentricity length by applying initial strain loads to the eccentricity lines according to Hooke's law:

$$\varepsilon_i = \frac{\Delta L}{L} = \frac{e - L}{L} = \frac{e - e_g}{e_g} \quad (3.4)$$

Here, the strain load ε_i is determined by the preferable eccentricity length e , and initial eccentricity length ($L = e_g = e_i$). For each individual eccentricity line, an individual stain is then determined to increase, reduce, or maintain its length depending on length e_g . Fictional beam stiffnesses are applied to be able to maintain the basic RFs member configuration.

Figure 3.8 shows the optimization procedure applied to a simplified problem. Different eccentricity lines with length e_i are optimized towards length e by reducing the length of member b . By modeling all members (b) as 'infinitely' stiff to shear and bending and 'infinitely' weak to axial stresses and shear, length e can be changed. Eccentricity lines are modeled 'infinitely' stiff to all directions with torsional resistance as exception to be able to maintain the member configuration. Consequently, fictional beam stiffnesses must be applied.



FICTIONAL BEAM STIFFNESSES AND FE

The following mechanical properties for deformation optimization analysis apply to the eccentricities:

$$\begin{aligned} I_{pp} &= 1 \quad cm^4 \\ C_w &= 1 \quad cm^6 \\ A, A_y, A_z &= 1.10^{13} \quad cm^2 \approx \infty \\ I_y, I_z &= 1.10^{13} \quad cm^4 \approx \infty \end{aligned}$$

The following mechanical properties for deformation optimization analysis apply to the members:

$$\begin{aligned} A &= 1 \quad mm^2 \\ I_{pp} &= 1 \quad cm^4 \\ C_w &= 1 \quad cm^6 \\ A_y, A_z &= 1.10^{13} \quad cm^2 \approx \infty \\ I_y, I_z &= 1.10^{13} \quad cm^4 \approx \infty \end{aligned}$$

In which:

$$\begin{aligned} A, A_y, A_z &= \text{Equivalent (shear) area} \\ I_{pp} &= \text{Tors. moment of inertia (St. Venant)} \\ C_w &= \text{Warping tors. constant} \\ I_y, I_z &= \text{Moment of inertia} \end{aligned}$$

To allow FE analysis, RF lines are divided at each intersection where they are rigidly connected in all directions. At all polygon midpoints, near the edges of the design, hinged supports are created. Hence, the structure can be optimized. The optimization procedure is applied in the RFD by using Karamba's FE solver^[20] that allows geometrical nonlinear deformation analysis but, can also be applied within other FE software capable to coop with this. Geometric nonlinear analysis updates the RFs' equilibrium equations in the deformed state.

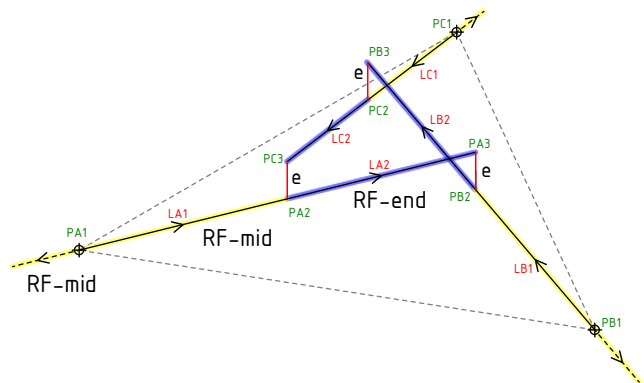


Figure 3.8: Explanatory scheme for eccentricity optimization method (left), line structure applied in the optimization process. All lines are divided and rigidly connected at all intersections

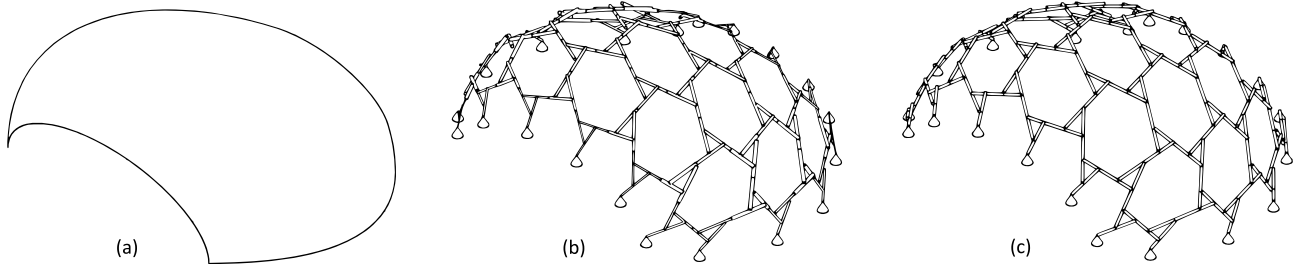


Figure 3.9: The RF based on a NURBS surface (a) with mean eccentricities per unit that depend on surface curvature (b) and optimized eccentricities by means of the strain method (c) that is visualized by member diameter

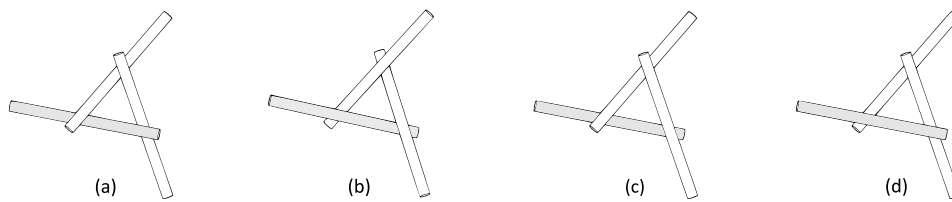


Figure 3.10: Four possible three-member unit styles. Unit style (a) is the result when using a dome subdivided by means of a geodesic polyhedron as basic geometry in the RFD

Karamba's incremental method creates a solution that approximates geometric non-linearity and results in an unavoidable drift that should be considered during the form finding process. It means that when the optimization process is repeated using the same parameters, none of the solutions are exactly the same. By internalizing data, one can store the preferred geometry which makes the algorithm deterministic.

3.3.3 REDRAWING THE OPTIMIZED GEOMETRY

The optimization procedure has no influence on the configuration of structural members and unit style that depends on the geometry of the basic surface. A geodesic polyhedron for example, results in unit-style and member configuration a (Figure 3.10). The initial surface shape can be approached by choosing a new value for e that is close to the mean length of e_g .

Although the members are modeled as 'infinitely' stiff in bending, the optimization of line e requires redrawing the RF geometry. Hence, member straightness and perpendicularity of eccentricities can be guaranteed. The traveling salesmen problem is introduced to reorganize all geometrical data, required for redrawing,

TRAVELING SALESMEN PROBLEM

The redrawing process of the geometry is possible by means of solving the traveling salesmen problem. As described above, the resulting geometry after optimization is not directly usable for further use since members are not completely straight and eccentricities not lie exactly perpendicular to them.

The redrawing process is started by reorganizing the data between members and eccentricities. To make this possible, all lines are joined into polylines based on their vector direction in space. All polylines can now be redrawn by connecting their two extreme points with a new linear line. However, to be able to redraw the eccentricities, the data need further reorganization.

The eccentricity lines are determined through a mathematical determination of the lines' neighboring linear equations. This requires sorting the lines such that they are consecutive neighbors (A, B, C, D, etc.). When considering triangles, the number of possible combinations to create this consecutive order is one: the consecutive order is always maintained. However, when considering rectangles, the number of sorting options, the routes, is three resulting in the problem that a consecutive order is more difficult to create.

The problem of having multiple routes to create order is called the traveling salesmen problem. In computer science and mathematics, the traveling salesmen problem shows that the number of possible routes increases with a factor $(n-1)/2$ when increasing the polygon sides: n is the number of polygon sides. Therefore, an unambiguous algorithm is created.

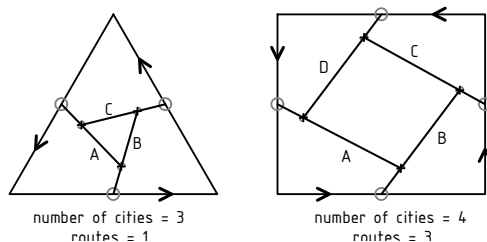


Figure 3.11: Traveling salesmen problem

The traveling salesmen problem is solved when the shortest route between 'cities' has been found^[21]. In order to find this solution for an RF, one can establish an iterative algorithm. However, the developed algorithm in the RFD sorts the line by means of the direction of polygon edges of a nearby geometry. This results in a fast and unambiguous solution enabling distinction of members from eccentricities.

First, by means of Delaunay triangulation, a panel geometry is drawn within the optimized geometry. The panel geometry is drawn by using the midpoints, PA1-PC1 of each member (Figure 3.8). Four-member units use midpoints PA1-PD1 and require additional joining of these two triangles into a rectangle. Second, the closest panels that to line parts LA2-LC2 are sorted per unit. Third, the geometry and eccentricities can be redrawn by using the polygon edge direction (\rightarrow) of the sorted triangles or rectangles (Figure 3.11).

The resulting RF geometry is completely linear and has perpendicular eccentricity lines where eccentricity lengths are optimized with millimeter precision. Increasing the precision is possible by implementing a loop. However, this seemed to be unnecessary: in practice, a higher precision does not produce major differences on a global scale of meters. Furthermore, a loop increases computational complexity.

ROOFING

The panel geometry used for redrawing the RFs' geometry indicates that it can, if supplemented with other covering panels, be used for something else. Undoubtedly, the RF needs covering in a practical application.

Thus, a similar geometrical procedure is used to simulate roofing. To cover the holes within the panels, curves within these gaps are able to create a pentagonal or hexagonal curve network. Within this curve, an average midpoint can be found: the start points of the green lines. With these points a new panel geometry can be created (Figure 3.13). The four-member RFs need a further triangulation to close the panel geometry. Panels can be used for grid load application which is discussed in the next chapter.

3.4 CONCLUSION

This chapter described the form finding procedure for single- and multi-unit RFs. Whereas a single-unit RF can be easily created by moving the intersection points, a multi-unit RF requires a more advanced algorithm. To create a ten-unit RF, one can use an exact approximation of the geometrical shape using geometric equations. The resulting design however, is limited to ten-units. The RFD has been developed to overcome this problem and is suitable to design three- and four-unit RFs.

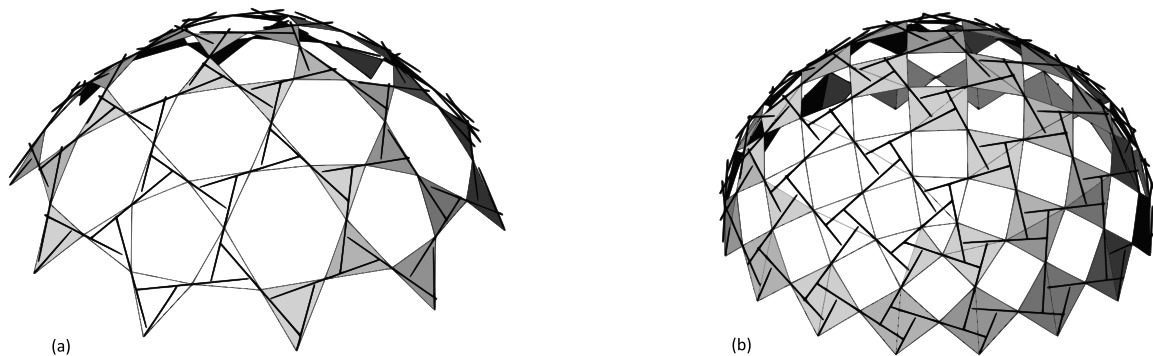


Figure 3.12: Sorting geometry to rebuild RF geometry for a three- (a) and four-member (b) RF

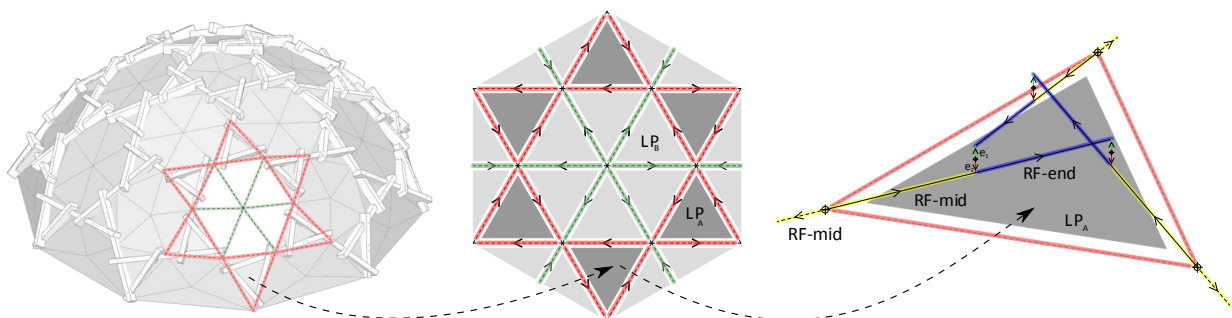


Figure 3.13: The sorting geometry in red with in green the additional geometry to create a closed structure and simulate load panels to be used for grid load application to simulate roofing



The described theory could cover the design of reciprocals; however, the structural timber and reciprocal behavior has not yet been thoroughly discussed. Therefore, the next chapter purely focusses on the structural system of RFs with respect to timber engineering by evaluating theory and practical examples.

The acquired knowledge is then used in the design of a reciprocal timber connection to be implemented in the RFD. This page shows an RF design variety that already can be created by means of the RFD with circular members and not regarding connections. Furthermore, a schematic explanation of the RFD is added including the order of theoretical steps discussed in this chapter.

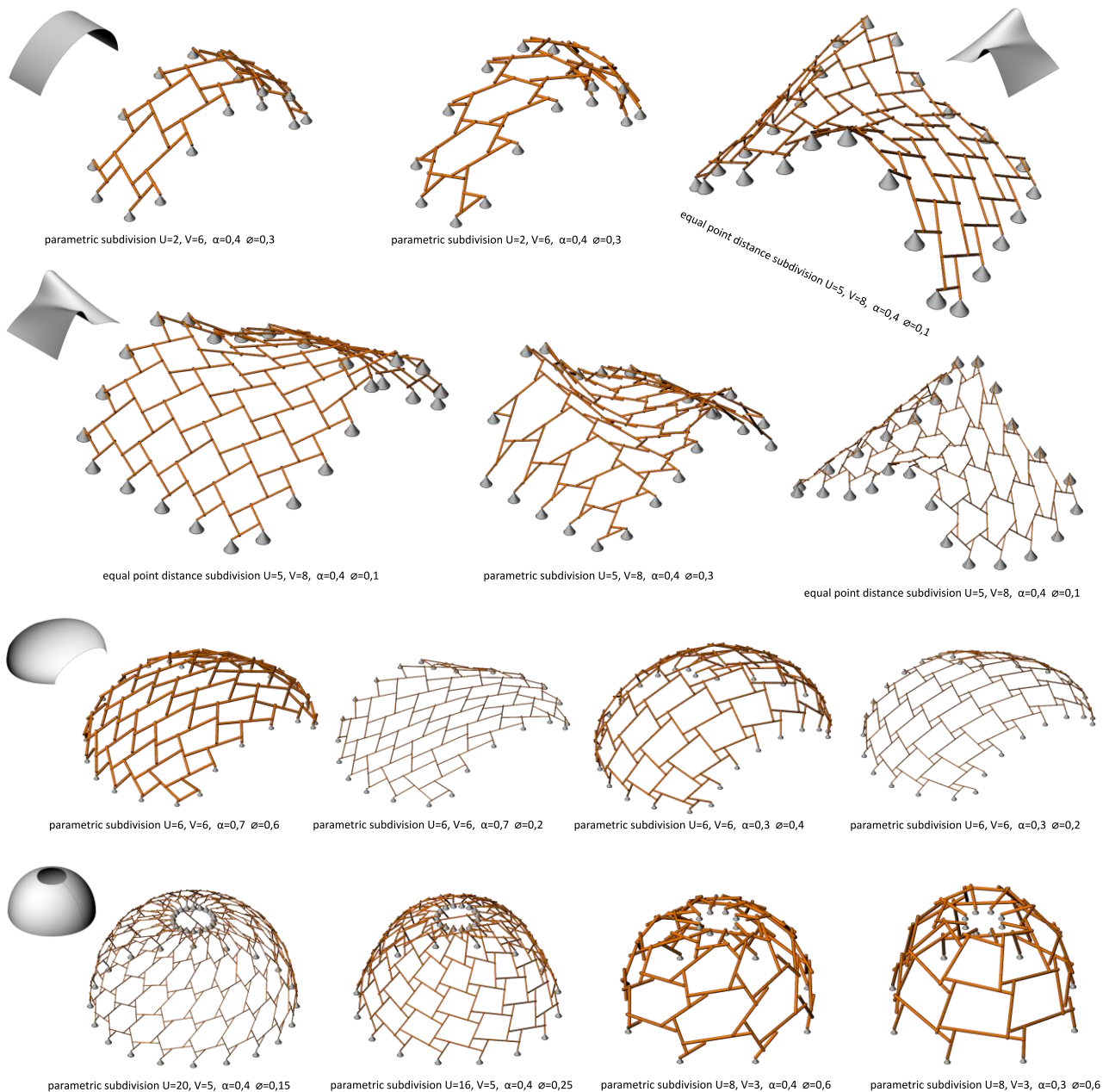


Figure 3.14: RF designs based on standard untrimmed NURBS surfaces subdivided by means of parametric curvature or equal point distance. The number of subdivisions (U,V), scale factor (α), diameter (ϕ), and basic surface are displayed next to the design



3.4.1 SCHEMATIC OVERVIEW OF THE RFD

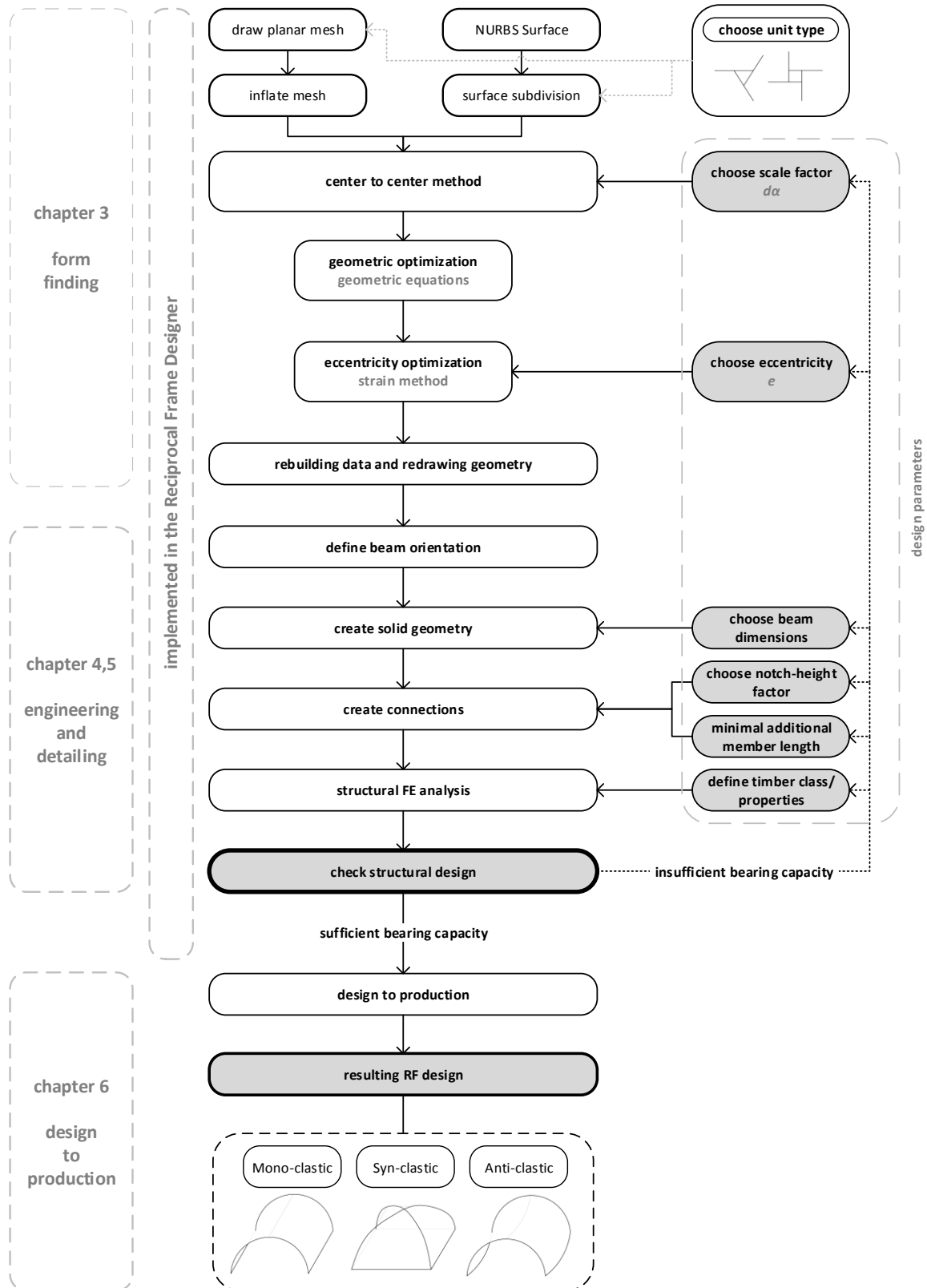
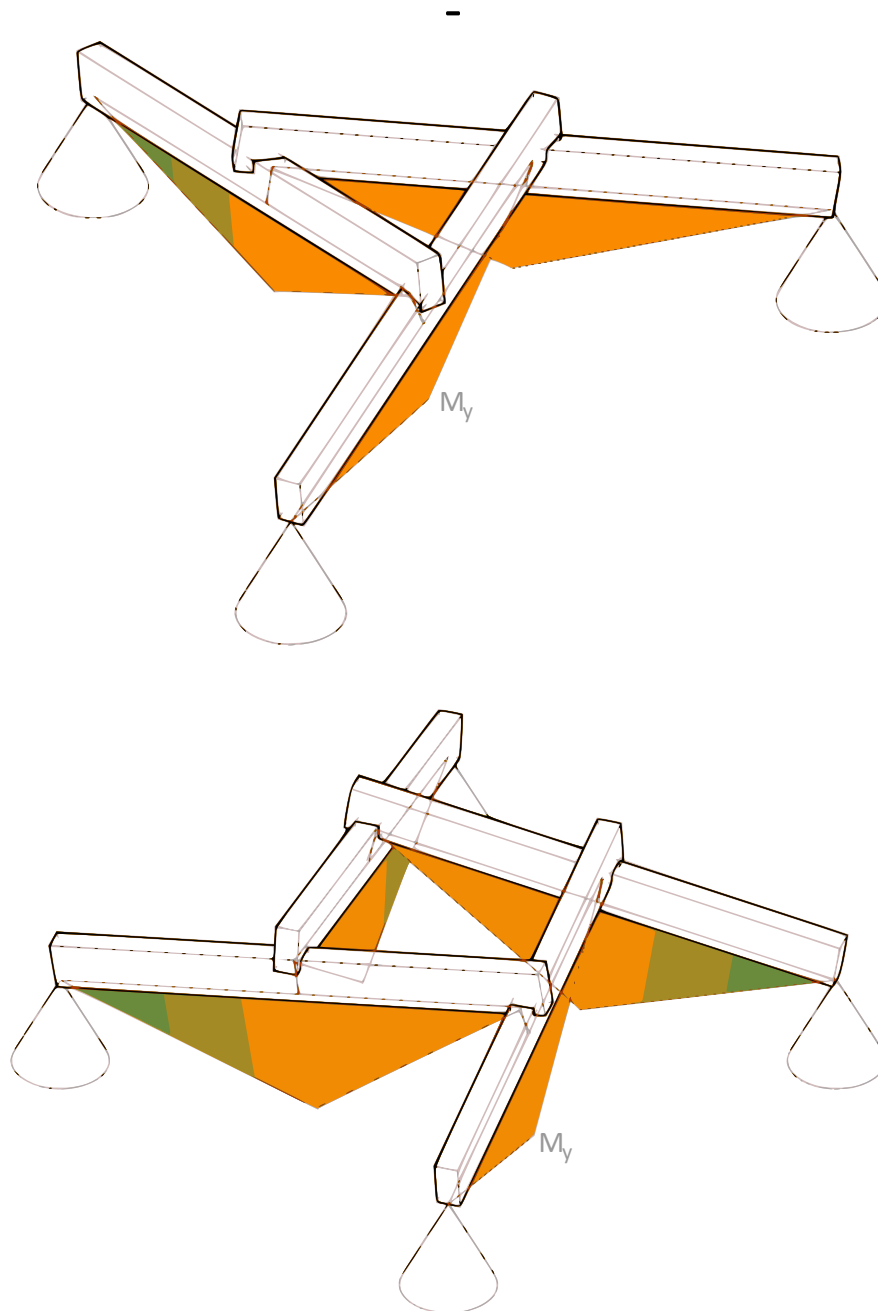


Figure 3.15: Flow diagram of the RFD and its theoretical explanation divided per chapter

TIMBER AND STRUCTURAL BEHAVIOR

This chapter evaluates the structural system of RFs with respect to timber engineering by evaluating theory and practical examples. The acquired knowledge is used in the design of a reciprocal timber connection.



4 STRUCTURAL BEHAVIOR

The structural system of a Reciprocal Frame (RF) has a clear identity and can be placed in the family of section active space, or beam grid structures. However, in regular types of space structures, forces are mainly being transferred by normal forces and all members meet each other at their extremities. This is in contrast with RF structures where:

- The members do not meet at their extremities but at intermediate supports;
- Forces are primarily or partly transferred by shear and bending.

These characteristics result in circumstances where an intuitive understanding of the load path cannot always be immediately established. This chapter therefore defines the structural system by means of hierarchy, mechanical schematization, and other properties to be able to define a structural design.

4.1.1 BASIC PRINCIPLES

To create a force equilibrium in an RF, the minimum number of elements in an RF unit is three. This force equilibrium is depending on the unit style as described in chapter 2.3 and is demonstrated below.

In one-unit and concentric RF systems, e.g. a planar system, the resultant force F - that is identical to the vertical support reaction at point B - can be determined by considering a stationary equilibrium (Figure 4.1). Suppose that an equally distributed vertical load q is acting on each, simply supported, individual element with length l . The vertical reaction at the outer support location A, can now be determined by dividing the total load by the number of elements. Consequently, the vertical reaction at the outer supports (A_v) must be equal to the total load ql_{total} resulting in $A_v = ql$.

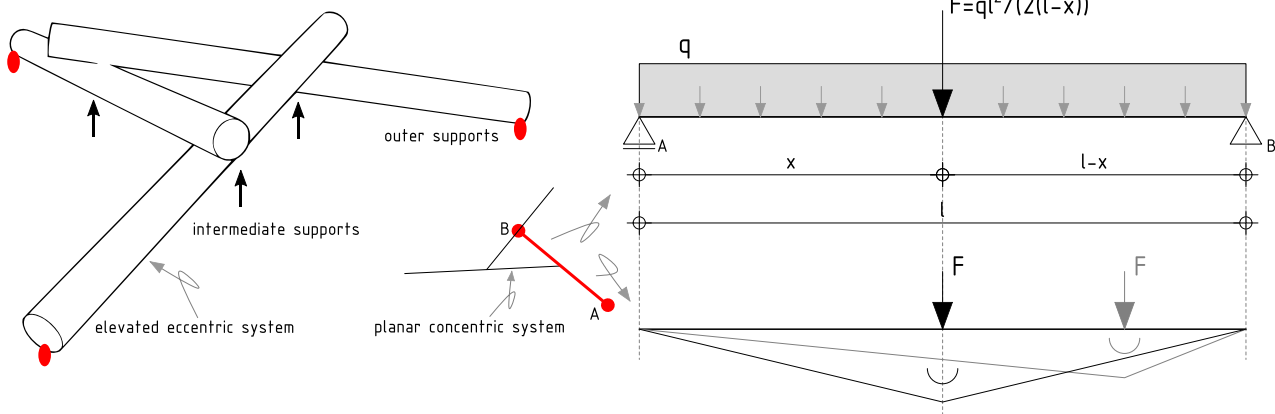


Figure 4.1: Structural principle for an 3RF system with eccentric jointing (left) and the mechanical schematization for an element in a concentric 3RF system (right)

The force that is acting on the beam can now be determined by first taking the moment equilibrium at A:

$$\begin{aligned} \sum M_A = 0; & \quad -Fx + B_v l - \frac{1}{2}ql^2 = 0 \\ \rightarrow & \quad B_v = \frac{Fx}{L} + \frac{1}{2}ql \end{aligned}$$

The vertical equilibrium:

$$\begin{aligned} \sum F_v = 0; & \quad -F + B_v - ql + A_v = 0 \\ \rightarrow & \quad A_v = F - B_v + ql \end{aligned}$$

Substituting B_v :

$$\begin{aligned} \text{subs.} \quad B_v &= \frac{Fx}{L} + \frac{1}{2}ql \\ \rightarrow \quad A_v &= F - \left(\frac{Fx}{L} + \frac{1}{2}ql \right) + ql \\ A_v &= F - \frac{Fx}{L} + \frac{1}{2}ql \\ A_v &= F \left(1 - \frac{x}{L} \right) + \frac{1}{2}ql \end{aligned}$$

Equilibrium and symmetry result in $A_v = ql$:

$$\begin{aligned} A_v = ql \quad \rightarrow \quad ql &= F \left(1 - \frac{x}{L} \right) + \frac{1}{2}ql \\ \frac{1}{2}ql &= F \left(1 - \frac{x}{L} \right) \\ F &= \frac{ql}{2 \left(1 - \frac{x}{l} \right)} \end{aligned}$$

This results in the force F and support reaction B_v :

$$-B_v = F = \frac{ql^2}{2(l-x)} \quad (4.1)$$

This formula is applicable to determine force distributions for all single unit and concentric RF systems with equal member length.



4.2 MECHANICAL SCHEMATIZATION

The mechanical schematization of the system described above is clear. A simply supported beam that is statically determined can easily be calculated by hand following mechanical equilibrium.

However, when calculating larger eccentric RF structures with multiple units, it becomes inevitable to use Finite Element Method (FEM) software to determine the force distribution because of an RFs' statically indeterminacy^[22]. This requires an unambiguous and clear schematization.

The force distribution in the three-beam eccentric RF system (Figure 4.1) is naturally in equilibrium when only self-weight is acting as loading (Figure 4.1). Here, a structural equilibrium is established utilizing friction and contact pressure between the elements without the need to apply additional connectors. Friction could be enhanced by using for instance the bark of three trunks.

When using concentric connections or when adding loads, additional measurements need to be taken. Notching or the use of steel fasteners can be implemented based on the mechanical schematization.

4.2.1 SCHEMATIZATION RELATION TO TIMBER

The mechanical schematization of a structure is coherent to the connection design or detailing. Structural detailing is the analyzation of all possible forces through a connection to facilitate force distribution^[23]. With regards to this research, that is focusing on timber RFs, bending resistant connections could require the use of many steel fasteners and could lead to large timber dimensions.

In general, it is physically impossible to create infinite bending stiff connections in timber but, glued (finger) joint or prestressed dowel connections can approximate infinite bending stiffness and can transfer moments. In other cases, the connection will always behave as a spring with certain stiffness that is independent from the overall beam stiffness. Its mechanical schematization is a combination between a hinge and infinite bending stiff connection. The stiffness magnitude of this bending stiff or so-called moment connection must be calculated correspondingly.

In timber connections, the most efficient way of transferring forces is by means of contact pressure^[23]. Contact pressure can be activated by utilizing the natural force equilibrium and friction between the members in RF structures. The mechanical schematization of the connection is then simply supported and the eccentricity between the elements must be as large as the beam's diameter (Figure 2.7).

When comparing a simply supported connection with a moment connection in timber, the following can be concluded^[23]:

- Moment connections require relatively more material with respect to axial and shear force connections;
- Introducing bending moments at connections will reduce intermediate moments;
- Force transferring by means of contact pressure is more efficient than by means of bending moments;
- A moment connection could contribute to the overall stability of a structure.

As discussed before, the number of connections in RF structures is relatively large compared to regular structures. Introducing bending moments at the connections correspondingly results in a large number of complicated connections and a large amount of materials in comparison to simply supported structures. Therefore, the connections will be mechanically schematized as simple as possible while ensuring local and overall stability. In other words, it is preferable to schematize a connection as simply supported if local and global stability will be guaranteed.

CONNECTION SPECIFICATION CONCENTRIC RFs

Figure 4.2 shows the beam releases that apply for concentric RF systems ($T = \leftrightarrow$ and $R = \nlessgtr$).

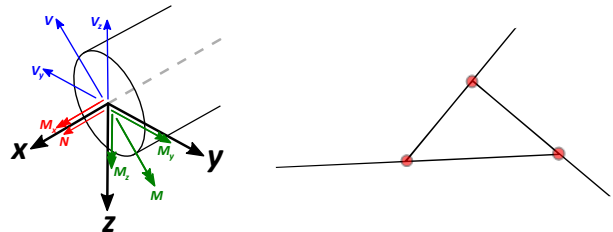


Figure 4.2: Mechanical schematization concentric RFs

● = Fixed: T_x, T_y, T_z, R_x, R_z . Free: R_y

CONNECTION SPECIFICATION ECCENTRIC RFs

Figure 4.3 shows the beam releases that apply for eccentric RF systems ($T = \leftrightarrow$ and $R = \nlessgtr$).

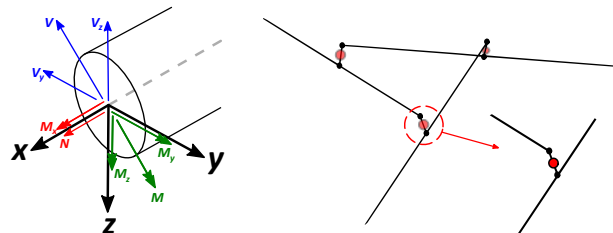


Figure 4.3: Mechanical Schematization eccentric RFs

● = Fixed in all directions

● = Fixed: T_x, T_y, T_z, R_x . Free: R_y, R_z



SUPPORT SPECIFICATION

Figure 4.4 shows the beam releases that apply to the supports of RF systems considered in this research ($T = \leftrightarrow$ and $R = \curvearrowright$).

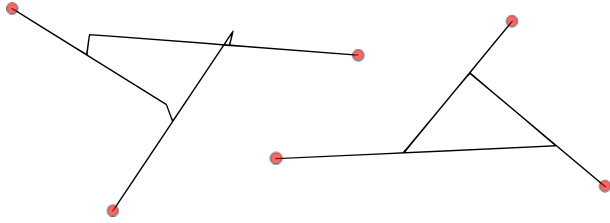


Figure 4.4: Mechanical Schematization Supports RFs

● = Fixed: T_x, T_y, T_z . Free: R_x, R_y, R_z

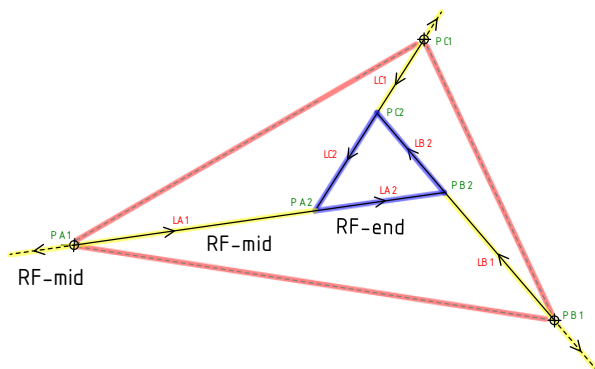
CLARIFICATION BOUNDARY CONDITIONS

In this research, supports are considered as hinges for the same reasons as for the connections. Normal forces for instance, that can occur in the members of eccentric systems, must be supported here resulting in a required horizontal restraint.

Beam releases and restraints -known as Boundary Conditions (BC's)- are defined at detailing level in their local axis systems. The BC's are a minimal required to guarantee a stable system and to ensure simply supported behavior. If one chooses to fix or restrain the connections in extra directions, bending or torsional moments need to be transferred. This BC modification could result in unpreferable force distributions throughout the structural design.

GEOMETRY

All BC's are defined to the beam end or starting points in their own local axis system. The local axis system is defining the beam orientation: its strong and weak axis. The global axis system is defining the structural design in Euclidian space by means of coordinates. These coordinates, to be referred to as points, are connected by lines that shape the RF.



A line always connects two different points. Lines are converted into beams to allow FEM calculation. In RFs, points are often both start- and end-point of different lines.

Consider for example the concentric system. Here, end-point PA2 of line LA1 and LC2 is the start-point of line LA2 (Figure 4.6). In the eccentric system, point PA2, is communal with the end-point of line LA1, e2, and the start-point of line LA2. The start- and end-point determine the line direction.

Line directions are unitized throughout each RF design by using an unambiguous hierarchy enabling unitized boundary condition assignation (Figure 4.5). This hierarchy slightly differs between con- and eccentric RFs.

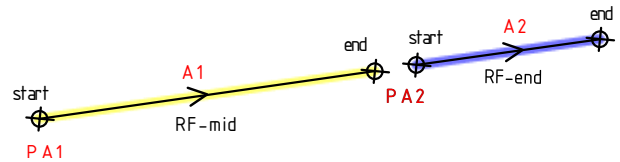


Figure 4.5: Line hierarchy and direction (>)

The BC's for the concentric system must be assigned to the end-points of lines RF-end (Figure 4.6). Free rotation of R_y will cause free rotation of R_z at adjacent members since this point connects three lines (Figure 4.2).

The BC's for the eccentric system must be assigned to the start-point of eccentricity line e1. Free rotation of R_x (torsion) and R_z (bending moment) will result in a simply supported beam consisting of at least a line RF-mid and RF-end.

Figure 4.5 indicates that a beam is created for a single-unit RF system by a line RF-mid and RF-end. The greater part of beams in multi-unit RF systems are created by two lines RF-mid and RF-end with supporting positions as exception. It is self-evident that this topology also applies to concentric systems.

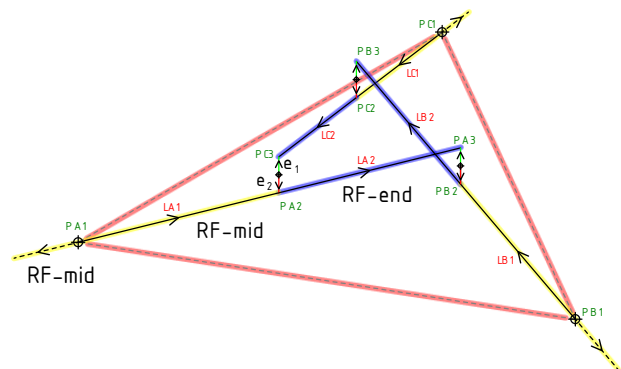


Figure 4.6: Line directions (>) concentric RF design (left) and Line directions (>) eccentric RF design (right)



4.2.2 LOADS

The structural line topology has a direct relation with load application and the consecutive load distribution to the structure. This chapter therefore explains on how to apply loads to RF structures, the schematization, to be able to analyze force distributions in RFs.

In linear static structural calculations, loadings such as point loads, line loads, and grid loads are distinguishable and can be applied in the direction of their local or global axis system. The choose of loading type depends on structural geometry and loading type. A grid loading for example, can ascend from flooring or roofing.

LOAD SINGLE-UNIT RF

An RF structure should ideally be covered with flooring or roofing to create a functional design which can be considered as secondary structure. Grid loads that are applied to a secondary structure should be transferred to the RF and will lead to varying line loads on the RF.

The schematization on how to determine these varying line loads is discussed below by considering a concentric and single-unit RF.

First, imagine an RF that is loaded by an equally distributed load over area A in vertical direction. Consider the RFs as simply supported at the edges.

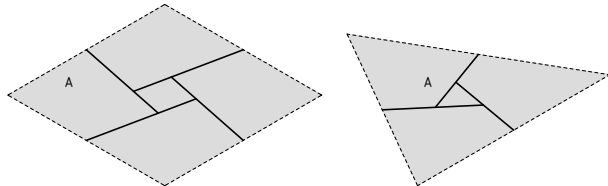


Figure 4.7: Single-unit RFs with area A

Second, one need to specify the loading area per individual beam. This area can be calculated by dividing the total loading area by the number of beams. Figure 4.8 specifies the actual and simplified loading areas that will naturally result in different line loads.

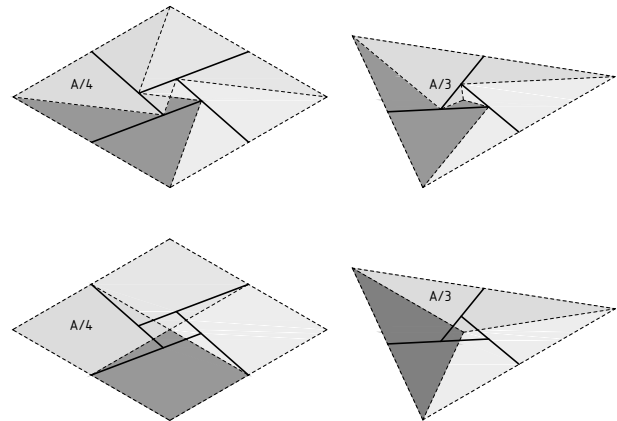


Figure 4.8: Actual area and simplified area per beam

The simplification of the loading areas per beam will result in different line loads (specified as q -loads in the figures). The actual line load is determined by using the actual loading area whereas the simplified q -load is most convenient to use in practice since it will probably lead to normative mechanical behavior.

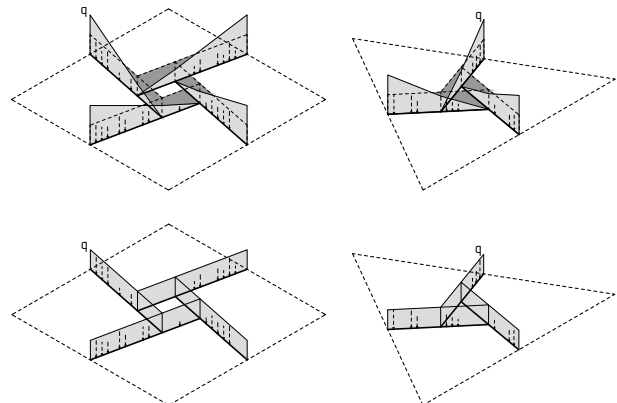


Figure 4.9: Actual q -load an simplified q -load per beam

The procedure to determine line loads for single-unit RFs differs from the determination of loads on a multi-unit RF. However, it shares the fact that it relies on the type of secondary structure.

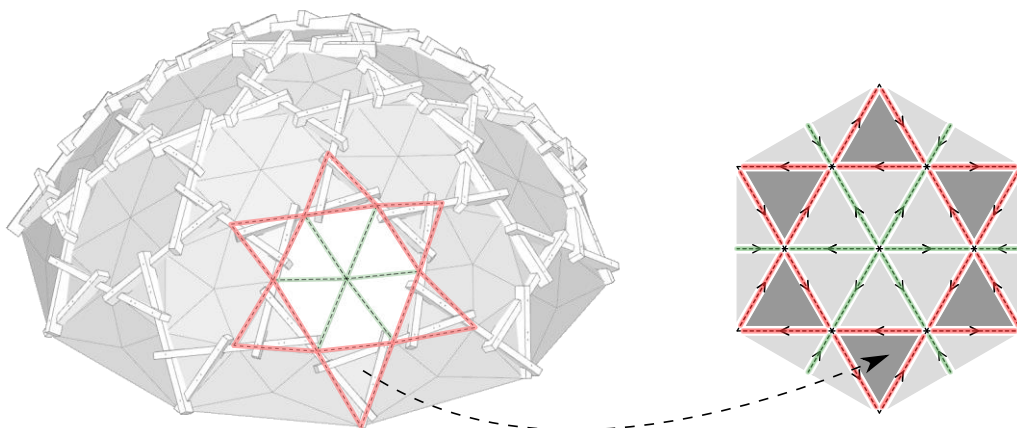


Figure 4.10: Load panels (in gray) for a multi-unit RF

LOAD MULTI-UNIT RF

The loading areas are described as load panels and could represent a secondary structure. The design of this structure can easily be determined for concentric RFs where the load panel shape can be multiplied for multi-unit RFs. The load panel design for multi-unit and eccentric RFs however, is not straightforward since every beam is oriented in a different manner.

The most convenient way of connecting beams in a multi-unit and eccentric RF with load panels is by means of triangles. A triangle has the unique property that its face is always planar which is essential in FEM software to be able to define its geometry and to apply loads. In addition, planar faces will result, in general, in a more feasible and cheaper secondary structure.

Figure 4.10 shows a solution on how to distribute triangular load panels over an eccentric multi-unit RF. The geometrical rules that are the basis for this design are thoroughly discussed in chapter 3 but, all triangles share the property that at least two of its points are connected to the start point of line part RF-mid (Figure 4.5).

This property, together with an evenly distributed panel pattern, ensures to schematize reality as well as possible. The schematization however will always be an abstraction of reality.

In FEM software, load panel edges need to be represented by beams to be able to transfer loads from the load panels to the RF. The load transferring beams should not strengthen the main RF structure since in general, a secondary structure will not strengthen the main structure and only has the function to bear itself. Furthermore, a secondary structure could start to structurally behave as a space structure which is not preferable.

Therefore, adapted BC's are added to the load transferring beams to ensure that the secondary structure will not strengthen and supports the main structure. All load transferring beams are consequently schematized as simply supported. Figure 4.11 shows that the RF structure is present within LP_A . The dashed green and red lines indicate the load transferring beams. Beams indicated in green are fully fixed at their start point because they here do not intersect with the RF.

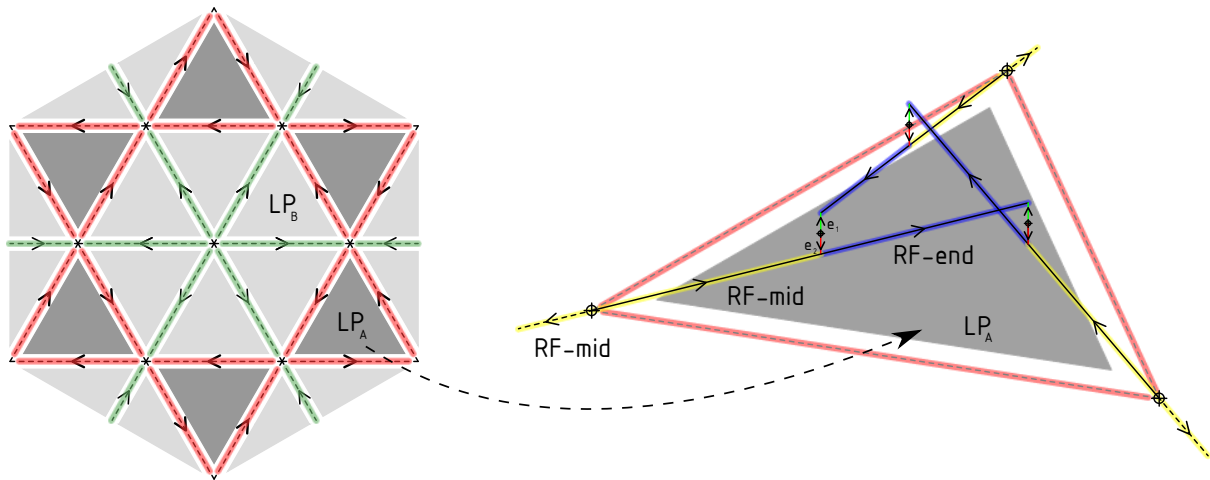


Figure 4.11: Load panel geometry with respect to the RF

| LP _A | Translation | | | Rotation | | |
|-----------------|-------------|------|------|----------|------|------|
| | x | y | z | xx | yy | zz |
| Start beam | Rel. | Fix. | Fix. | Rel. | Rel. | Rel. |
| End beam | Fix. | Fix. | Fix. | Fix. | Rel. | Rel. |

| LP _B | Translation | | | Rotation | | |
|-----------------|-------------|------|------|----------|------|------|
| | x | y | z | xx | yy | zz |
| Start beam | Fix. | Fix. | Fix. | Fix. | Fix. | Fix. |
| End Beam | Rel. | Fix. | Fix. | Rel. | Rel. | Rel. |

| e ₂ | Translation | | | Rotation | | |
|----------------|-------------|------|------|----------|------|------|
| | x | y | z | xx | yy | zz |
| Start beam | Fix. | Fix. | Fix. | Rel. | Fix. | Fix. |
| End beam | Fix. | Fix. | Fix. | Fix. | Fix. | Fix. |

| RF-mid, RF-end, e ₁ | Translation | | | Rotation | | |
|-----------------------------------|-------------|------|------|----------|------|------|
| | x | y | z | xx | yy | zz |
| Start beam | Fix. | Fix. | Fix. | Fix. | Fix. | Fix. |
| End Beam | Fix. | Fix. | Fix. | Fix. | Fix. | Fix. |

Table 4.1: Boundary conditions specified for each individual line segment

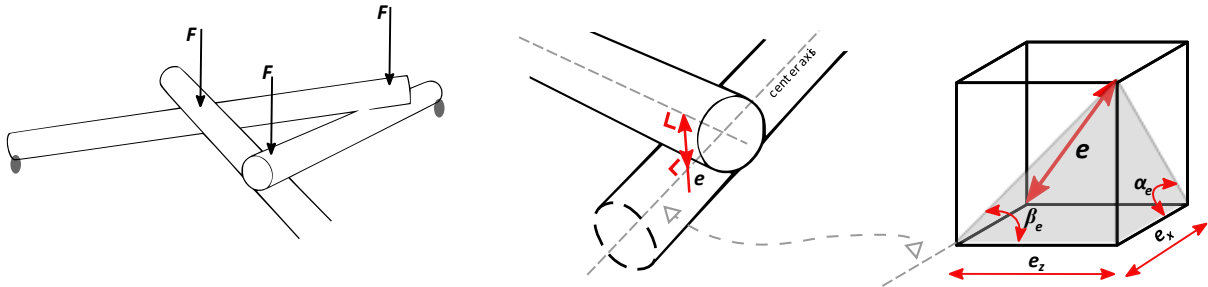


Figure 4.12: Load F applied at beam intersection, clarification of eccentricity e

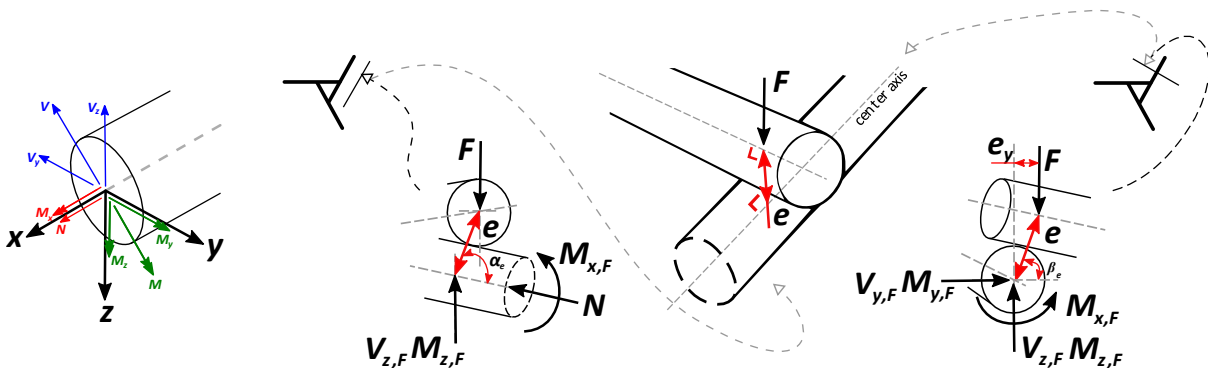


Figure 4.13: Influence of force F on internal force distribution

4.3 STRUCTURAL BEHAVIOR

The previously described BC's and load application methods allow the determination of mechanical behavior in an RF. This chapter discusses how applied loads can be transferred from the RF by internal forces to the supports, and what kind of influence geometry has on the interplay of forces.

4.3.1 GENERAL

An initiative understanding of the load path cannot always be immediately established but, can be determined for simple single-unit and concentric systems as explained before. This differs for multi-unit and eccentric systems but, a few things can be schematically clarified.

When comparing a three-unit RF with a four-unit RF, a tree-unit naturally provides stability to shear and bending when considering springs at the connections. A four-unit RF does not naturally provide stability to shear and bending resulting in a transformation from square to parallelogram (Figure 4.14).

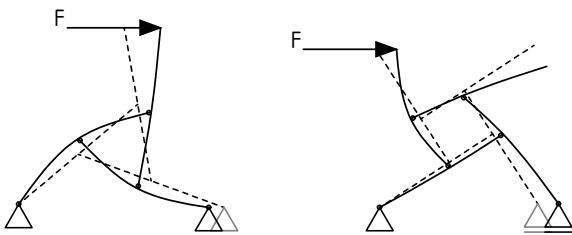


Figure 4.14: Comparison in deformation between RFs

It shows that a four-unit RF requires additional measurements to ensure a structurally stable design. Additionally, resultant forces need to be transferred by bending, shear and normal forces to be able to create an equilibrium (Figure 4.13). In general, this is unfavorable for lightweight structures where normal forces are preferred over bending moments.

This phenomenon can be minimized by shifting the engagement length between the elements, by introducing bending moments at the connections using steel connectors (not practical), or by changing the curvature of vaulted RFs.

Furthermore, the conceptual idea of implementing a shear, bending moment, and normal force ratio in a global geometrical form-finding optimization procedure can be established. Structural optimization per individual beam according to the internal force flow could minimize material consumption.

4.3.2 THE INFLUENCE OF ECCENTRICITY

With respect to concentric RFs, eccentricity between beams in an eccentric RF result in additional internal forces that are caused by line geometry and applied BC's. All eccentricity lines -that connect the beams in the mechanical model- are designed as the shortest line between the intersecting beams (Figure 4.12). In general, forces will naturally search for the shortest load path by which it is attempted to make this an assumption close to the actual structural behavior.

The geometrical rule of defining the eccentricity line (e) as the shortest between both beams' center axis vectors, ensures that line e is perpendicular to both intersecting beams. Thus, angle α_e is equal to 90° and distance e_x is equal to line length e (Figure 4.12). Although line e is perpendicular to both center axes of the RF beams, length e_z is unequal to length of line e . Correspondingly, angle β_e is unequal to 90° .

As if angle β_e is unequal to 90° , a lever arm between force F and the supporting internal force $V_{z,F}$ is created. This lever arm will cause extra internal forces in the supporting beam. The horizontal and vertical forces, - that lead to corresponding bending moments- can be expected. Torsional bending moments however, are not preferable in the mechanical calculation and do occur but, will in practice not evolve.

TORSION

The difference between a mechanical schematization and the actual situation leads in the bespoke situation to unpreferable torsional moments in the structure when performing a FEM calculation. Torsional moments cannot occur in practice when there is little movement (slack) in the connection in the direction of distance e_y (Figure 4.15). This research assumes that slack will be possible: deformation can barely be prevented in timber connections resulting in no torsion.

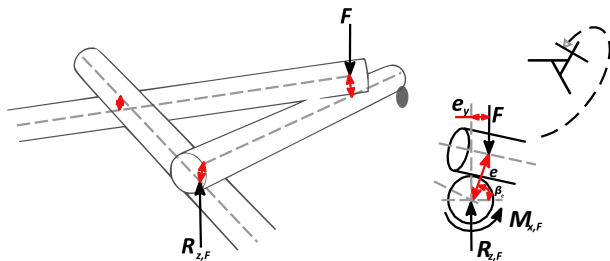


Figure 4.15: Formation of a torsional moment

To avoid that a torsional moment will affect the total force distribution in the system, one can choose to decrease the torsional moment resistance of the beams to for instance one percent of its capacity. This will result in a negligible torsional moment and a more like reality behaving force distribution throughout the structure when assuming possible slack (also see 4.4.2)

In short, lever e_y between action force F and reaction force $R_{z,F}$ will cause a torsional moment $M_{x,F}$ that can be decreased by reducing the beams' torsional resistance resulting in a more realistic force distribution.

4.3.3 REDUNDANCY

The force distribution in an RF is determined by its geometry and detailing. All individual beams transfer their internal forces to their neighboring beams or to the

supports trough connections. A collapse of one of the beams or connections -both to be referred to as parts in this context- will have a direct effect on the force distribution in an RF. Beams have to find alternative load paths when one part fails to be able to prevent general collapse. Alternative load paths correspondingly lead to a changed force distribution. The capability of a structure to redistribute forces is circumscribed by redundancy.

MECHANICS

Structures with big redundancy are able to redistribute forces through non-failed parts when one or others failed. In this research, a part is considered as failed when one or more have reached their Ultimate Limit State (ULS). When a structure has no redundancy, failure of one part will lead to general collapse which should always be prevented.

The applied connection design has a direct influence on redundancy. In RFs, failure of a beam part will result in bending moments at the connections that, when not resisted, will lead to a general collapse. By allowing bending in the connections, one can increase stiffness and, correspondingly increase redundancy.

TIMBER

When regarding redundancy in timber structures at material level, resistance against tension parallel to the grain is very high but, shows brittle behavior at failure. Brittle behavior can be avoided by choosing for instance larger beam dimensions (implemented in Eurocode 5 by volume factors), by reducing structural utilization, by adding reinforcing screws, or by using composite timber such as Cross Laminated Timber (CLT).

In comparison to tension parallel to the grain, tension resistance of timber perpendicular to grain is very low. They however share the fact that both show brittle failure when exceeding the allowable stress levels. The measurements described above to prevent brittle failure also applies to tension parallel to the grain.

The addition of screws or varying grain direction can add extra tension resistance in a direction perpendicular to the grain and will increase a beams' plasticity. Plasticity is naturally showed when loading timber in compression parallel to the grain by internal buckling behavior of the grains. This results in a relatively high allowable compression strength with respect to compression perpendicular to the grain.

The redundancy behavior of timber with respect to RF design is further briefly discussed in chapter 5. The subject of redundancy for RFs is explained in more detail by Garavaglia et al^[24].



4.4 THE INFLUENCE OF CHANGING PARAMETERS

The parameters that are described in chapter 2.3.5 determine the global form of an RF and influence correspondingly the structural behavior. In addition to this, chapter 4.3.1 showed what kind of influence the beam configuration has on stability when considering concentric and single-unit RFs. This chapter purely focusses on the differences between three- and four-unit RFs by evaluating the total structural design.

4.4.1 COMPARISON 3RF AND 4RF

The evaluation between a three- and four-beam RF assembly is started by evaluating a rectangular floor or roof span of twenty by twenty meter. This span is covered by both concentric RF systems and shares the same geometric assumptions and loading. The beam length and loading area per unit, indicated in blue, for example is the same (Table 4.2). An elaboration of the structural calculation can be found in annex 1.

The difference in configuration causes that the four-unit system uses a larger number of beams and connections in comparison to the three-unit RF resulting in a larger total beam length. The length however, results in a lower beam load reducing required beam dimension.

Although the total beam length of the four-unit system is larger, the calculations not explicitly show smaller required beam depths when looking at the timber volume that show a 9,6 percent difference. In addition to this has been showed that four-unit RFs not naturally provide stability. Furthermore, more connections results in larger production time, materials thus cost, and often cause a large part of the total displacement.

Despite that the calculations where conducted for one design and load, it can be suggested that three-unit RFs are structurally more efficient with respect to four-unit RFs. Therefore, the next part of this research will focus on three-unit RFs.

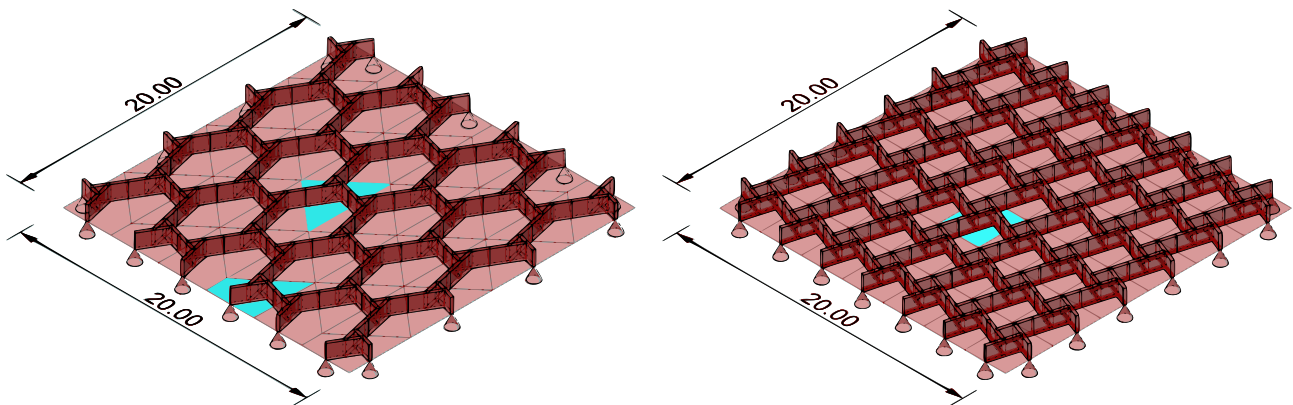


Figure 4.16: Two concentric RF systems, 3RF (left) and 4RF (right) with the same individual member length and area per unit (blue)

| | 3RF | 4RF |
|---|---------------------------|----------------------------|
| Vertical load | 5 kN/m ² | 5 kN/m ² |
| Area per unit | 9,5 m ² | 9,5 m ² |
| Number of areas | 42 | 42 |
| Number of beams | 73 | 97 |
| Number of supports (sup.) | 20 | 28 |
| Number of connections | 126 (=42 · 3) | 168 (=42 · 4) |
| Average beam length | 3,1 m | 3,4 m |
| Average beam length ex . sup. | 2,0 m | 2,0 m |
| Total beam length | 229,8 m | 329,2 m |
| Percentual difference total length | 35,6 % | |
| Structural dimension GL24h (ULS) | 0,22 x 1,0 m ² | 0,18 x 0,94 m ² |
| Total timber volume | 50,6 m³ | 55,7 m³ |
| Percentual difference total volume | 9,6 % | |

Table 4.2: Geometrical differences between 3RF and 4RF system, result of calculation

4.4.2 INFLUENCE OF ECCENTRICITY AND ENGAGEMENT LENGTH

The comparison between the concentric three- and four-unit RF show that a three-unit RF is more beneficial to use regarding material use and structural efficiency. This comparison illustrates the influence of varying the number of members per unit but, the other parameters such as engagement length and eccentricity have not yet been discussed.

This chapter therefore discusses the influence of these parameters on the structural behavior for an RF with unitized member configuration and unit style that are characteristic for RFs. The RF designs have been made by using 'The RFD'.

GEOMETRY

These two RF designs, spanning both ten meters, differ in applied eccentricity. By varying the eccentricity from 160 mm to 80 millimeters, parameters such as, engagement length, and the overall member length will change too.

The engagement length, determined by the scale factor, has been kept the same. Varying this parameter will have the same effect as for varying eccentricity e ; the structural design will increase or decrease in height resulting in an increased or decreased enclosed volume: the volume within the RF (Figure 4.17).

By decreasing the eccentricity between the beams to 80 millimeters, the average beam length is reduced. Consequently, when comparing both systems, it can be concluded that the total required beam length will become smaller if the eccentricity is reduced. As written before, the total beam length does not necessarily correlates to material use which depends on mechanics.

MECHANICS

Changing the geometry by varying the eccentricity has a great influence on the mechanical behavior. This influence is examined by evaluating mechanical consequences for several loading types. Furthermore, the influence of reducing the RFs' torsional capacity is examined in order to determine whether this is allowable and responsible.

The mechanical behavior is examined by using a linear static FEM calculation using the FEM software Oasys GSA. Application of loads and BC's resulted in mechanical ranges that are displayed in the table on the next page. Beam sizes have not been determined.

The loading types that are all being applied to the structure in global z-direction and are defined as self-weight, point load, and load panel. Self-weight of the structure is defined as 1 kN/m^1 acting as equally distributed load over the beam length.

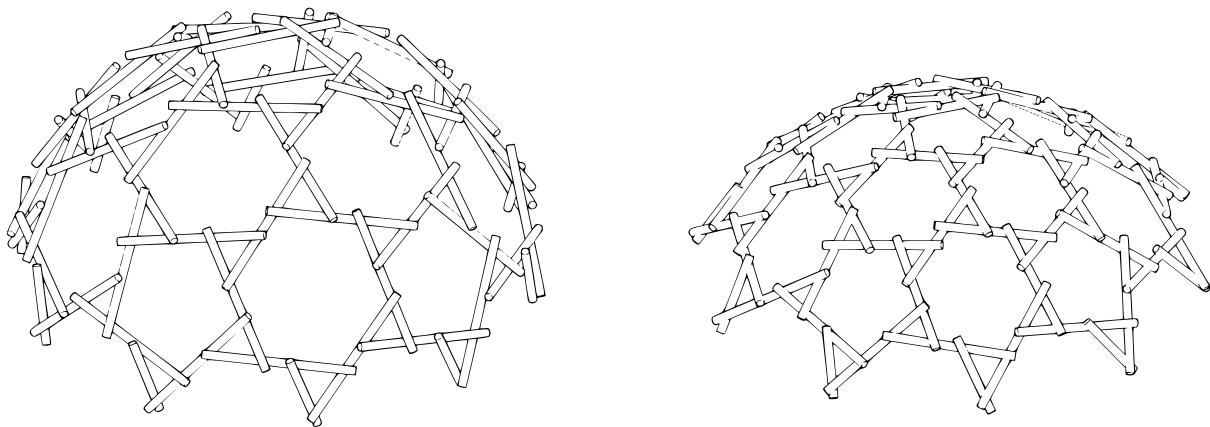
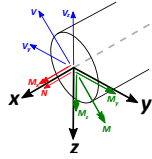


Figure 4.17: RF inspired by a geodesic dome with $e = 160 \text{ mm}$ (left) and $e = 80 \text{ mm}$ (right)

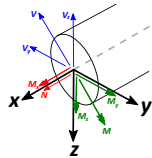
| | Eccentricity = 160 mm | Eccentricity = 80 mm |
|----------------------------|-----------------------|----------------------|
| Diameter RF dome | 10 m | |
| Total unscaled beam length | 154 m | 126 m |
| Minimum beam length | 1,3 m | 1,2 m |
| Maximum beam length | 2,6 m | 2,3 m |
| Average Beam Length | 2,4 m | 1,9 m |
| Floor area | 72 m ² | |
| Enclosed volume | 230 m ³ | 120 m ³ |

Table 4.3: Geometrical properties $e = 160 \text{ mm}$ & $e = 80 \text{ mm}$

| | Eccentricity = 160 mm | | | | | | Eccentricity = 80 mm | | | | | |
|-----------------------------|------------------------------------|-------|---------------------|-------|------------------------------------|-------|------------------------------------|-------|---------------------|-------|------------------------------------|-------|
| | Self-weight 1 kN/m ¹ | | Point loads 5 kN | | Load panels 1 kN/m ² | | Self-weight 1 kN/m ¹ | | Point loads 5 kN | | Load panels 1 kN/m ² | |
| | pos. | neg. | pos. | neg. | pos. | neg. | pos. | neg. | pos. | neg. | pos. | neg. |
| F_x [kN] | 10,0 | -15,0 | 40,0 | -60,0 | 10,0 | -15,0 | 2,5 | -15,0 | 10,0 | -80,0 | 2,5 | -12,5 |
| F_y [kN] | 4,0 | -4,0 | 15,0 | -15,0 | 4,0 | -4,0 | 6,0 | -2,0 | 30,0 | -15,0 | 5,0 | -2,0 |
| F_z [kN] | 8,0 | -8,0 | 25,0 | -25,0 | 8,0 | -6,0 | 4,0 | -4,0 | 20,0 | -20,0 | 4,0 | -2,0 |
| M_{xx} [kNm] | 0,6 | -0,8 | 2,0 | -2,5 | 0,8 | -0,6 | 0,2 | -0,3 | 1,0 | -1,5 | 0,2 | -0,2 |
| M_{yy} [kNm] | 3,0 | -3,0 | 12,5 | -10,0 | 3,0 | -2,5 | 1,5 | -1,5 | 8,0 | -6,0 | 1,0 | -1,0 |
| M_{zz} [kNm] | 2,0 | -2,5 | 8,0 | -10 | 1,5 | -2,0 | 1,0 | -2,5 | 4,0 | -8,0 | 0,5 | -1,3 |

Table 4.4: Mechanical range when varying e with torsional beam stiffness ($M_{xx} \wedge M_{yy}$ = free, rest = fixed)



| | Eccentricity = 160 mm | | | | | | Eccentricity = 80 mm | | | | | |
|-----------------------------|------------------------------------|-------|---------------------|-------|------------------------------------|-------|------------------------------------|-------|---------------------|-------|------------------------------------|-------|
| | Self-weight 1 kN/m ¹ | | Point loads 5 kN | | Load panels 1 kN/m ² | | Self-weight 1 kN/m ¹ | | Point loads 5 kN | | Load panels 1 kN/m ² | |
| | pos. | neg. | pos. | neg. | pos. | neg. | pos. | neg. | pos. | neg. | pos. | neg. |
| F_x [kN] | 10,0 | -15,0 | 40,0 | -60,0 | 10,0 | -12,5 | 2,5 | -15,0 | 10,0 | -80,0 | 2,5 | -12,5 |
| F_y [kN] | 4,0 | -3,0 | 15,0 | -10,0 | 4,0 | -3,0 | 6,0 | -2,0 | 30,0 | -10,0 | 5,0 | -2,0 |
| F_z [kN] | 8,0 | -8,0 | 25,0 | -25,0 | 8,0 | -6,0 | 4,0 | -4,0 | 20,0 | -20,0 | 4,0 | -3,0 |
| M_{xx} [kNm] | - | - | - | - | - | - | - | - | - | - | - | - |
| M_{yy} [kNm] | 2,5 | -3,0 | 10,0 | -12,5 | 2,5 | -2,5 | 1,0 | -1,5 | 6,0 | -8,0 | 0,8 | -1,0 |
| M_{zz} [kNm] | 1,5 | -2,0 | 6,0 | -8,0 | 1,5 | -2,0 | 0,5 | -1,5 | 2,0 | -8,0 | 0,3 | -1,3 |

Table 4.5: Mechanical range when varying e without torsional beam stiffness (M_{xx} = free, rest = fixed). Green is equal to figure 4.4

This applied value is quite large because actual self-weight results in negligible values: timber is a lightweight building material. Round timbers with a diameter of 160 mm and density of 350 kg/m³ give a self-weight of:

$$q_{\text{self-weight}} = \pi (0,16/2)^2 \cdot 350 = 7,0 \text{ kg/m}^1 = 0,07 \text{ kN/m}^1$$

Point loads are applied to all beam intersections. Load panels and BC's have been applied as explained under 4.2.2. Both tables that are displayed above, indicate that the different types of load application will not lead to major differences in mechanical behavior.

The tables furthermore show that the mechanical range change when decreasing the beams torsional resistance to one percent of its original. Where some moments change direction, others will become slightly smaller or greater but, in general, the individual beams will start to behave as simply supported and show more realistic results (Figure 4.18). It is self-evident that by reducing the torsional stiffness of the beam, torsional moments will become neglectable small. Consequently, reducing the beams' torsional resistance will lead to more reliable results with respect to this research.

When looking at all mechanical ranges with respect to the different eccentricities, one can conclude that when decreasing the eccentricity, normal force F_x and shear force F_y increases and moment M_{xx} , moment M_{yy} , and shear force F_z decreases (Figure 4.20). The reduced curvature that is a result of the reduced eccentricity, causes that internal forces will be transferred more in vertical bending while the variant with larger eccentricity will transfer its forces more by bending and shear in all directions. Its curvature correspondingly results in lower normal forces.

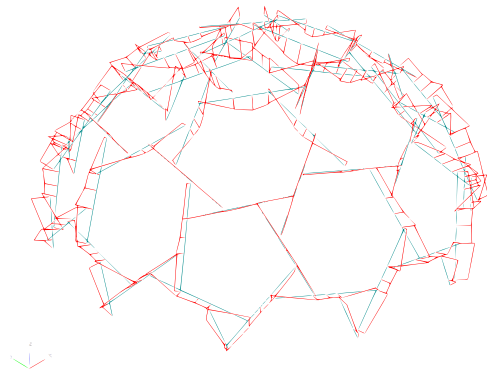


Figure 4.18: Schematic overview of M_y

4.5 CONCLUSION AND DISCUSSION

Normal forces in the connections could lead to force transferring by means of contact pressure which is, as written before in this chapter, the most efficient way of transferring forces in timber structures^[23]. This has yet to be proved by a connection design of which the required BC's have been determined. The chosen BC's will result in simply supporting beams throughout the RF which is beneficial for timber design.

It has been showed that a mechanical equilibrium for single unit RFs can thus be easily determined by using these BC's and an equally distributed line load. However, when regarding an eccentric an multiple unit RF, this statement does not apply anymore making the use of FEM software indispensable.

By using this software in a concentric three- and four-unit RF design, and by a schematization of the deformation, three-unit RFs seemed to be structurally superior to four-unit RFs. Especially when regarding deformation, four-unit RFs can be easily parallelized i.e. deformed in a parallelogram. This is different in comparison to three-unit RFs that are structurally stable from itself. In addition to this, four-unit RFs result in to greater material use. The further work of this research is therefore focused on three-unit systems.

The effect of different loading types on an eccentric RF has furthermore been reviewed. Since all loads where acting in the same direction, no outstanding differences could be distinguished but, the load panel geometry proposal proved to be a workable method to be able to apply area loads to an eccentric RF.

The variation of eccentricities between the beams in these tree-unit systems influences the force distribution throughout the system. An RF will more start to behave as beam grid structure when reducing the eccentric. Increasing the eccentricity between the beams result in greater bending moments. The connection design, to be discussed in the next chapter, determines whether this is beneficial or not.

The design of connections and beams will also influence redundancy. Global collapse due to local failure should always be prevented. An addition of screws for example helps to increase or introduce plastic behavior in timber elements that naturally show brittle collapse.

The findings of this chapter will be practically applied in the next chapter that discusses a connection design especially suited for RFs. It also discusses the corresponding structural calculations and the design procedure.

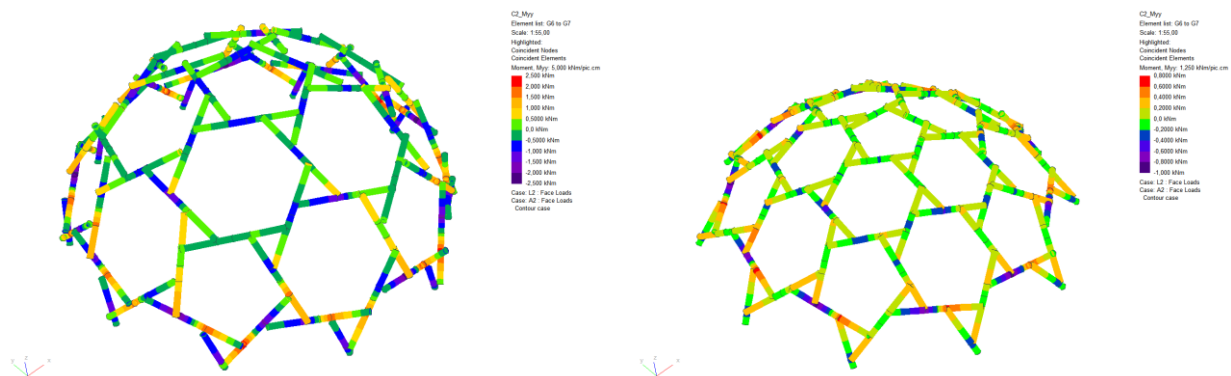


Figure 4.19: Schematic overview of bending moment M_{yy} without torsional beam stiffness and $e = 160$ mm (left) $e = 80$ mm (right)

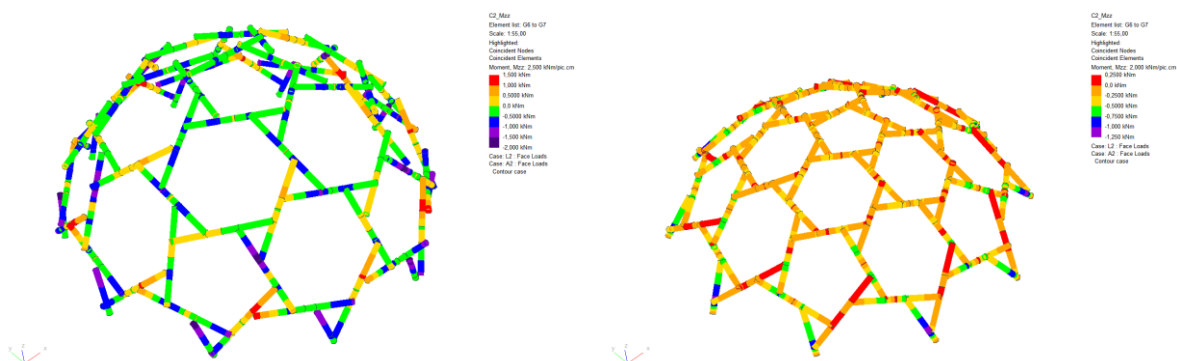


Figure 4.20: Schematic overview of bending moment M_{zz} without torsional beam stiffness and $e = 160$ mm (left) $e = 80$ mm (right)



DETAILING AND APPLICATION IN THE RECIPROCAL FRAME DESIGNER

This chapter proposes a connection design that is especially suited for RFs and has been added in the RFD to allow for design to production. By elaborating the design to production steps and design procedure of the in this chapter completed RFD, one should be able to use the tool or its theory for practical RF design.

-



5 DETAILING

In this research, detailing is the identification of forces found at intersecting timbers; the connections, recognizing its consequences and the design of possible facilities to engage these consequences. This chapter focusses on the design of an appropriate timber connection design especially suited for RFs. First, the chosen section type and material is discussed. Second, a connection design is proposed that is based on a practical RF design.

5.1 CONCEPT

To be able to design a connection, one first has to choose the cross-section type. This decision is in this research influenced by availability, practicability, mechanical need and processability by industry standard machines. The following cross-sectional types have been regarded that can be used for RF construction:

- Circular cross-sections;
- Rectangular cross-sections;
- Varying rectangular cross-sections.

In addition to this, the cross-section in an RF structure needs to resist:

- Bending in multiple directions;
- Axial compression and corresponding buckling;
- Axial tension.

5.1.1 CONSIDERING CROSS-SECTIONS AND MATERIALS

Circular cross-sections are generally known and applied as round wood structure. Although they are not very efficient in bending in one direction, they are very well suitable to bear two way bending and compression simultaneously. In practical applications, logs are often unbarked which is needed to improve insect decline. Additionally, cylindrical milling improves dimension accuracy: the members will become exactly round.

The milling largely or completely removes the stronger sapwood but, is required in CAM applications to create dimensionally accurate connections. Circular cross-sections with CAM detailing are often made circular with cylindrical milling subsequently to a CAM process. In this case, material is not used optimally. The milling process needs to be well controlled to be able to create fitting connections. Rectangular cross-sections however, are more dimensionally accurate because they already have been processed and are therefore more common to be used in CAM. In timber industry, rectangular cross-sections are created by solid sawn wood that in small dimensions can be applied in composite timbers: the engineered wood products.

The maximum depth of solid timber is limited to the tree size. In Sweden for example, the maximum dimensions of solid timber are limited to a depth of 245 millimeter and a length of five meter^[24]. Greater dimensions require engineered wood products. These include composite wood products bonded together with adhesives or other fixation methods.

ENGINEERED WOOD PRODUCTS

The use of engineered wood products has been arising from the shortage of old grown timber. It turned out that these materials show smaller variation in mechanical properties than sawn timber. Large and strength reducing knots for instance, are often removed during the manufacturing process. Furthermore, low-strength areas are more distributed by so called smearing-out effects. With respect to beam sections, engineered wood products such as LVL, CLT, and GL are based on veneers or sawn timber and are briefly discussed below. The discussion results in a preferred material that will be further elaborated in this research.

Cross Laminated Timber (CLT) is made from sawn timber boards that are stacked in a grain direction that varies perpendicular each layer. Consequently, a more homogeneous stress capacity can be created in comparison to solid timber: tension resistance of timber perpendicular to the grain is very low. CLT is produced as panel in which strand lay-out depends on the strength requirements and manufacture. When used as member, the panel has to be sawn into the required member dimensions based on structural need. One can for example decide to vary the member depth over the length. This increases the complexity of an RFs assembly.

Glued Laminated (GL) timber however, is often already produced by an highly automated fabrication process in the required section size. Glulam consists of sawn timber joined together by finger joints. Gluing the laminated timbers together will shape the final member that has axially orientated grains. It results, when not reinforced, just as with sawn timbers, in low mechanical strength perpendicular to the grain. Members can have a curved or varying shape depending on the mold shape. Curved members are often made from smaller laminates that are easier to bend.

Laminated Veneer Lumber (LVL) is not made from laminates but from veneer that is subtracted from rotary peeling trees into veneer subsequently glued together. This type of engineered wood product is comparable to plywood and structurally superior to the other described products: defects in the wood are removed and grains can be oriented in different directions.



WHAT TO USE?

Although LVL can show proper mechanical behavior, it requires more glue in comparison to glulam which could be environment unfriendly. Furthermore, it is available in a limited number of widths since it is manufactured as board resulting in slender beams good to resist bending in one direction. CLT uses less glue and could, just as with LVL, be made with varying grain directions. This can be beneficial at notches.

Glulam is not made with varying grain directions and is widely available in standardized dimensions. It does not need additional sawing to create members. Furthermore, the fact that designs are limited by maximum dimensions will not occur that fast. In fact, to take the RFD to practice, the in this research cooperating industry partner 'Heko Spanten' explained that they prefer using glulam for members instead of CLT.

Although glulam may not be the most beneficial engineered wood product to be applied in an RF from structural point of view, it could be interesting to investigate consequences of application. For instance, what kind of reinforcing strengthening is needed. Consequently, this research continues with the application of rectangular glulam cross-sections in RF design and its application in the RFD.

5.1.2 THE EFFECT OF ECCENTRICITY

In addition to the described section and material preferences, the parameter eccentricity is of paramount importance to be able to design a connection for an RF. As discussed before, member depth can be dependent on the eccentricity. A member depth smaller than the eccentricity results in required notching. However, steel can also be added but this is not preferable in RF design. By applying steel connectors, the RF advantage of using relatively simple connections is nullified. Therefore, it is tried to keep the RFs jointing as simple as possible. A first design step required to reach this goal is given below.

POTENTIAL DESIGNS

Figure 5.1 shows the possible connection designs that could be possible in RFs. First, when the eccentricity is larger than the member depth, detailing principle one should be implemented. It results in the need to add extra space filling elements to the connection. Second, if the eccentricity is equal to the member depth, connection topology two is created. Here, elements rest exactly onto each other. However, when the members arrive under an angle, rectangular members do require notching although member depth equalizes eccentricity. The third and fourth example shows that smaller eccentricities require one- or double-sided notching.

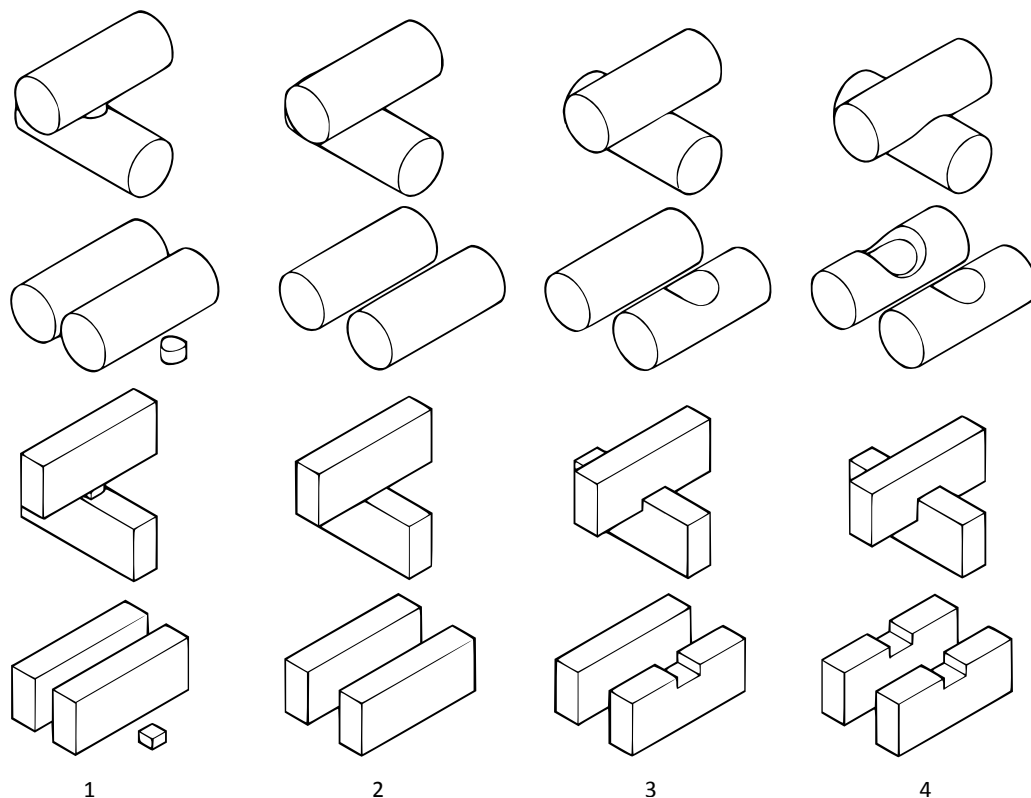


Figure 5.1: Possible connections in an timber RF and its influence on the cross-section coherent to eccentricity

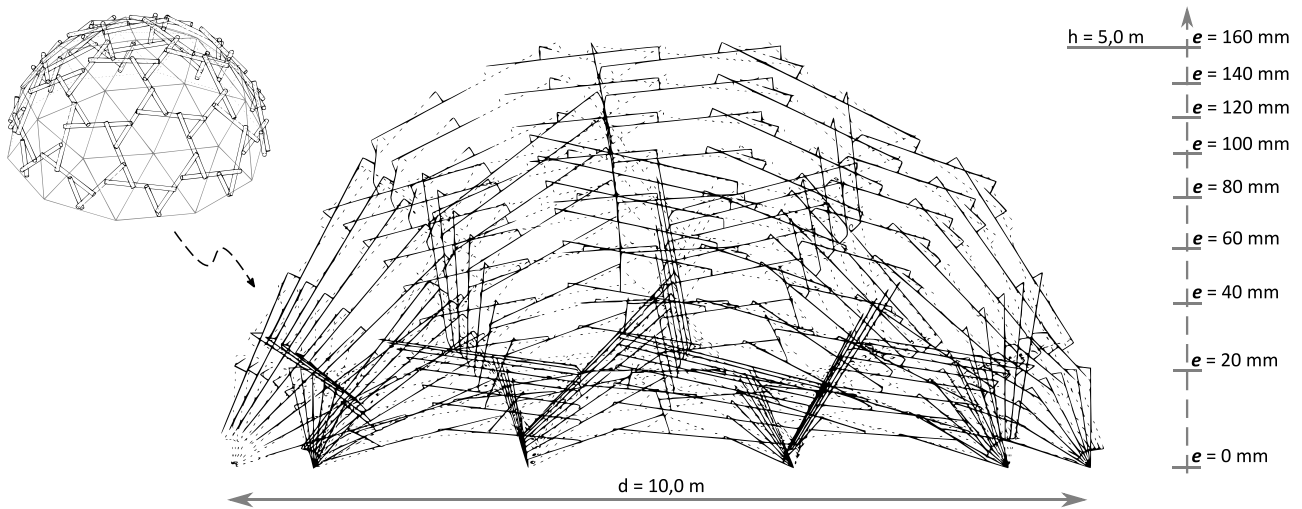


Figure 5.2: Eccentricity and its influence on the structural height on a standard unit style RF dome created with the RFD

ECCENTRICITY AND MEMBER DEPTH

The effect of increasing the eccentricity while preserving the scale factor is determined by the eccentricity optimization method (see 3.3.2) and results in an higher RF structure (Figure 5.2). It seems that relatively small eccentricities and thus member depths are required when not using notching to create structural height.

Load application to this structure most likely will result in a larger required member depth than the eccentricity length. Therefore, and because the angular reason described above, notching seems unavoidable in RF design. Furthermore, by keeping the eccentricity independent on member depth, one creates structural freedom and enables necessary transferring of shear and axial forces. The for the RFD developed detailing divides these notches over both intersecting members causing equal section weakening (Figure 5.4).

The RFD enables furthermore to vary this division over the height of the notch along the member. Increasing the notch at the end of the members will cause a reduced notch halfway the member.

This process is visualized below where the notch at the end of the member is decreased leading to an reduced notch halfway the member.

Reducing the notch height at the beam ends increases a members' shear resistance but, increases the bending moment resistance.

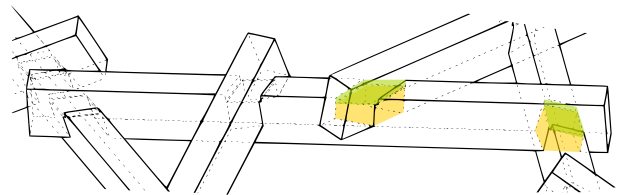


Figure 5.3: Varying the notch height division. In this case a factor of 0.8 has been taken

As written under 4.4.2, decreasing eccentricity causes that internal forces will be transferred more in vertical bending while RFs with larger eccentricity will transfer its forces more by bending and shear in all directions. Correspondingly, low curvature decreases normal forces. A notch height division must be attuned to this.

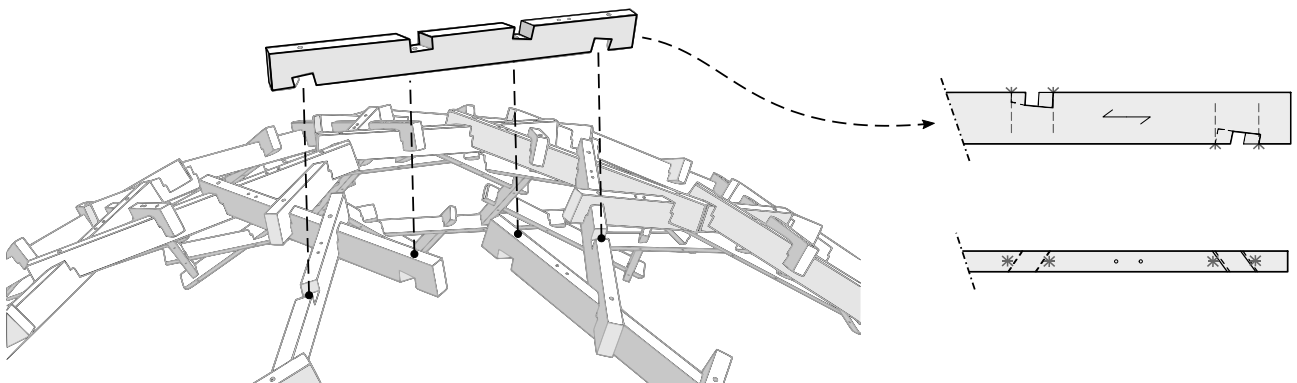


Figure 5.4: Detailing concept applied in the RFD with reinforcing screws and timber grain direction

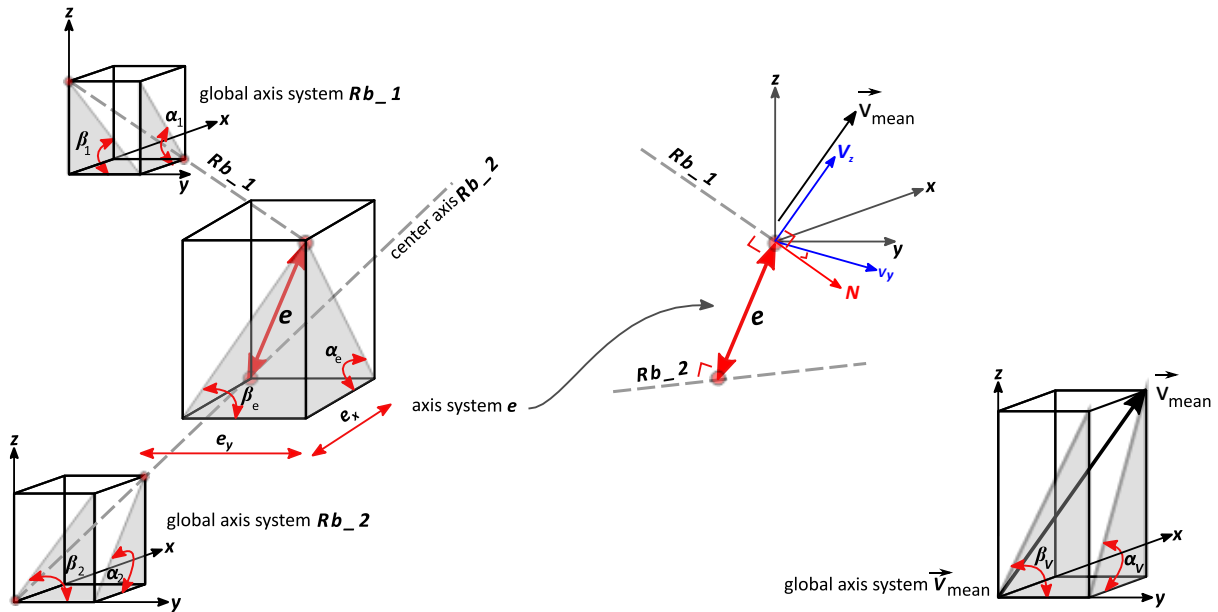


Figure 5.5: Axis systems present between two intersecting RF members Rb_1 , Rb_2 and the eccentricity e

5.1.3 DEFINING THE LOCAL AXIS SYSTEMS

The notching geometry can only be determined by using a predefined unambiguous geometrical rule that determines the member orientation within the RF. This rule should be governing for multiple unit RFs and should be independent of the unit style. In general, members are oriented by means of their local axes system.

PRINCIPLES AND EXPLORATION

Figure 5.5 shows the number of axis systems present at one beam intersection. They all determine the geometry of an RF but are not used to define the member orientation.

A first exploration on how to determine the beam orientation was made by taking the mean point of a basic surface and use that point to determine all beams Z-vectors. However, this did not result in great member orientations. Especially when surfaces have intricate geometries, there exists no point that can be used to define local axis systems for all members.

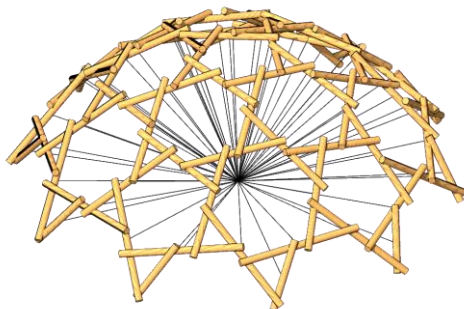


Figure 5.6: Orienting beams around a predefined point does not always provide usable results

APPLIED AXIS SYSTEM

The eccentric jointing in RFs causes the need for a mathematical approach to be able to orient rectangular members such that they are mechanically properly positioned around their strong axis. Subsequent to the experiment with beam orientations around a predefined point, it was found that the eccentricity lines may be usable in the definition of a local axis system. The mathematical determination of the eccentricity lines by means of the shortest distance between two vectors causes perpendicularity. This perpendicularity property is used in the RFD to define the local axis system: it results in mechanically correct solutions.

Local axis systems that define the member orientation are defined in the RFD by sorting two eccentricity lines along a members' center point and by taking their mean vector direction as local vertical axis (Figure 5.7):

$$\vec{V}_{mean} = \frac{\vec{V}_1 + \vec{V}_2}{2} \quad (5.1)$$

This exact beam orientation is used to structurally check beam dimensions and connections with FE software.

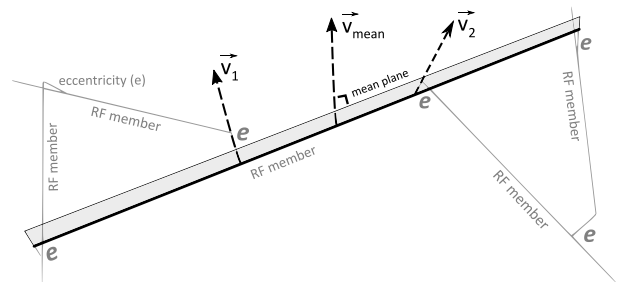


Figure 5.7: Beam orientation based on eccentricities

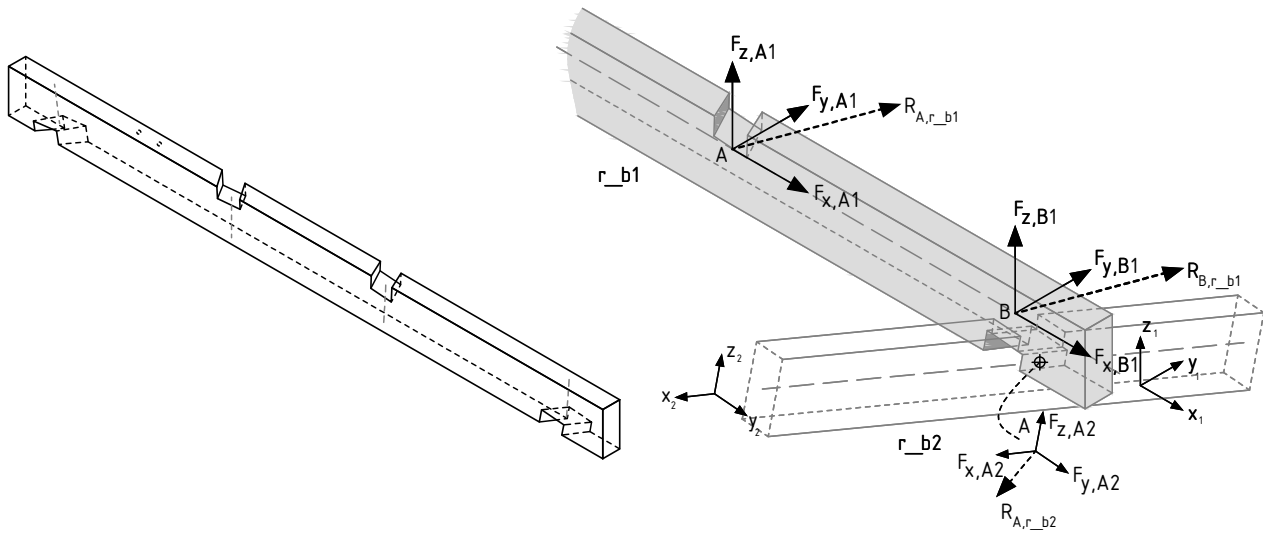


Figure 5.8: Detailing principle with planes (left), local force and axis systems (right)

5.2 STRUCTURAL DESIGN

The exact section orientation used for detailing is also used in the FE analysis included in the RFD to define force distributions and enable structural checks. UC failure is directly visualized by colored indications (Figure 5.2). Forces are transferred at the notched planes and by self-drilling screws (Figure 5.8). The complete calculation on how to structurally verify the connection according to timber Eurocode 5^[25], is added in annex 2. It is the manual elaboration and exploration of a parametrized calculation implemented in the RFD.

5.2.1 FE ANALYSIS WITHIN GRASSHOPPER

In addition to the computational modeling of the connection that is included in the RFD. The structural design of the connection and members are also checked within the RFD according to the regulations described in Eurocode 5 (EC5). This is possible by a direct connection within grasshopper to the FE software of Oasys GSA. The FE engine of GSA runs in a background process. By means of the plugin Geometry Gym, developed by Jon Mirtschin, every step that is normally taken within GSA can be automated and programmed into Grasshopper.

Among others, this includes load application, boundary conditions, member geometries and orientations. The effect of design changes on the structural behavior can be immediately visualized because its influence on the force distribution is calculated directly. Parameters can be changed until the EC5 checks are satisfied.

The data structure is kept within Grasshopper enabling a matching link between geometrical data and corresponding forces. It allows to combine structural checks with geometrical form finding and visualization of UC exceeding locations. All forces are linked to the geometrical data. This is a necessity given the RFs nature of having an intricate geometry: all notches could differ.

FORCE DISTRIBUTIONS

To ensure force equilibrium between the connecting members, the resultant forces between member r_b1 point B, and member r_b2 point A, need to be equal (Figure 5.8). This is checked in the RFD by the general expression for resultant forces in a perpendicular axis system:

$$\vec{R}_i = \sqrt{(F_{x,i}^2 + F_{y,i}^2 + F_{z,i}^2)} \quad (5.2)$$

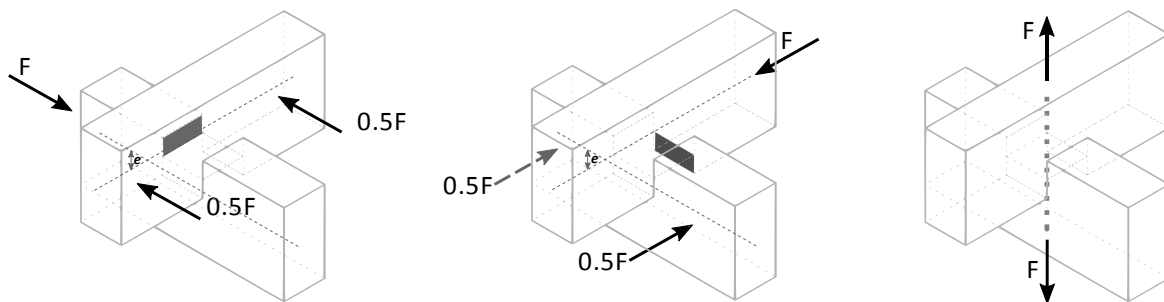


Figure 5.9: Forces are transferred at the notched planes and by self-drilling screws (indicated by the dashed line)

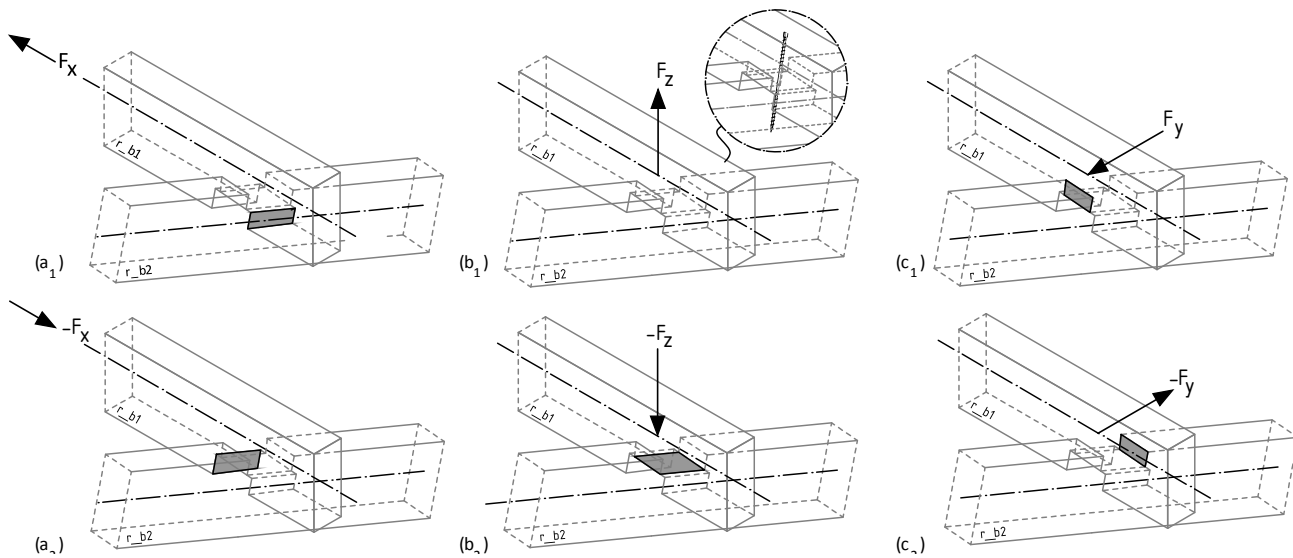


Figure 5.10: The transferring of forces in the connection by notch planes or self-drilling screws

FORCE TRANSFERRING

The resultant forces showed that there is an equilibrium of forces using the BCs' described under in 4.2.1. In this research it has been assumed that every individual force is taken by a separate part of the connection. In practice however, forces will most likely spread through multiple parts but, dividing the forces per part is a workable and save approach.

Figure 5.10 shows that each different plane or screw in the connection bears a different force. The eccentricity between the members cause a lever arm between plane center where the force engages and the member center axis. This lever arm together with the angular geometry causes stresses perpendicular to the grain.

The calculations discussed in annex 2 showed that in order to resist these stresses additional measurements are needed. In this respect, self-drilling screws are added to the locations next to the notches that will increase redundancy and resistance to tension perpendicular to the grain.

CLT may not require this reinforcement but is , just as glulam, weak in compression perpendicular to the grain and strong in compression parallel to the grain: the grains in glulam are oriented axially. Consider for example force F_x that causes compression under an angle to the grain on beam r_{b1} and compression exactly perpendicular to grain to beam r_{b2} . Since compression perpendicular to the grain is normative over compression parallel to the grain, the compression force acting to an angle on beam r_{b1} , does not need to be checked. In addition to this, all members are automatically scaled to reach a specific length to be able to transfer force F_x .

5.2.2 AUTOMATED SCALING

It is self-evident that members used for FE analysis have a different length than the members used to determine the solid geometry. Members in the FE analysis need to connect exactly at line intersections whereas with solid members a small cantilever must be created to be able to create the notch and protruding part (Figure 5.11).

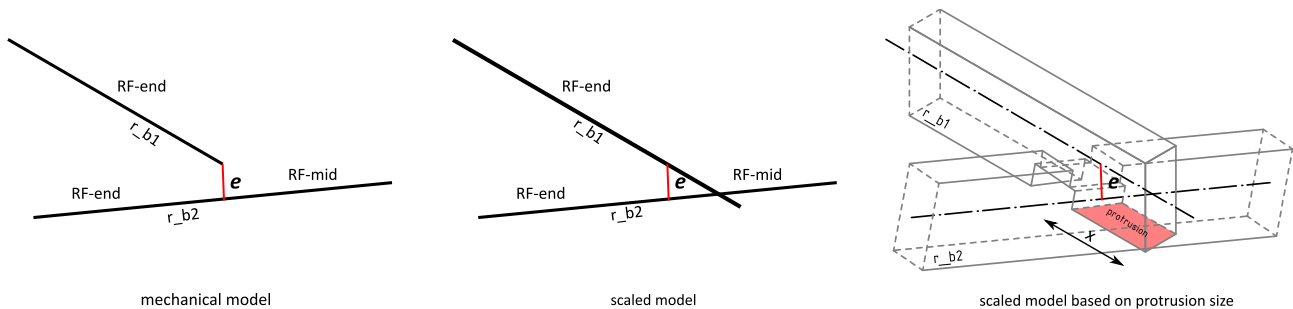


Figure 5.11: Difference between mechanical model used for FE analysis and the solid scaled model. The protrusion is indicated in red

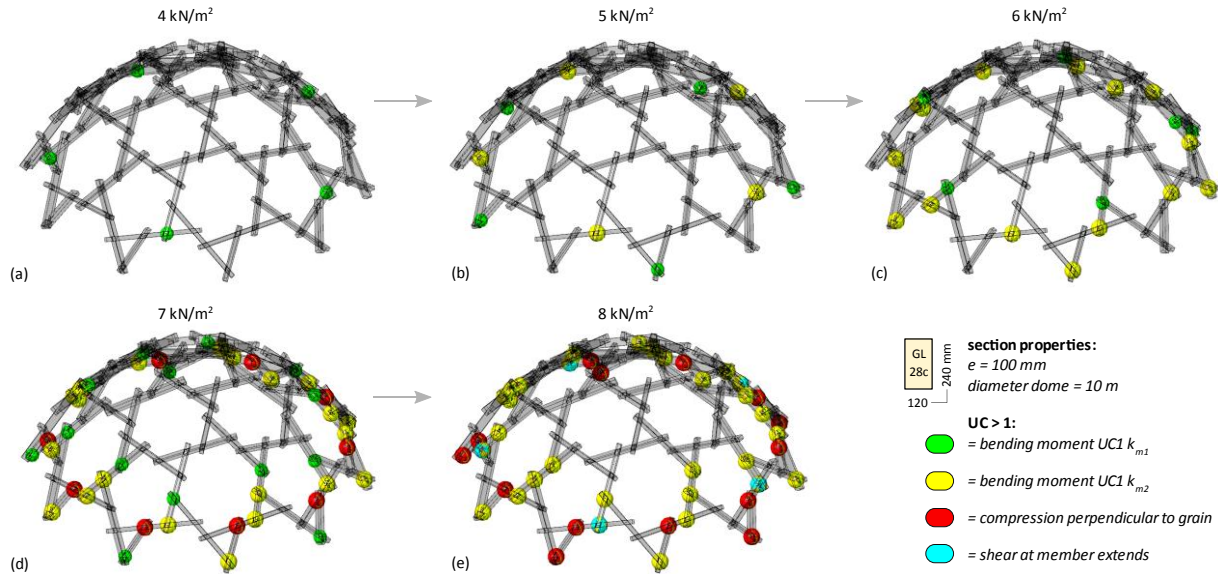


Figure 5.12: Increasing the area load onto load panels first results in UC exceeding thus failure by bending moments where after the structure fails in more mechanisms. The UC exceeding is visualized by different colors within the RFD

Member dimensions in the RF are scaled conform the following formula:

$$S_{\text{scaling_factor}} = \frac{\text{round}(L, 1) + x}{L} \quad (5.3)$$

In which members are scaled around their midpoints towards the to one decimal rounded beam length L plus the required additional beam length x (protrusion).

However, although this method creates rounded dimensions and protruding members, the member orientation and angular relations within the RF require additional scaling to create uniform protrusions. After trying several scaling methods based on geometrical angle ratios between the members, no unambiguous scaling rule could be determined. It cannot be stated that a governing rule does not exist but, within this research is has not been found.

Therefore, a scaling rule based on the actual protrusion size has been developed. This method measures every protrusion size where after it can be decided whether it satisfies the preferable length. When a protrusion is too long, the member size will be reduced. Too short protrusions will be lengthened to the preferred length that can be determined using the calculations described in annex 2.

CONSEQUENCES

The UC exceeding in annex 2 shows that strengthening by means of reinforcement perpendicular to the grain is unavoidable when using glulam (GL28C). However, the advantage of combining geometrical and structural design is that parameters can directly be changed to modify an RFs geometry or member depths to satisfy the checks. The members are reinforced with self-drilling screws close to the notches (Figure 5.13).

In addition to this, at some locations in the structural design of an RF, tensile forces at the connection occur. Since this force cannot be withstood directly by the system, it must be transferred by a dowel type connection in the form of a special type of self-drilling screw (Figure 5.10).

The varying installation speed of this double-threaded screw that is created by its thread geometry, insures that beams are drawn towards each other enabling force transferring by the designated planes. When using bolts, re-tightening may be needed due to shrinkage which is not necessary when using this screw. Furthermore, the shank of this screw is the strongest part. Consequently, tensile forces could be the highest here by which its position is designed exactly in between the neighboring members.

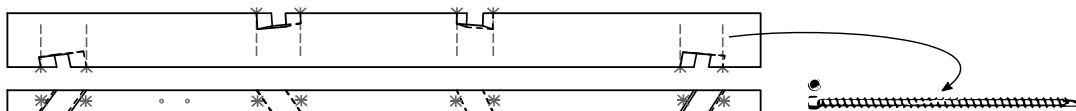


Figure 5.13: Section reinforcement by full threaded self-drilling screws



Self-drilling screws can almost always be applied without the use of pre-drilled holes. This direct instalment, together with their special shape, results in a greater withdrawel strength compared to traditional screws. With respect to this connection, the screw adds redundancy to the connection because they introduce plastic behavior to parts that would otherwise show brittle behavior. Furthermore, it ensures a peak stress capacity that could be preferable during the implementation of the structure.

OVERALL STRENGTH, STIFFNESS AND STABILITY

The implementation of the structure will be discussed in the next chapter but, it can already be stated that the connection requires some slack to enable installation. This slack will have an effect on the total deformation of the structure when not restored after installation. Connection settlement due to slack can be determined by varying the scale factor explained under the form-finding chapter.

However, requirements with respect to deformation are not obligated and are project specific. Structural deformation can be calculated in GSA using a decreased (shear) modulus of elasticity in combination with the characteristic value of the considered load. Loads, naturally can be applied as line, grid or point load. To check the deformation, the complete model needs to be exported from the RFD as GSA file (b) (Figure 5.15). Hence, this also allows to visualize for instance the stresses and check the stability. Overall stability of the considered RF is guaranteed with the chosen BC's and the three-unit triangular system (Figure 4.14).

5.3 CONCLUSION

This chapter discussed the detailing concept and its application in the RFD. The implementation of FE analysis and the normative EC5 checks within the RFD, allows to dynamically edit the RFs' design to find an optimal design.

Figure 5.12 indicates that structural failure first occurs by bending moments where the force redistribution value k_m is applied to the different moments as discussed in annex 2. Loads are applied to this structure in vertical direction to the load panels (4.2.2). It seems that overall and lateral buckling does not need to be considered and thus is not normative. Increasing the gird load first results in failure by bending moment where after the structure fails in compression perpendicular to the grain and shear. Editing the parameters such as eccentricity will lead to different results as discussed in chapter 4.

Although the applied glulam may not be the most beneficial material in comparison to CLT, the required reinforcement is limited. Furthermore, this adds strength during implementation and increases redundancy. The amount of labor may be the same as with CLT since CLT needs to be sawn into members.

These results may be promising but, implementation and roofing have not yet been fully developed. Therefore, the next chapter focusses on the development of taking the RFD to practice by discussing the design to production process. Below, a roofing concept is displayed that could be a basis for further research focusing on RF roofing.

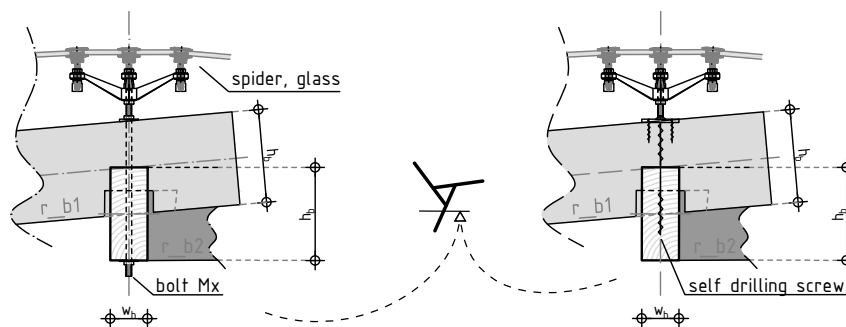


Figure 5.14: Roofing concept using a spider to elevate the glass from. The Glass can have a similar geometry as the load panels

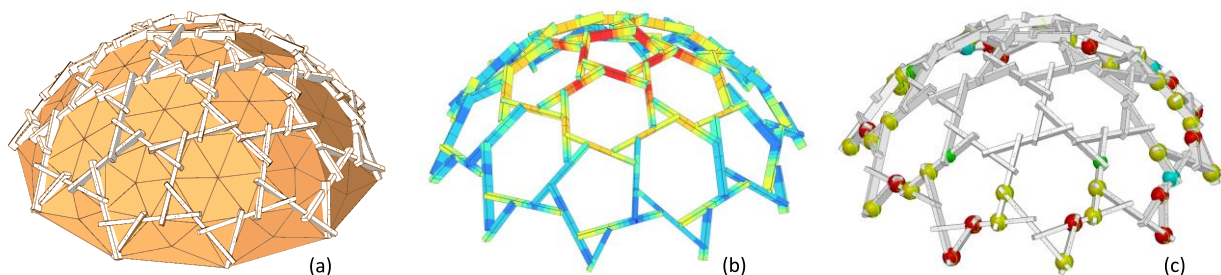
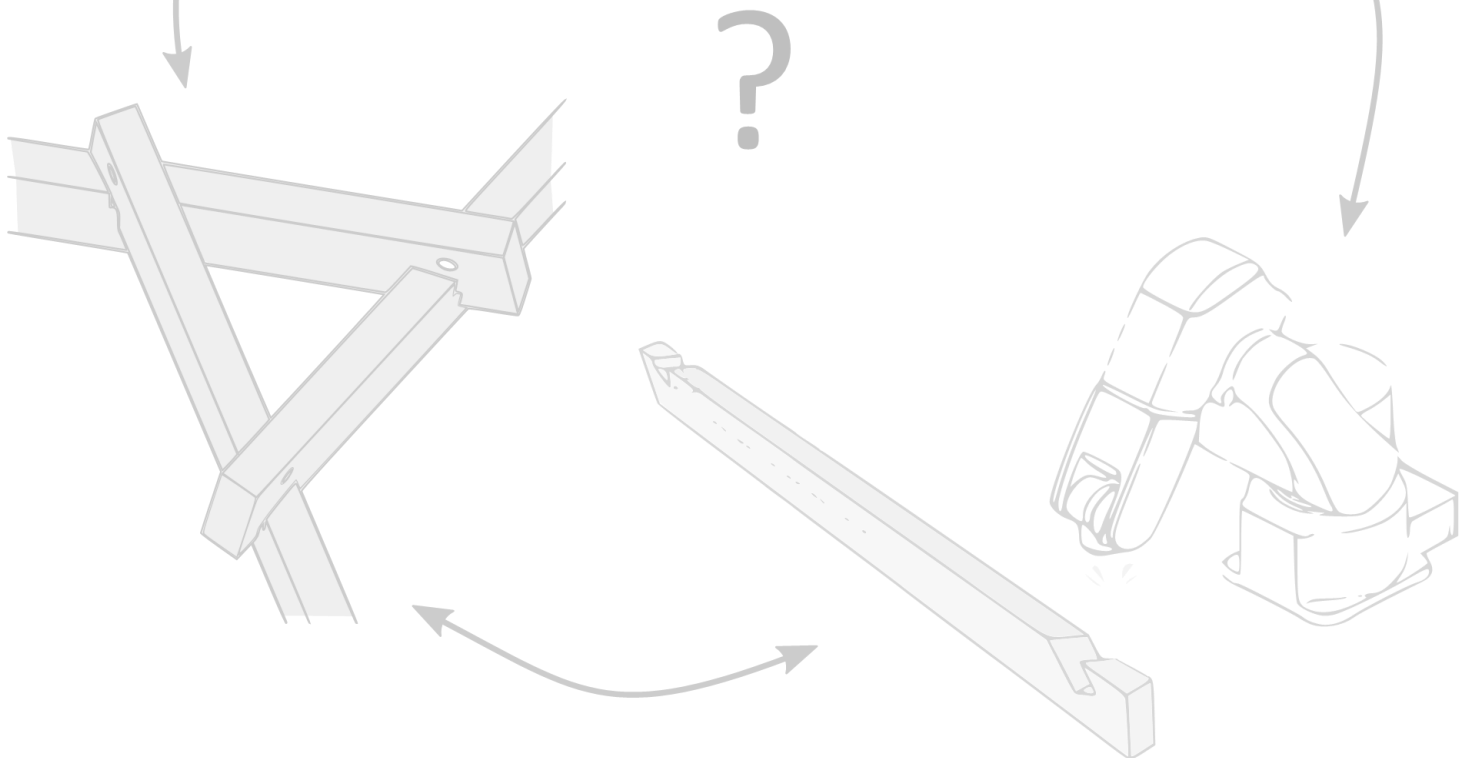


Figure 5.15: Load panels (a), illustrative FE model in GSA showing M_y (b), UC's > 1 showing timber failure in the RFD

DESIGN TO PRODUCTION

This chapter discusses the design to production process by means of the practical models that were made for this study.



6 DESIGN TO PRODUCTION

RF designs made by the RFD can result in intricate geometries in which notches and members all differ. The combination of this parametric system with CAM however, makes it suitable for practical applications. In fact, it makes timber a perfect material for free form architecture^[21].

Robotic manufacturing gets slowly implemented in today's construction. Assembling for instance, prefabricated robotically machined elements already is adopted. This chapter shows how these kinds of processes have been designed and implemented to test the feasibility of the RFD. The design to production process is crucial to test the RFDs feasibility and practicality. The subject will be introduced by discussing practical models made to recognize improvements.

6.1 FIRST MODELS

The first practical model was made to explore the design to construction workflow from Rhino to an actual model. At this point, the RFD was not yet completely developed but, the parametric model that uses the exact approach based on geometric translations, was already finished. A laser cutting machine was used to cut out members from plywood.

In this model, all members use one point to determine their local axis system. As discussed, this is not a proper approach but, for this test regarded as suitable.

6.1.1 CONNECTION

By means of this model it became clear that one needs a certain member height to create structural height. The model furthermore showed that notching is insurmountable to be able to determine member placement relative to neighboring members. Notching simplifies member placement during implementation.

All connections have been notched at one side for matters of simplicity: the connection was not yet developed. The parametric model failed to orient all notches at one side of the member which was preferable. Furthermore, additional iron wiring was needed to secure the model. This could have been avoided by using double sided notching.

Laser cutting the members from plywood only allowed two-dimensional (2D) notching. Members however need three-dimensional (3D) notching that can be tested by using for instance 3D printing.

6.1.2 FIRST 3D PRINTED MODEL

The first printed 3D model showed that with the applied connection principle, that divides the notches over both member sides, a tight-fitting joint can be achieved. In addition to this, the test revealed that member marking to identify their orientation relative to neighboring members is necessary. Member placement can otherwise be very difficult. The RF design becomes a puzzle without placement marks.



Figure 6.1: model of parametric model based on the analytic approach made by laser cutting plywood

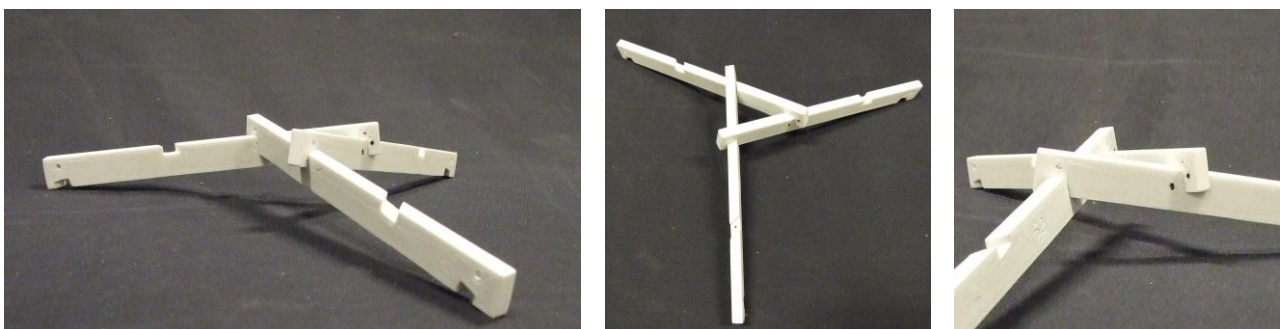


Figure 6.2: 3D printed model of connection to explore its feasibility



Since the members were not marked to identify their orientation, it took a while to assemble the three members into one unit. Hereafter, all members were marked with black dots. In addition to this marking, the model revealed that the protrusion size needs to be equalized in the overall design as discussed in the previous chapter. It furthermore showed that the notch division simplified construction and identification of member placement enormously.

6.2 COMPLETE 3D PRINTED RF MODEL

These lessons have been applied in the construction of a complete 1:20 scale model, that is also made with 3D printing. Here, all members have been identified with two dots at their topside at the side with the highest point Z in space. This is parametrically added in the RFD.

Applying this rule to the RF, that is based on a geodesic dome, results in two-indications per unit (Figure 6.5). This model was the first test to verify whether it is possible to assemble the complete structure. It tested the practicality of the RFD.

To be able to transfer the model to practice, one has to first unfold the structure (Figure 6.3). The unfolding transformation can be determined by using the members' orientation plane to determine the necessary transformation angle to a plane situation. It is of paramount importance that members have similar numbering between the complete and unfolded model which is included in the RFD. Hence, the model can be prepared for 3D printing, that in this case was conducted using wood filament, or by full-scale manufacturing.



Figure 6.3: Baked RFD model and its unfolded version ready for design to production. Diameter of the full-scale dome is 10 meter

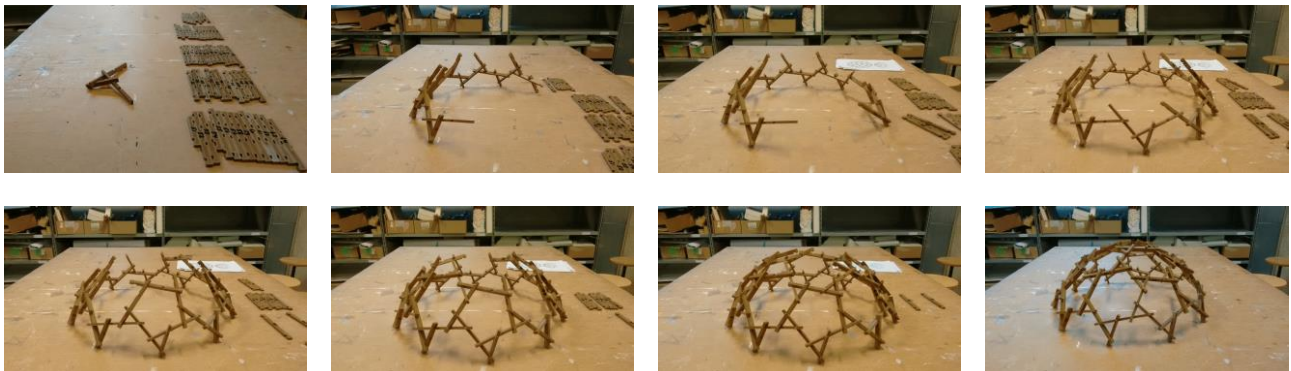


Figure 6.4: The construction of the 1:20 3D printed dome in chronological order

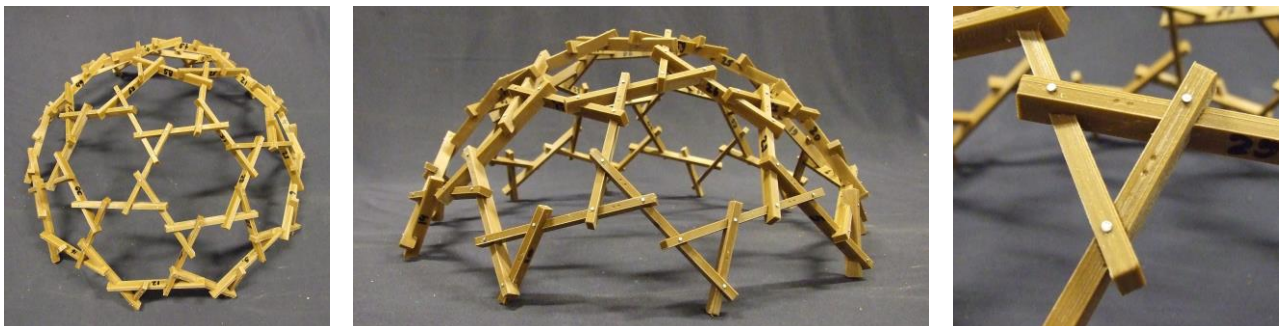


Figure 6.5: 3D printed RF dome with dotted marks on the beams to identify member placement in space

6.3 TRANSFERRING THE RFD TO PRACTICE

The construction sequence used to assemble the RF dome (Figure 6.4), showed that starting at the bottom will create problems at the top. Here a member does not have enough translation freedom to get installed. Consequently, construction of the RF dome needs to be started at the top of the design. Subsequently, members can be inserted by rotation and lifting the RF by for instance a stable and temporary lifting tower. This construction method was also used to construct Buckminster Fullers' Aviodome built in Holland and Hawaii.

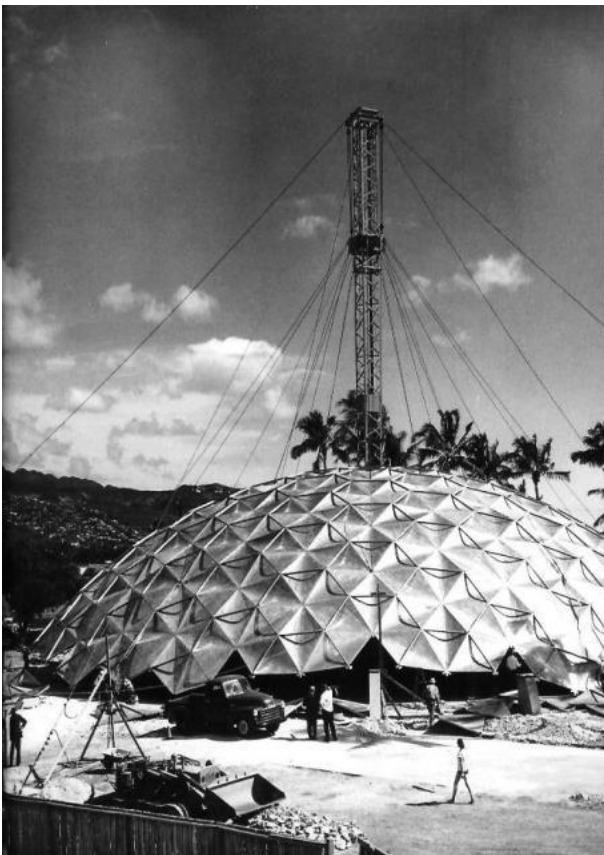


Figure 6.6: Fuller dome construction, Honolulu, Hawaii, 1957

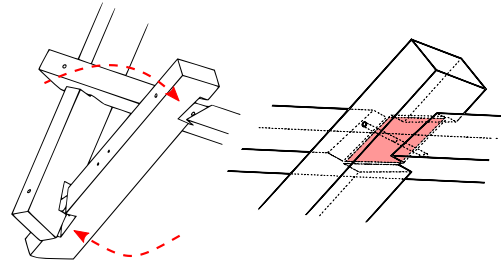


Figure 6.7: Slack in the connection to enable installation

This dome is slowly elevated while simultaneously mounting new construction elements to the dome at ground level. It seems a safe construction method since workers do not have to work at height. Furthermore, the lightweight aluminum does not require heavy lifting and are closely fitting. However, this is in contrast to the RF dome that requires some slack in the connection to be able to rotate the beams into position (Figure 6.7). The required slack size depends on the reciprocal geometry.

Allowing some slack in the connection is also a precautionary measurement to prevent non-fitting joints due to wood swelling and shrinkage caused by moisture and temperature changes. It adds however the drawback that, in order to create structural force transferring, first some connection settlement is required. This settlement can be predicted by varying the scale factor during the design process within the RFD.

A full-scale connection mock-up has been built in corporation with timber industry to determine the slack size and determine connection feasibility. Since, there was no application for a complete dome, a practical application has been found in the form of reciprocal table legs. This model allowed to verify the design to production process and to check the practicality of the RFD and included connection. Although a full-scale model gives great insight, it is advised to first make a 3D printed model by which possible errors become visible. Thus, most errors can be prevented before making a full-scale model.

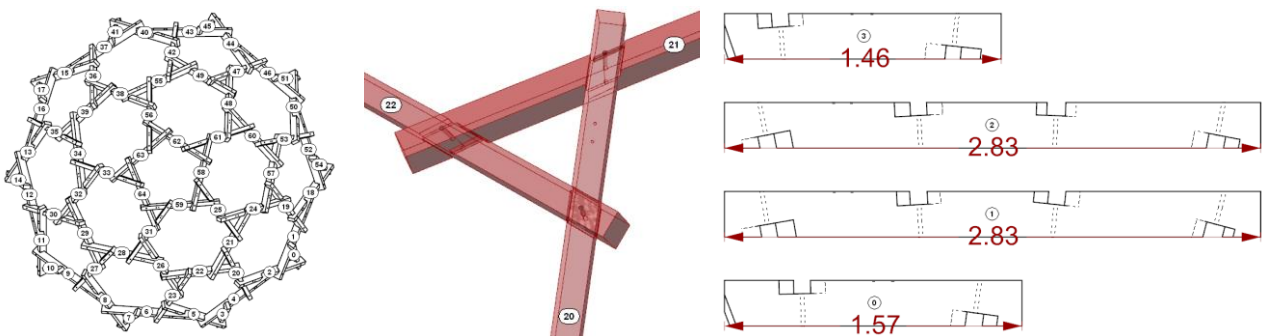


Figure 6.8: Numbering the members and checking measurements



6.3.1 MOCK-UP

The method of first making a 3D printed model and thereafter making a full-scale model has been applied in the fabrication of a connection mock-up. In this process, it is not just a matter of sending the CAD file to the factories' CNC machine. Information need for instance be transferred without data loss and designs have to take machine capabilities into account. It requires the integration of design, engineering, fabrication, and logistics into one seamless process^[21].

INFLUENCE OF CAM ON THE DESIGN

The full-scale mock-up was made at the for this research collaborating timber industry partner Heko Spanten that has two Hundegger machines. Heko has one 4-axis, and one 5-axis Hundegger K2i machine that are fitted with a variety of machining tools including milling tools and drilling equipment. These machines are especially suited to machine timber connections.

The Hundegger machines are originally designed for the German and Austrian timber housing industry and are even capable to handle round timber. For these machines it does not matter whether they handle hundred different, or hundred identical elements. However, for Heko this does matter since they cannot standardize quality control when there is a lack of identical elements. This results in the fact that it is cheaper to produce identical elements.

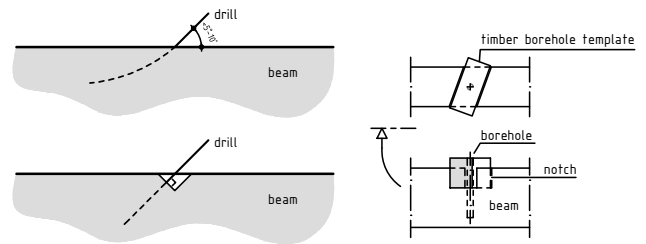


Figure 6.9: The Hundegger machines of Heko cannot drill under angles that are not perpendicular to the beam due to possible drill warping

The proposed connection could have drilled holes at all notch locations depending on the applied roofing that could include bolts. These holes cannot be made by Heko's Hundegger machines that only allow drilling perpendicular to the beam. The capabilities of the machine determine the freedom of connection design.

Drilling with automated machinery under angles smaller than 5 to 10 degrees, may result in curved and unprecise drill holes: the drill may not find directly its correct position. This can be avoided by using a pre-milled hole, or by using a mold (Figure 6.9). Consequently, although the machine can make the notch, manual labor is needed for completion. The relatively simple notch that characterizes the connection can easily be made by the milling tool of the 5-axis Hundegger machine. Its simplicity reduces machine time and thus cost.

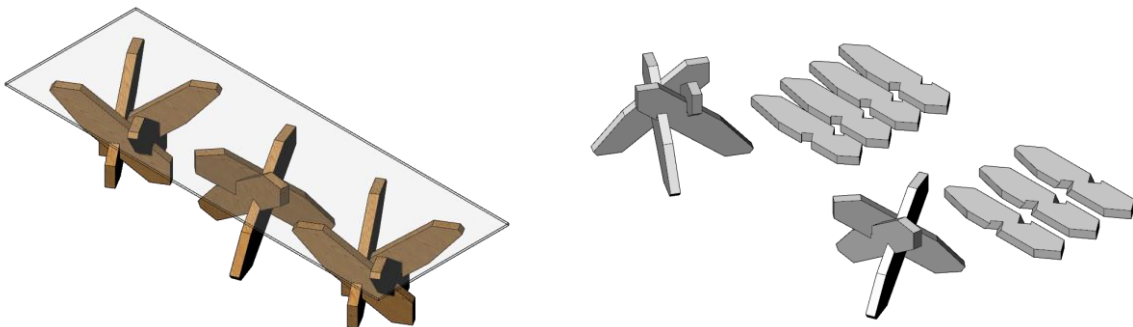


Figure 6.10: Practical application for the connection mock-up

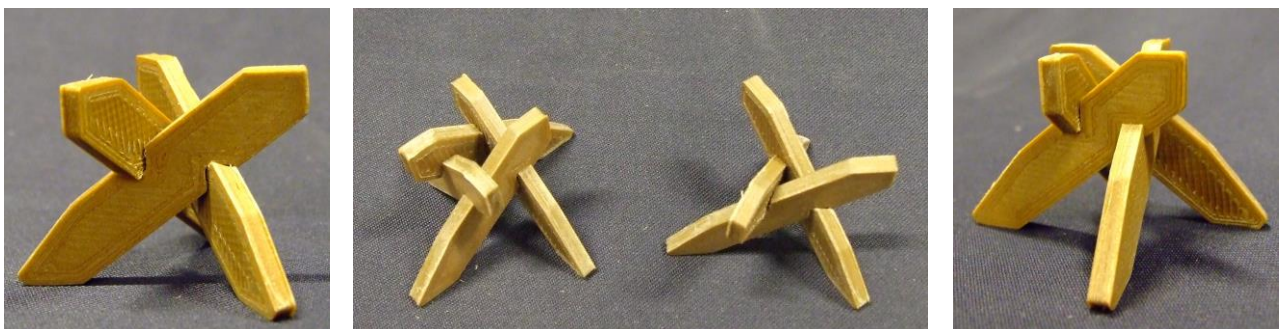


Figure 6.11: 3D print of scaled model before fabrication of full-scale mock-up

6.3.2 TRANSFERRING THE RFD TO CAM

The connection design correlates to the type of machine that is being used. Consequently, in general, it is beneficial when the timber manufacturer is known in the connection design phase. However, the designed connection is relatively simple to manufacture with CAM.

By varying the parameters within the RFD, a preferable design RF can be established. It is preferable, that design changes, that influence the RFs line geometry, are taken in the earliest advance. The further the design process has been developed, the further computational time increases. Increasing data is represented by the amount of geometrical data that needs processing. Lines within the RF need for instance two points in space for specification whereas solid beams need eight points. Including connections adds 32 points to the data increasing computational time when changing parameters in this stage exponentially. The RF dome that is discussed in this chapter takes about 1,5 minutes of calculation time including UC checks.

BAKING AND EXPORTING THE FILES

After all the parameters are adjusted into a satisfying design the model can be 'baked' into Rhino. Baking will transfer the Grasshopper data to a Rhino model making it suited for manual modification, file export, etc.

To be able to transfer this baked NURBS design to CAM software, one need to export the model to a .sat file. This transforms the NURBS geometry of the members into a mesh. The resulting file then needs to be imported into the timber industry standard software 'cadwork'.

Cadwork is used in timber industry to design complete structures suited for CAM. First, after importing the .sat file to cadwork, all members require numbering in which the numbering that is applied in the RFD should be used. Second, by an automated process, the CAM files, suited for Hundeggers Cambium software that controls the machines directly, must be generated (Figure 6.13). Third, nestings that determine machine control based on timber stock and available tools need to be generated within Cambium (Figure 6.12). Hence, a simulation of production can be started.

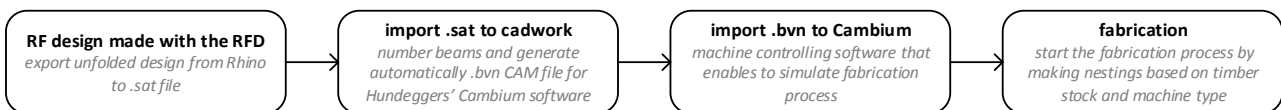


Figure 6.12: Flow diagram to transfer the RFD to practice

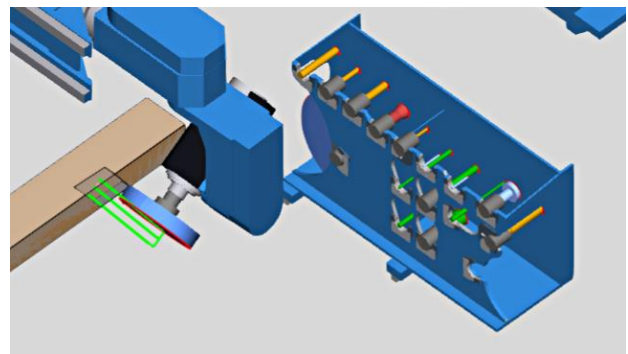
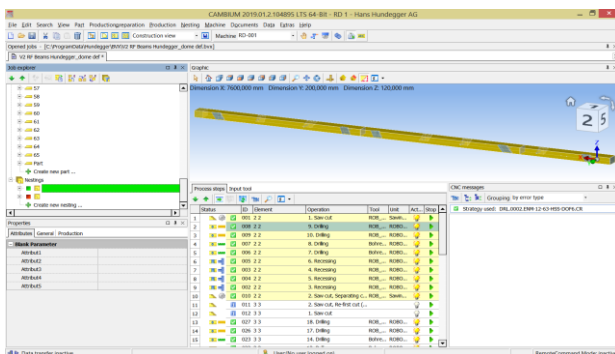


Figure 6.13: Hundeggers' Cambium CAM software showing a nesting and a simulation of the fabrication process using Hundeggers Robot Drive machine



Figure 6.14: Fabrication of the mock-ups with the milling tool of a Hundegger K2i at Heko Spanten



6.4 CONCLUSION

This chapter discussed the design to construction process of the RFD by means of several practical models. It showed that it is possible to manufacture a structural RF design made by means of the RFD with timber industry standard machines.

The simple double notch connection principle reduces machine time and cost. From a structural point of view, a more complex connection could be more preferable but, this also increases machine time and manufacturability that should always be considered.

Therefore, communication with manufacturing parties is a necessity. The available machinery determines to a great extent the practicability of the design (Figure 6.14).

Figure 6.15 shows the full-scale models after the milling and sawing operations performed by the Hundegger machine. To assemble the model a tolerance of at least four millimeters was necessary due to the confined geometry.

Further research with respect to the design to production process can focus on the clustering and generation of identical members and on reducing computational steps.

The research showed that although it is possible to transfer the design to practice, there are still some manual operations between the RFD within Rhino and CAM software. In the future, direct exporting files from Rhino may become possible. A global flow process on how this design process could look is visualized below (Figure 6.16).



Figure 6.15: Full scale mock-up made with Hundegger K2i at Heko Spanten

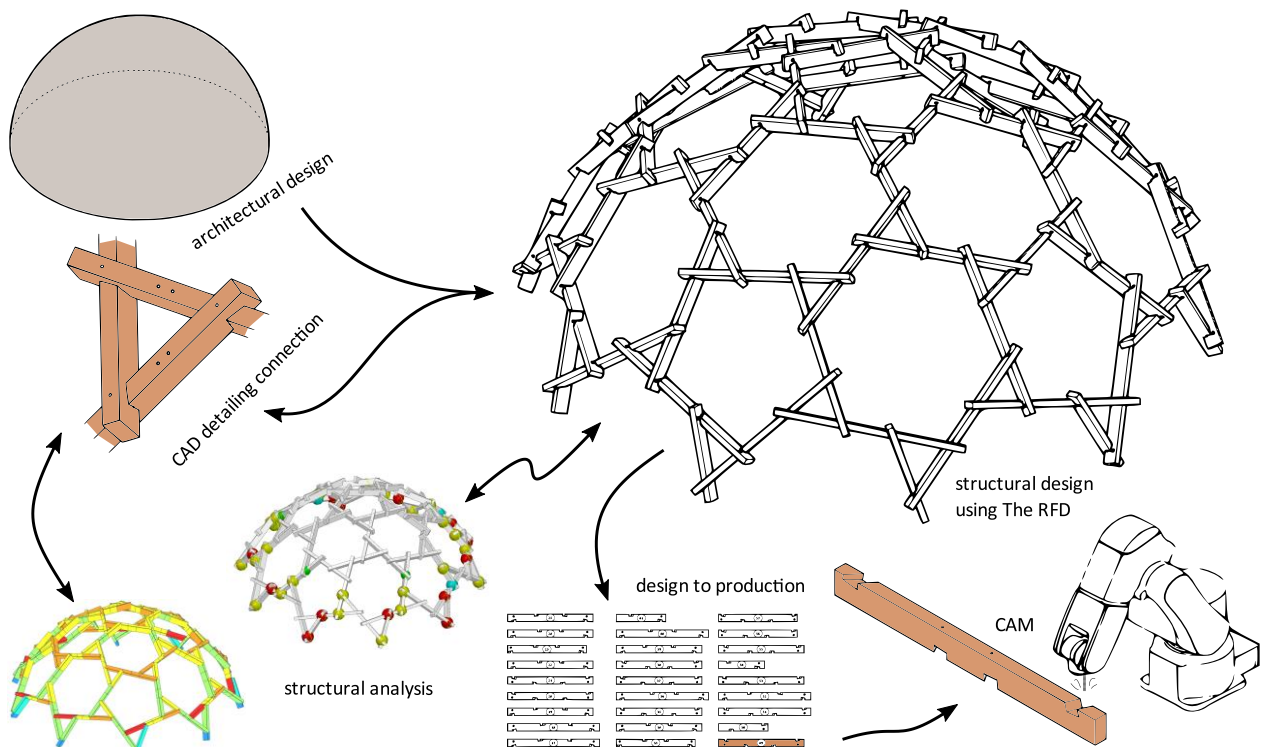
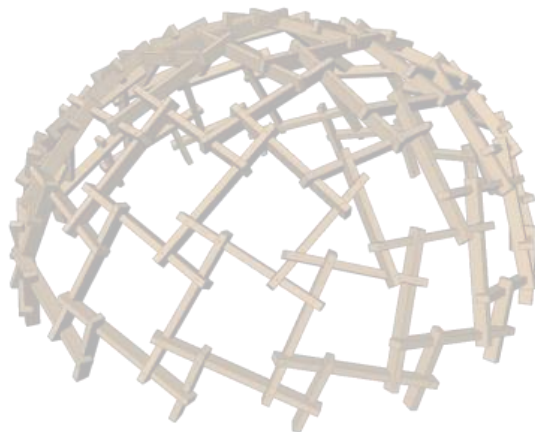
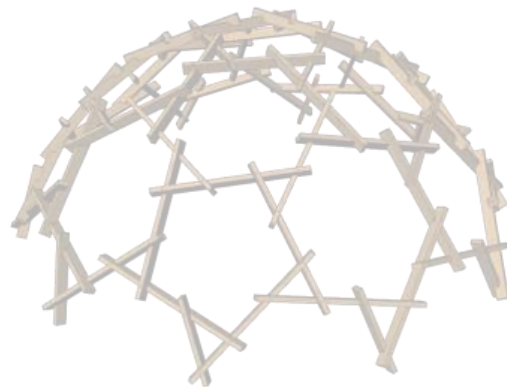
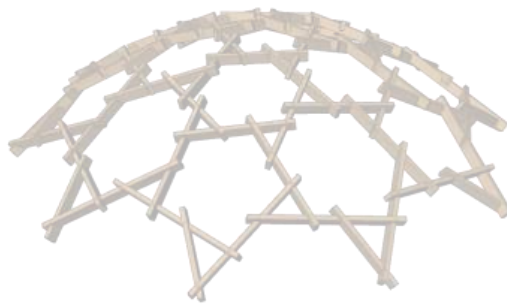


Figure 6.16: Design to production process within the RFD

SUMMARIZING CONCLUSIONS AND RECOMENDATIONS

This chapter presents the conclusions and recommendations based on all previous chapters.





7 SUMMARIZING CONCLUSIONS AND RECOMMENDATIONS

This final chapter discusses the overall conclusions and corresponding recommendations divided per subject. These are based on the in dept and theoretical conclusions described at the ends of all previous chapters.

7.1 CONCLUSIONS

This research presented a complete design to production method for free form Reciprocal Frame (RF) structures. The applied theory is based on the literature study and on new development throughout the research process. This resulted in the creation of the scientific basis for the Reciprocal Frame Designer (RFD) which is this research' final product. Consequently, the stated research goal has been met:

'The goal of this research is to develop a computational design to production tool for vaulted timber reciprocal frame structures using an optimized connection typology and a sustainable timber-based material'

TIMBER

The RF principle lends itself for using residual flows from industrial timber production. Furthermore, timber is a renewable and carbon storing material approving its use in an ecological and sustainable sense with the advent of climate change. Timber in lightweight construction is beneficial considering relative high strength with respect to low density. In this research, glulam timber appeared to be preferable and is used in all RF designs.

Some advantages of RF structures are that they can create curved geometries by using straight members, can span longer distances than the individual member length, can be joined using low tech techniques, and have proven their applicability in times when the availability of materials, especially timber, was scarce. Where historical RF applications seemed to be induced by material shortages, complex examples of today have an investigative and aesthetic function. This research could result in practical timber reciprocal architectures as cutting-edge timber engineering finds more and more practical applications.

RF DESIGN

The complex nature of RFs requires computational design methods to enable structural (FE) analysis, detailing design (CAM), prediction of geometrical configurations, and dimension prediction. In recapitulation, to find the appropriate architectural and structural shape which is designated as form finding. The RFD has been designed to combine all these subjects into one powerful tool. A vital component in the RFD is the eccentricity optimization method.

The developed eccentricity optimization method allows effective and time efficient RF form finding. Changing parameters results in direct geometrical solutions. The RFD has been developed to design three- and four-unit RFs but, could also be used for other RF-unit systems or form finding problems such as the design of tensegrities. The eccentricity optimization method allows to digitally sculpt a structure into the desired shape.

The eccentricity variation analysis showed that eccentricities between RF members influence the force distribution throughout the system. An RF will start to behave as beam grid structure when reducing the eccentricity. Increasing the eccentricity results in greater bending moments.

By comparing the structural behavior of the unit types, three-unit RFs are structurally superior to four-unit RFs. Especially when regarding deformation, four-unit RFs can be easily parallelized without using additional measurements. Three-unit RFs are structurally stable from itself. In fact, four-unit RFs result in a larger amount of material use.

DETAILING

When considering the structural design of RFs at detailing level, relatively small eccentricities and member depths are required when not using notching to create structural height. Notching is unavoidable in RF design and keeps the eccentricity independent on the member depth. It creates structural freedom and enables necessary transferring of shear and axial forces. By applying notches, no steel plate connectors are needed ensuring an RFs benefit of using relatively simple jointing.

This, and the simple notch geometry, reduces machine time and cost. Automated inclusion of the detailing geometry in the structural analysis is however inescapable: every connection could be different. Within the RFD, forces are linked to geometry allowing an implementation of structural checks according to building regulations. These structural checks showed that at material level, the applied glulam may not be the most beneficial material. However, required reinforcement that prevents stress failure perpendicular to the grain is limited.



DESIGN TO PRODUCTION

A more complex detailing principle could be preferable (Figure 7.2) but, this also increases machine time. Manufacturability and required tolerances for assembly should always be considered. Therefore, communication with manufacturing parties during the design state is a necessity when using CAM. The available machinery determines to a great extent the practicability of the design.

Despite the fact that this research showed that it is possible to transfer the design to practice, there are still some manual operations between the RFD within Rhino and the CAM software. Although the computational steps are limited, it is not just a matter of file to factory. Furthermore, the load panel geometry proved to be a workable method enabling to apply area loads to an eccentric RF. This principle however cannot directly be used for roofing and requires further research for implementation in actual roofing applications. Roofing is often project specific and depending on the architectural design.

IN TOTAL

Although, in final analysis, the RFD provides a powerful tool to design a great variety of RFs, it is a standardized tool that works for more or less standard RF designs with similarity between the examples (Figure 7.1). There will never be one tool able to describe all possible design variations. However, architects and engineers are obsessed with inventing new and unprecedented things. This research hopes to contribute to that with the development of the RFD that introduces a new, and top down, design to production tool for Reciprocal Frames. It is just a matter of waiting for practical applications.

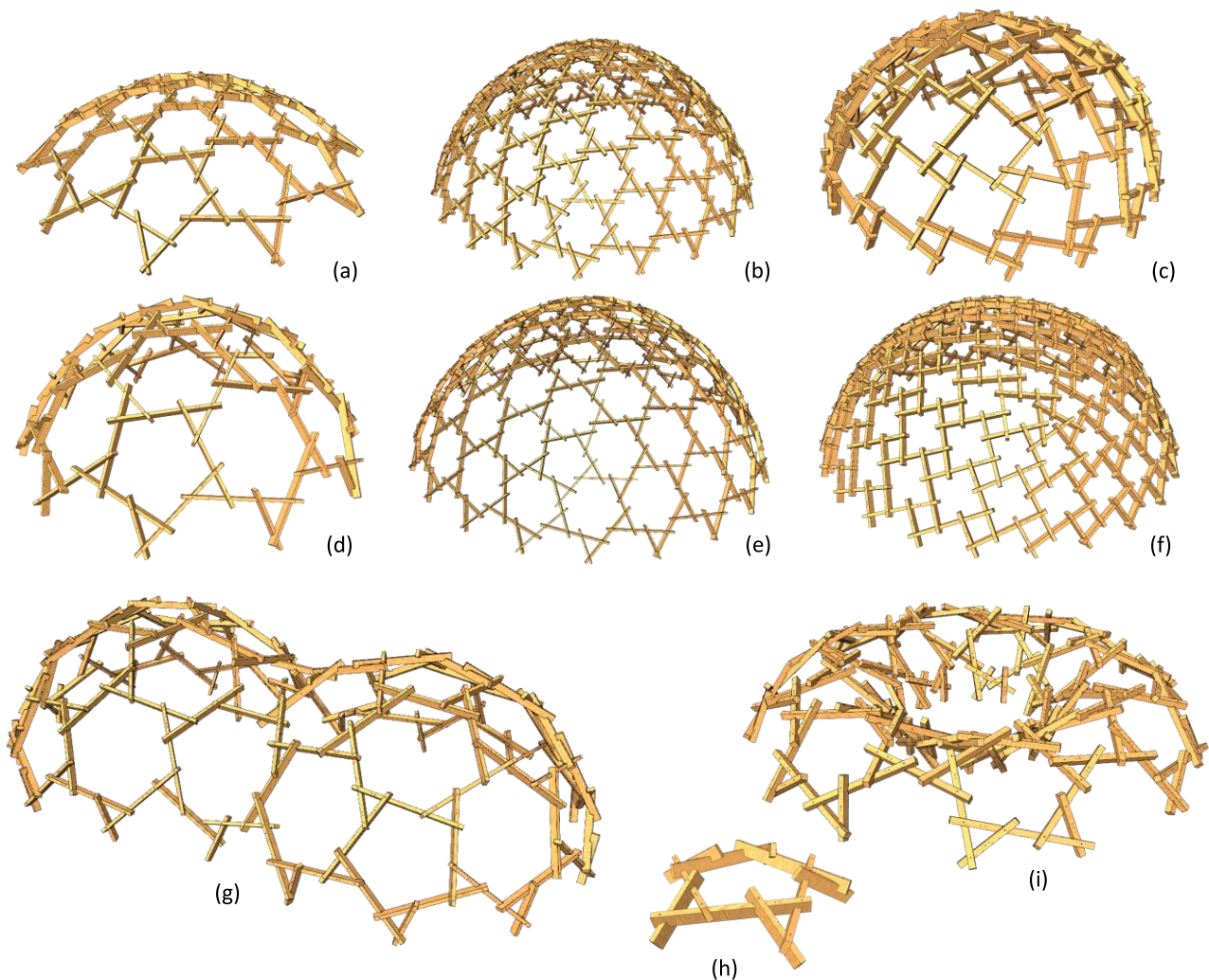


Figure 7.1: Examples of RF designs made with the RFD including detailing. The shapes are based on geodesic icosahedra (a, b, d, e, g, h), geodesic cube (c, f), and a torus (i)

7.2 RECOMMENDATIONS

Future work is encouraged by practical applications and should concentrate on elaborations on the body of work described above. Hence, possible directions are given below in the form of recommendations divided by subject.

TIMBER

The applied glulam timber needs reinforcement because of stresses perpendicular to the grain. Cross Laminated Timber (CLT) however, may be superior to glulam timber due to varying grain direction. Furthermore, CLT can be sawn in varying cross sections depending on the structural need which could improve structural efficiency and material use. This requires further research.

RF DESIGN

The proposed eccentricity optimization technique enables to design feasible RF designs and may be transferable to other form finding problems where digitally sculpting is required. An illustrative problem that requires further research could be found in tensegrity form finding. Here, a structural balance exists between compression and tension elements.

This in contrast with RFs which transfer its forces primarily through bending. Changing the parameters such as the scale factor and eccentricity will have an influence on the force distribution throughout an RF. The effect of overall changing these has been discussed in this research but, what the influence is when individually changing these parameters yet remains unclear and requires further research. Perhaps, parameters can be automatically changed based on force flow achieving a kind of structural optimization within the RFD.

In this respect, one can furthermore improve the RFD by increasing the possible RF designs by adding other RF-unit systems and by combining them. Hence, three- and four-unit RFs can for instance be combined which is not yet possible with the RFD. To achieve this, research should focus on surfaces subdivisions or paneling methods applied to different polygonal shapes. The member configuration and unit style depend on the subdivision geometry.

DETAILING

The detailing calculations show that compression perpendicular to the grain and axial tension are the governing failure mechanisms. Although the simple notching reduces machine time and simplifies construction, a more complex detailing could be beneficial. Figure 7.2 furthermore proposes two alternatives that in further research could be supplemented with possible roofing methods. Within this detailing, the effect of adding surface fasteners could be analytically investigated and proven by numerical or experimental research. These detailing alternatives however may increase complexity, machinability and practicability.

DESIGN TO PRODUCTION

Machine learning could reduce computational complexity and can be used on the clustering of identical members. Although the used Hundegger machines do not care whether they make hundred identical or similar parts, people who check member dimensions do care due to labor intensity. Machine learning can identify patterns in data to predict outcomes. However, identical members can also be found by using geometrical rules. This should be investigated.

In addition to this, the design to production process is not yet seamless. Errors could evolve at converging points between the different software. Further research should therefore focus on reducing the number of import and export steps. Rhino Inside is currently being developed and allows direct interaction between external software such as Revit. Therefore, it is just a matter of time before industry simplifies data exchange and finds a universal language.

A computational model however, will always stay an abstraction of reality. Therefore, it is advised to always make scale models by 3D printing or other techniques to verify the design to production process and dimensions. This has been proved with the RFD by which the author hopes to contribute to a new generation of timber design.

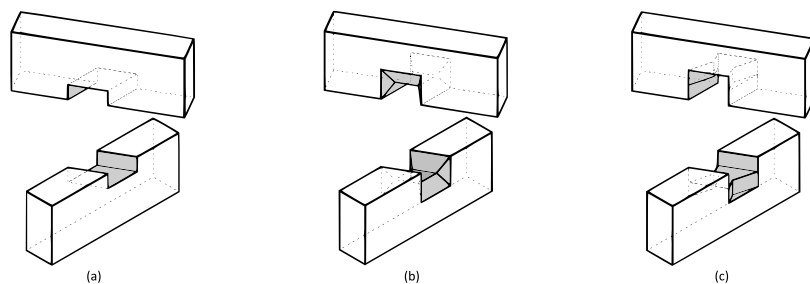


Figure 7.2: Alternative detailing (b, c) on the originally developed notching principle (a)



8 BIBLIOGRAPHY

8.1 REFERENCES

- [1] Thönnissen U. Hebelstabwerke / Reciprocal Frameworks Tradition und Innovation / Tradition and Innovation. Bilingual. Zürich: gta publishers; 2015.
- [2] Menges A, Schwinn T, Krieg OD. Advancing Wood Architecture: A Computational Approach. 2016. doi:10.4324/9781315678825.
- [3] Pugnale A, Sassone M. Structural Reciprocity: Critical Overview and Promising Research/Design Issues. Nexus Netw J 2014;16:9–35. doi:10.1007/s00004-014-0174-z.
- [4] Paris V, Pizzigoni A, Ruscica G. Brunelleschi 's herringbone hidden reciprocal structure and the form finding of its self-supporting bricks. Proc IASS Annu Symp 2017 2017.
- [5] Larsen OP. Reciprocal Frame Architecture. First edit. Oxford: Architectural Press - Elsevier; 2008.
- [6] Douthe C, Mesnil R, Baverel O, Gobin T, Tellier X. Design and construction of a shell-nexorade hybrid timber structure 2018:1–8.
- [7] Rizzuto JP, Popovic Larsen O. Connection Systems in Reciprocal Frames and Mutually Supported Elements Space Structure Networks. Int J Sp Struct 2010;25:243–56. doi:10.1260/0266-3511.25.4.243.
- [8] Pugnale A, Parigi D, Kirkegaard PH, Sassone M. The principle of structural reciprocity: history, properties and design issues. IABSE-IASS 2011 2011:414. doi:10.1007/s00004-014-0174-z.
- [9] Anastas Y, Rhode-Barbarigos L, Adriaenssens S. Design-to-Construction Workflow for Cell-Based Pattern Reciprocal Free-Form Structures. IASS 2016;57:159–76. doi:10.20898/j.iass.2016.188.737.
- [10] Veenendaal D, Block P. An overview and comparison of structural form finding methods for general networks. Int J Solids Struct 2012;49:3741–53. doi:10.1016/j.ijsolstr.2012.08.008.
- [11] Sénéchal B, Douthe C, Baverel O. Analytical Investigations on Elementary Nexorades. IASS 2011;26:313–20. doi:10.1260/0266-3511.26.4.313.
- [12] Rizzuto JP. Eccentricity Orientation of Bolted Connections in Space Structure Configurations Using Reciprocally Supported Elements. IASS 2014;1:49–62.
- [13] Gherardini F, Leali F. Reciprocal Frames in Temporary Structures: An Aesthetical and Parametric Investigation. Nexus Netw J 2017. doi:10.1007/s00004-017-0352-x.
- [14] Song P, Fu C-W, Goswami P, Zheng J, Mitra NJ, Cohen-Or D. Reciprocal frame structures made easy. ACM Trans Graph 2013;32:10. doi:10.1145/2461912.2461915.
- [15] Parigi D, Kirkegaard P, Sassone M. Hybrid optimization in the design of reciprocal structures. IASS-APCS 2012 Proc from Spat Struct to Spaces Struct 2012:8.
- [16] Baverel O. Nexorades: A family of interwoven structures - Phd. thesis. University of Surrey, 2000.
- [17] Douthe C, Baverel O. Design of nexorades or reciprocal frame systems with the dynamic relaxation method. Comput Struct 2009;87:1296–307. doi:10.1016/j.compstruc.2009.06.011.
- [18] Kilian A, Ochsendorf J. Particle-spring systems for structural form finding 2006:77–84.
- [19] Piker D. Kangaroo: Form finding with computational physics. Archit Des 2013;83:136–7. doi:10.1002/ad.1569.
- [20] Preisinger C, Arts A, Design S. Karamba — A Toolkit for Parametric Structural Design 2014. doi:10.2749/101686614X13830790993483.
- [21] Scheurer F, Stehling H. Lost in parameter space? Archit Des 2011;81:70–9. doi:10.1002/ad.1271.
- [22] Brocato M. Reciprocal Frames: Kinematical Determinacy and Limit Analysis. Int J Sp Struct 2011;26:343–58. doi:10.1260/0266-3511.26.4.343.
- [23] Jorissen AJM. Introduction to Timber Structures. 1st ed. Eindhoven: Eindhoven University of Technology; 2015.



- [24] Garavaglia E, Pizzigoni A, Sgambi L, Basso N. Collapse behaviour in reciprocal frame structures. *Struct Eng Mech* 2013;46:533–47. doi:10.12989/sem.2013.46.4.533.
- [25] Swedish Forest Industries Federation. Design of timber structures - Volume 1. vol. 1. 2015.
- [26] EN BS. 1-1: Eurocode 5: design of timber structures--Part 1--1: General--Common rules and rules for buildings. CEN, Brussels, Belgium 2004.
- [27] Bucher A, Hengesbach W. Fischer Power-Fast Screws and Fischer Construction Screws. Waldachtal: 2016.

8.2 FIGURES

FIGURE 1.1: THE STRUCTURAL PRINCIPLE OF A RECIPROCAL FRAME (RF) ASSEMBLY PORTRAYED BY NUMEROUS PEOPLE

Reprinted from 'An amiable vicious circle' from *Vicious Circles and Infinity: An Anthology of Paradoxes* by P Hughes and G Brecht, Penguin (1978).

HEADER LITERATURE

Digitally Fabricated Lamella Structure ©2017 Agustín Dieste

Figure 2.2: Early RF designs by Leonardo da Vinci - approx. 1235 AD (Left) and Villard de Honnecourt - approx. 1225 AD (right)

Thönnissen U. Hebelstabwerke / Reciprocal Frameworks Tradition und Innovation / Tradition and Innovation. Bilingual. Zürich: gta publishers; 2015.

Figure 2.3: Reciprocal frame history timeline. Years may be approximations

Photo A: Neolithic house at Bampo. Build around 4,000 BC 2008. <http://humanpast.net/shelter/shelter4k.htm> (accessed August 13, 2018).

Photo B-G, I-P, S: Thönnissen U. Hebelstabwerke / Reciprocal Frameworks Tradition und Innovation / Tradition and Innovation. Bilingual. Zürich: gta publishers; 2015.

Photo H: Pugnale A, Sassone M. Structural Reciprocity: Critical Overview and Promising Research/Design Issues. *Nexus Netw J* 2014;16:9–35. doi:10.1007/s00004-014-0174-z.

Photo Q: Douthe C, Mesnil R, Baverel O, Gobin T, Tellier X. Design and construction of a shell-nexorade hybrid timber structure 2018:1–8.

Photo R: KREOD Pavilion, London Olympics, Format Engineers. Retrieved November 1, 2017 from <http://formatengineers.com/projects/kreod-pavilion.html>. Copyright 2015 Format Engineers Ltd.

Photo T: Photo by Arjen Deetman ©2018

Figure 2.4: Reciprocal art structure made with laminated bamboo strips, designed by Shigeru Ban

Shigeru Ban Bamboo Roof. Rice Gall 2003. <http://www.ricegallery.org/shigeru-ban/> (accessed October 16, 2018).

Figure 6.6: Fuller dome construction, Honolulu, Hawaii, 1957

THE HILTON DOME, AND THE FIRST OF ITS KIND IN THE WORLD, WENT UP IN JUST 24 HOURS AT THE CORNER OF KALIA ROAD AND ALA MOANA BOULEVARD 2014. [HTTP://WWW.TIKIROOM.COM/TIKICENTRAL/BB/VIEWTOPIC.PHP?TOPIC=47716&FORUM=2](http://www.tikiroom.com/tikicentral/bb/viewtopic.php?topic=47716&forum=2) (ACCESSED APRIL 16, 2019).

ANNEX AND APPENDIX

9 ANNEX 1 : COMPARISON STRUCTURAL DIMENSIONS RF3, RF4 CONFORM EUROCODE 5

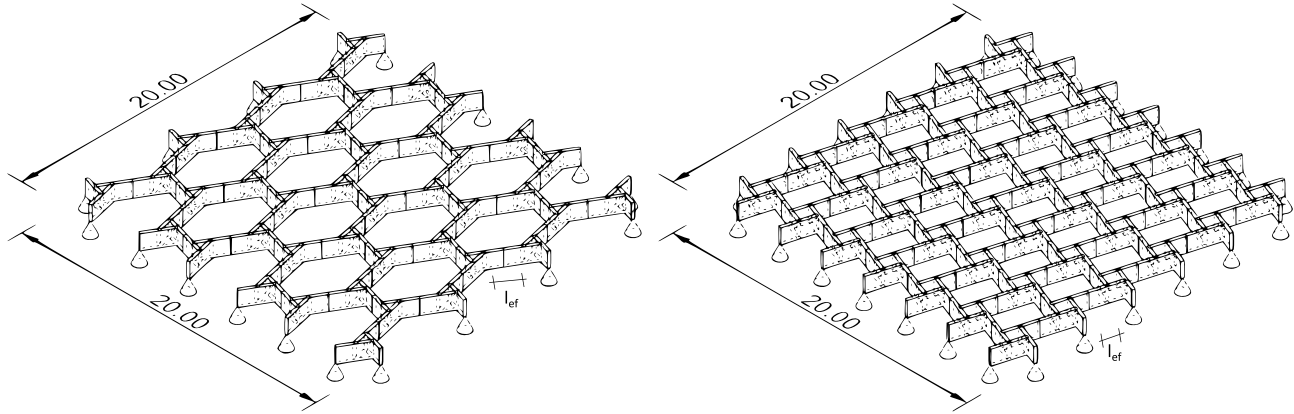


Figure 9.1: Design and dimensions RF3 (left) and RF4 (right)

9.1.1 MATERIAL PROPERTIES

The characteristic strength and stiffness properties for homogenous gleulam GL24h are:

| | | | |
|---------------------------|---|---|--------------------------|
| $f_{m,g,k} = f_{c,0,g,k}$ | = | Bending strength = compression strength | 24 N/mm ² |
| $f_{t,0,g,k}$ | = | Tension strength | 16,5 N/mm ² |
| $f_{v,g,k}$ | = | Shear strength | 2,7 N/mm ² |
| $E_{0,g,mean}$ | = | Modulus of elasticity | 11 600 N/mm ² |
| $G_{g,mean}$ | = | Shear modulus | 720 N/mm ² |
| $\rho_{g,k}$ | = | Density | 380 kg/m ³ |

The design value of the bending strength for the Ultimate Limite State (ULS) calculation is determined by:

$$\begin{aligned}
 f_{m,g,d} &= \text{Design value bending strength} \\
 &= \frac{f_{m,g,k}}{\gamma_m} k_{mod} k_h k_l \\
 &= \mathbf{17,3 \text{ N/mm}^2}
 \end{aligned}$$

In which:

| | | | |
|-------------|---|--|---------------------------------------|
| $f_{m,g,k}$ | = | Characteristic bending strength GL24h | In this case: 24 N/mm ² |
| γ_m | = | Partial factor for glued laminated timber | 1,25 |
| k_{mod} | = | Modification factor considering load duration and humidity. Climate class: 1 (indoor). Load duration class: Short (wind/snow load on roof) | 0,9 |
| k_h, k_l | = | Volume factors depending on element dimensions | 1,0 |

The volume factors k_h and k_l must be applied to brittle behaving timber elements in tension and/or bending covering possible force distribution. For laminated wood they are determined by:

$$\begin{aligned}
 k_h, k_l &= \text{Height and length factor. The height factor } k_h \text{ has to be used in bending and the length factor } k_l \text{ has to be used in tension situations for LVL.} \\
 &= 1,0 \leq k_h = \left(\frac{600}{h} \right)^{0,1} \leq 1,3 \\
 k_h &= \mathbf{1,0}
 \end{aligned}$$

In which:

| | | |
|-----------|---|-----------------------|
| h_{ref} | = | Reference beam height |
|-----------|---|-----------------------|

In this case:
1,0 m



The reference beam height h_{ref} is calculated by means of the rule of thumb for simply supported timber roof structures:

$$\begin{aligned} h_{ref} &= L_{span}/19 \quad \vee \quad b_{ref} = h_{ref}/5 \\ &= \mathbf{1,0 \, m} \end{aligned}$$

In which:

$$\begin{aligned} L_{span} &= \mathbf{\text{Length of span}} \\ b_{ref} &= \mathbf{\text{Reference beam width} = } h_{ref}/5 \end{aligned}$$

In this case:

$$\begin{aligned} &\mathbf{20,0 \, m} \\ &\mathbf{0,2 \, m} \end{aligned}$$

9.1.2 LOADS

The structures 3RF and 4RF are being loaded by a uniformly distributed and theoretical load of:

$$\begin{aligned} q_d = G_d + Q_d &= \mathbf{\text{Design value of the theoretical design load consisting of the static load } G_d \text{ and the variable load } Q_d} \\ &= \mathbf{5,0 \, kN/m^2} \end{aligned}$$

9.1.3 DETERMINATION OF STRUCTURAL DIMENSIONS IN ULS

The required beam height in the Serviceability Limit States (SLS) is normally determined by the characteristic load q_k and the stated deformation requirement. Since this requirement is not mandatory conform EC2 but project specific, the beam dimensions resulting from the ULS calculation are taken into account. However, when considering a deformation requirement of $u_{max} \leq L_{span}/250 = 80 \, mm$ could lead to normative beam dimensions (avoidable by adding precambers during manufacturing). For the maximum bending moments and force distribution see 0 and 9.1.5.

ULS RF3

The required beam height in the ULS for the RF3 system is:

$$\begin{aligned} h_{b,3RF} &= \mathbf{\text{Required beam height 3RF}} \\ &\geq \sqrt{\frac{6 \cdot M_{yd}}{b \cdot f_{m,g,d}}} \quad \left(W = \frac{1}{6}bh^2 \quad \wedge \quad \sigma_d = f_{m,g,d} = \frac{M_{yd}}{W} \rightarrow h_{b,3RF} \right) \\ &= \mathbf{1,0 \, m} \end{aligned}$$

In which:

$$\begin{aligned} M_{yd} &= \mathbf{\text{Maximum bending moment } M_y \text{ in the ULS (Figure 9.5)}} \\ b_{ref} &= \mathbf{\text{Preferable beam width } \approx h_{ref}/5} \end{aligned}$$

In this case:

$$\begin{aligned} &\mathbf{630 \, kNm} \\ &\mathbf{0,22 \, m} \end{aligned}$$

ULS RF4

The required beam height in the ULS for the RF4 system is:

$$\begin{aligned} h_{b,4RF} &= \mathbf{\text{Required beam height 4RF}} \\ &\geq \sqrt{\frac{6 \cdot M_{yd}}{b \cdot f_{m,g,d}}} \quad \left(W = \frac{1}{6}bh^2 \quad \wedge \quad \sigma_d = f_{m,g,d} = \frac{M_{yd}}{W} \rightarrow h_{b,4RF} \right) \\ &= \mathbf{0,94 \, m} \end{aligned}$$

In which:

$$\begin{aligned} M_{yd} &= \mathbf{\text{Maximum bending moment } M_y \text{ in the ULS (Figure 9.11)}} \\ b_{ref} &= \mathbf{\text{Preferable beam width } \approx h_{ref}/5} \end{aligned}$$

In this case:

$$\begin{aligned} &\mathbf{450 \, kNm} \\ &\mathbf{0,18 \, m} \end{aligned}$$

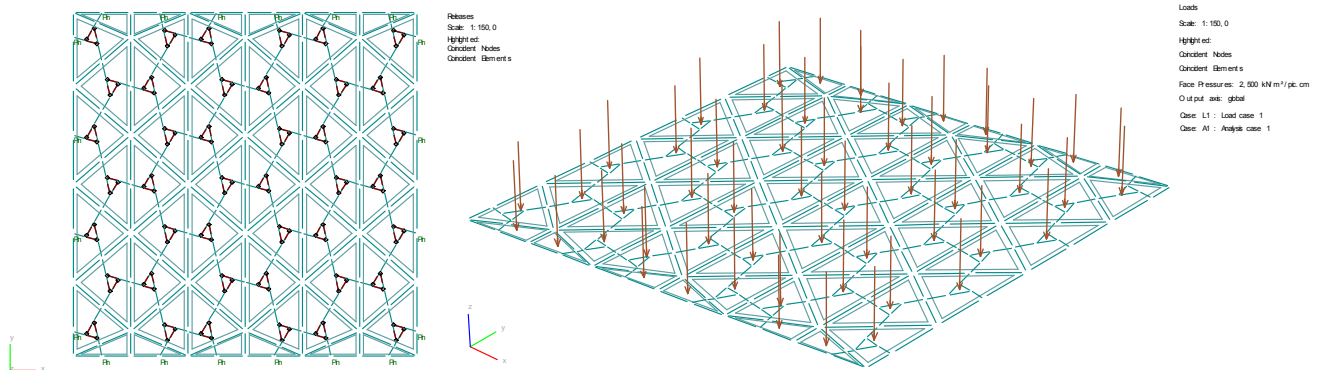
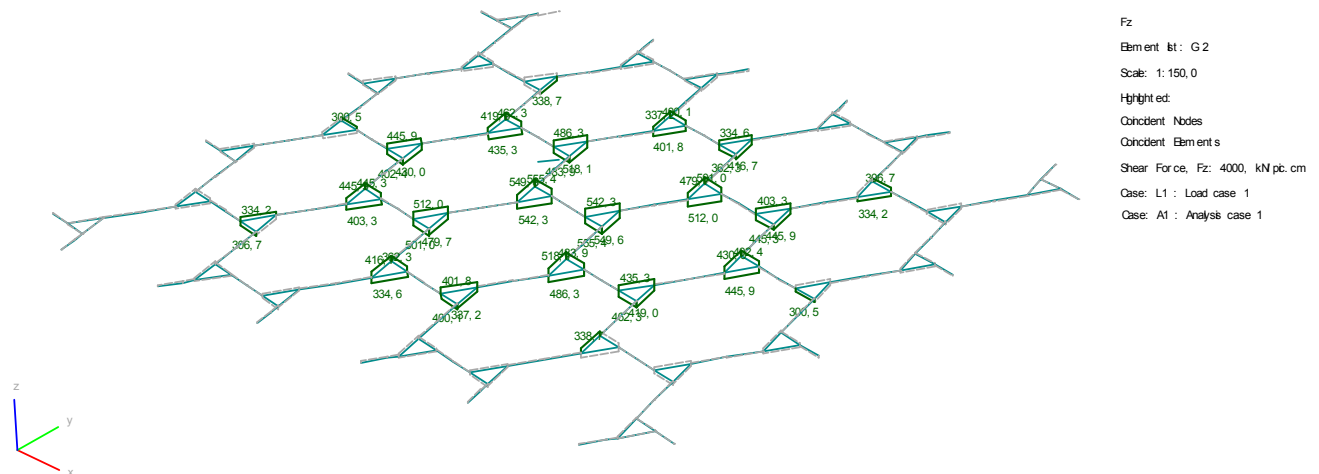
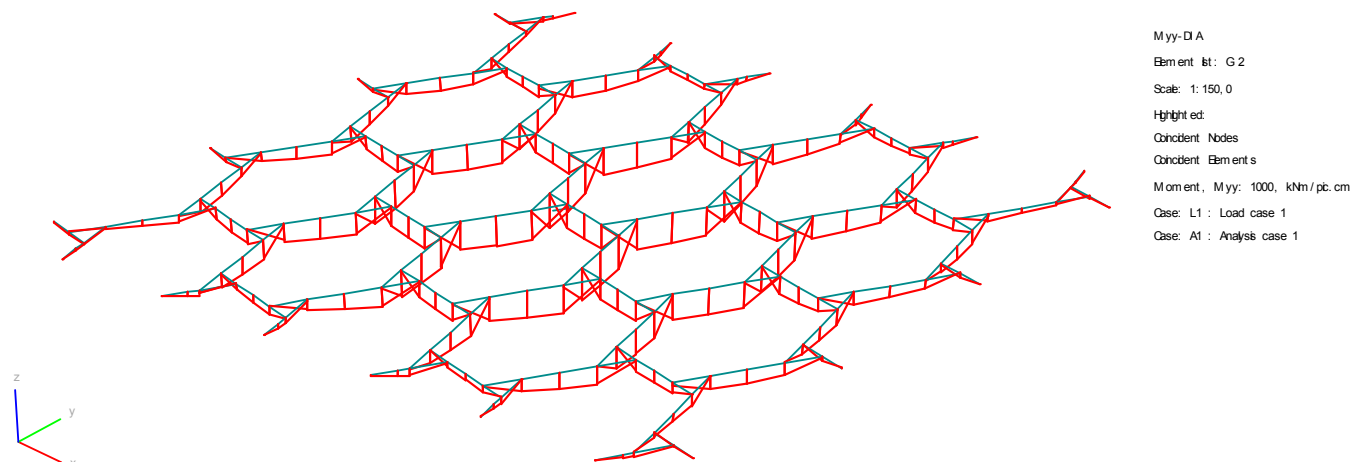
TOTAL

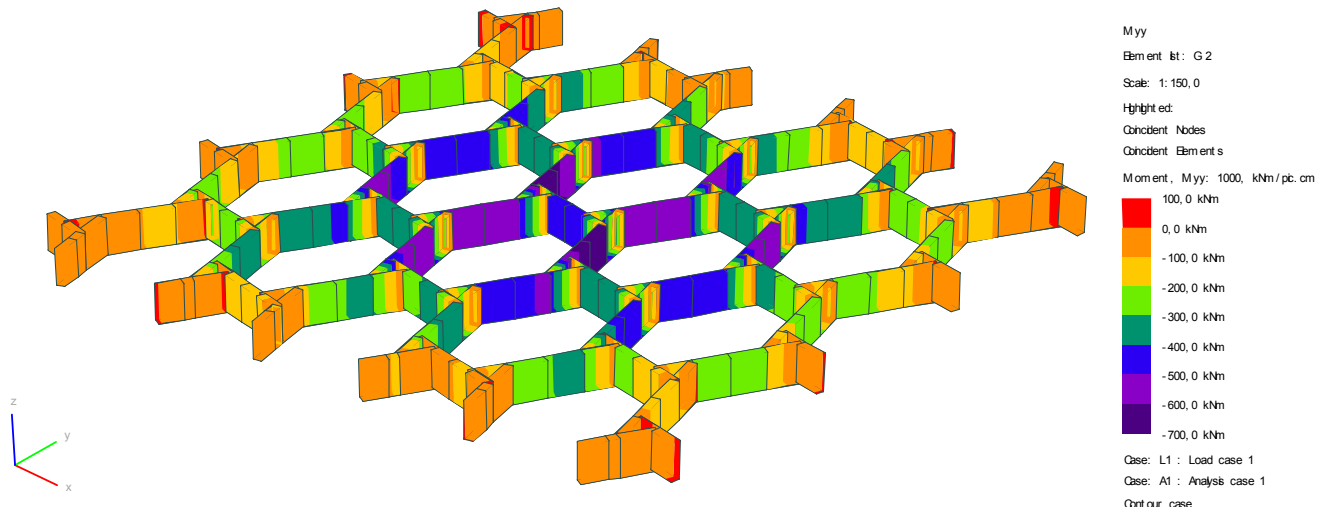
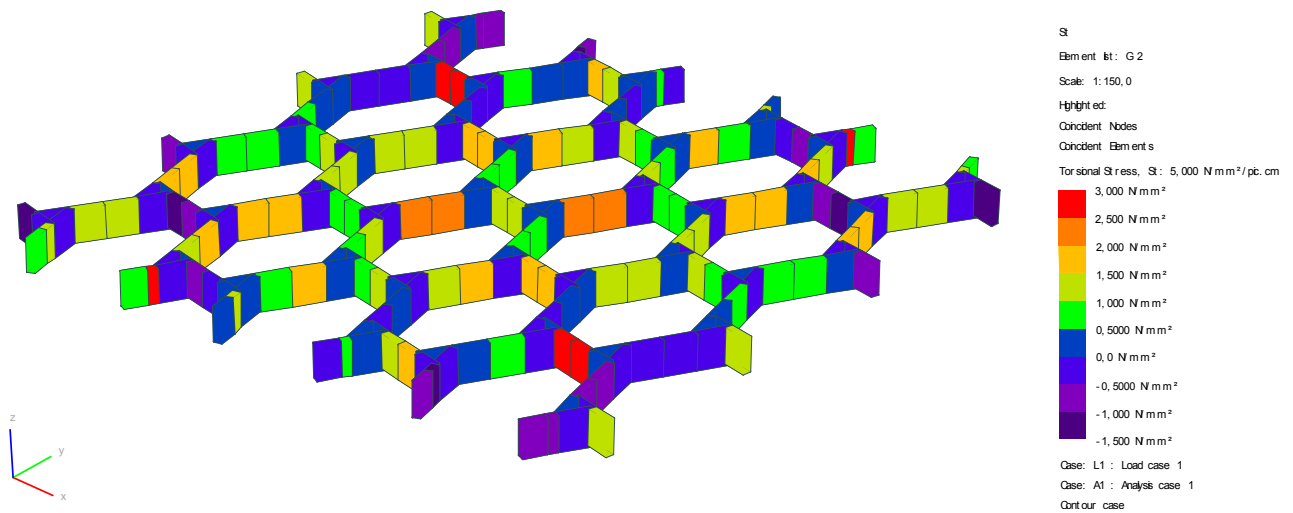
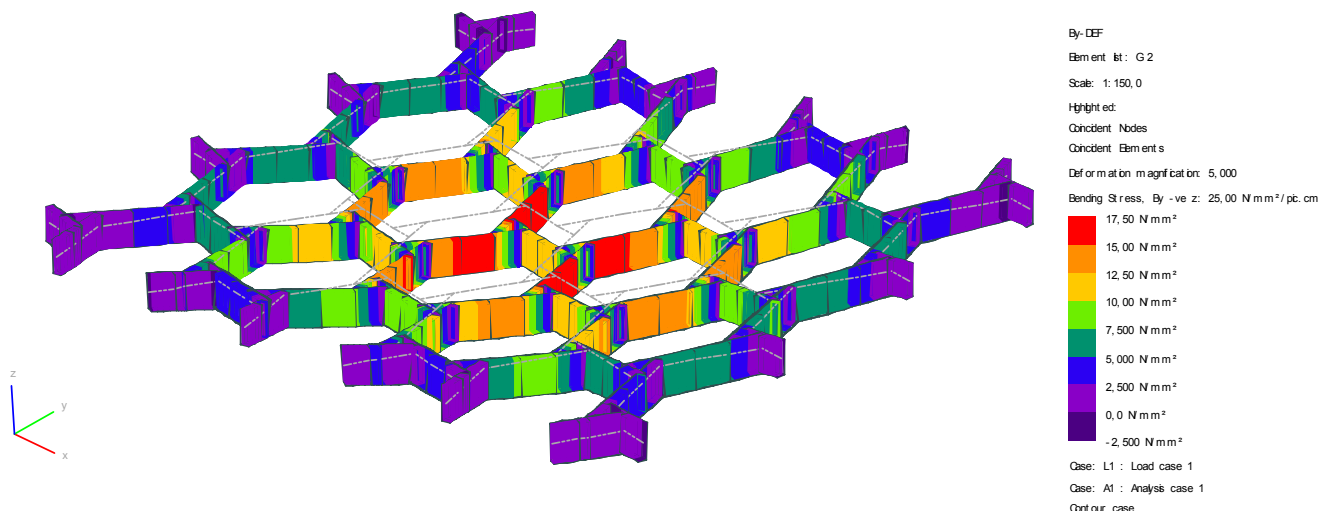
The total volumes of required GL24h are for both systems:

$$\begin{aligned} V_{RF3} &= A_{beam} \cdot L_{total} = 0,22 \cdot 1,0 \cdot 229,8 &= \mathbf{50,6 \, m^3} \\ V_{RF4} &= A_{beam} \cdot L_{total} = 0,18 \cdot 0,94 \cdot 329,2 &= \mathbf{55,7 \, m^3} \\ \text{Difference} &= V_{RF4} - V_{RF3} = 55,7 - 50,6 &= \mathbf{5,1 \, m^3} \\ \text{Percentual diff.} &= |V_{RF3} - V_{RF4}| / \left(\frac{1}{2}(V_{RF3} + V_{RF4}) \right) &= \mathbf{9,6 \, \%} \end{aligned}$$



9.1.4 GSA DATA RF3

Figure 9.2: Joint definitions and 2D load panels including supporting structure ($q = 5,0 \text{ kN/m}^2$)Figure 9.3: Major shear forces $300 \text{ kN} < F_z < 500 \text{ kN}$ Figure 9.4: Course of bending moment M_y

Figure 9.5: Bending moment distribution M_y Figure 9.6: Torsional stress distribution T_s for a beam dimension of $220 \times 1000 \text{ mm}^2$ Figure 9.7: Deformed bending stress distribution B_y for a beam dimension of $220 \times 1000 \text{ mm}^2$



9.1.5 GSA DATA 4RF

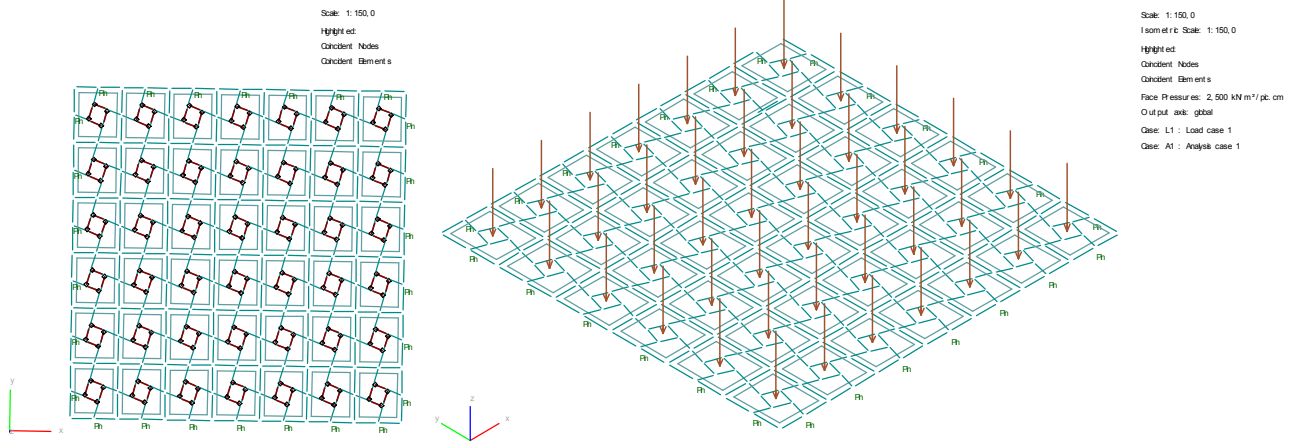


Figure 9.8: Joint definitions and 2D load panels including supporting structure ($q = 5,0 \text{ kN/m}^2$)

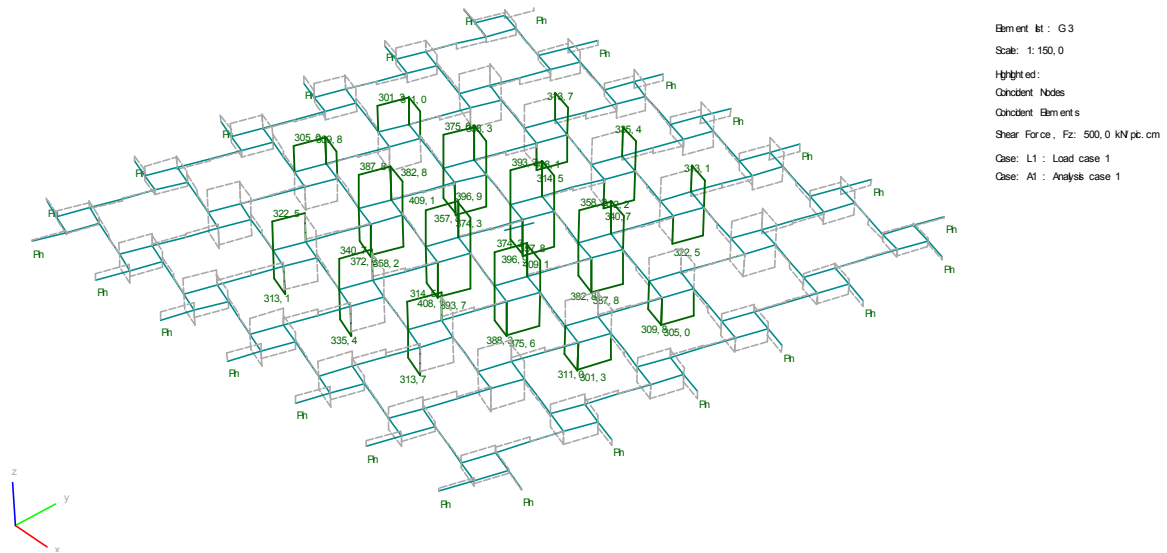


Figure 9.9: Major shear forces $300 \text{ kN} < F_z < 450 \text{ kN}$

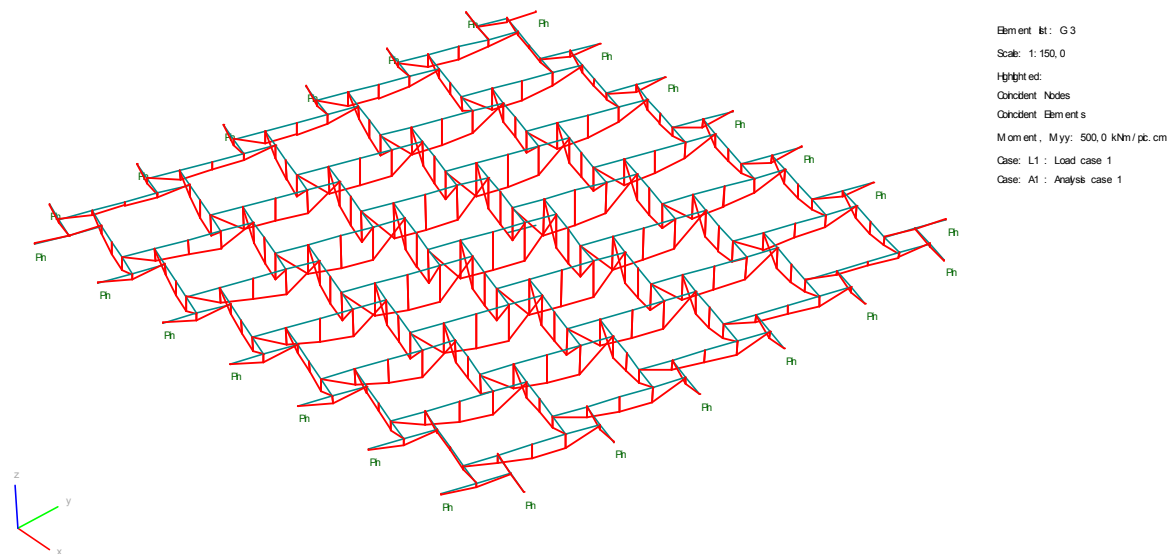


Figure 9.10: Course of bending moment M_y

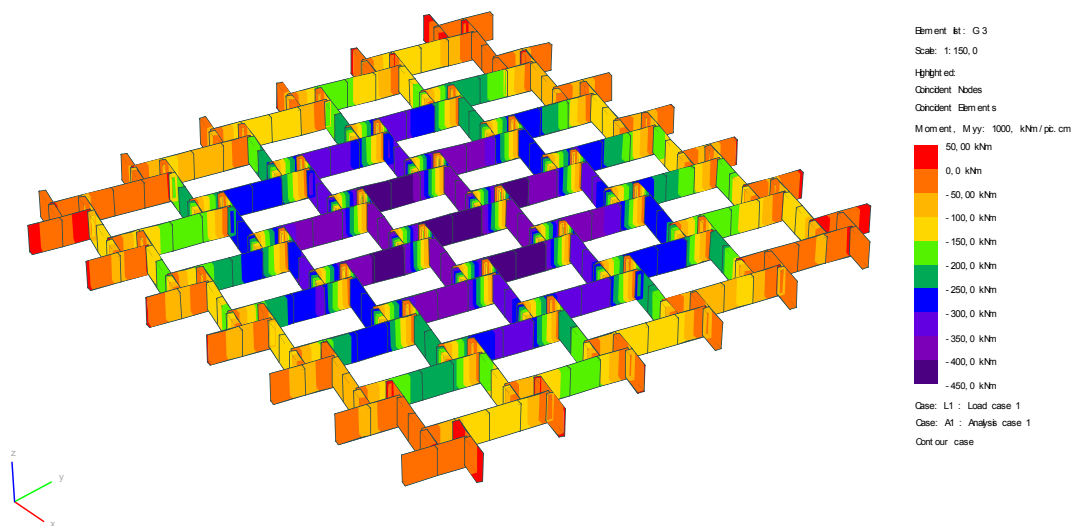


Figure 9.11: Bending moment distribution M_y

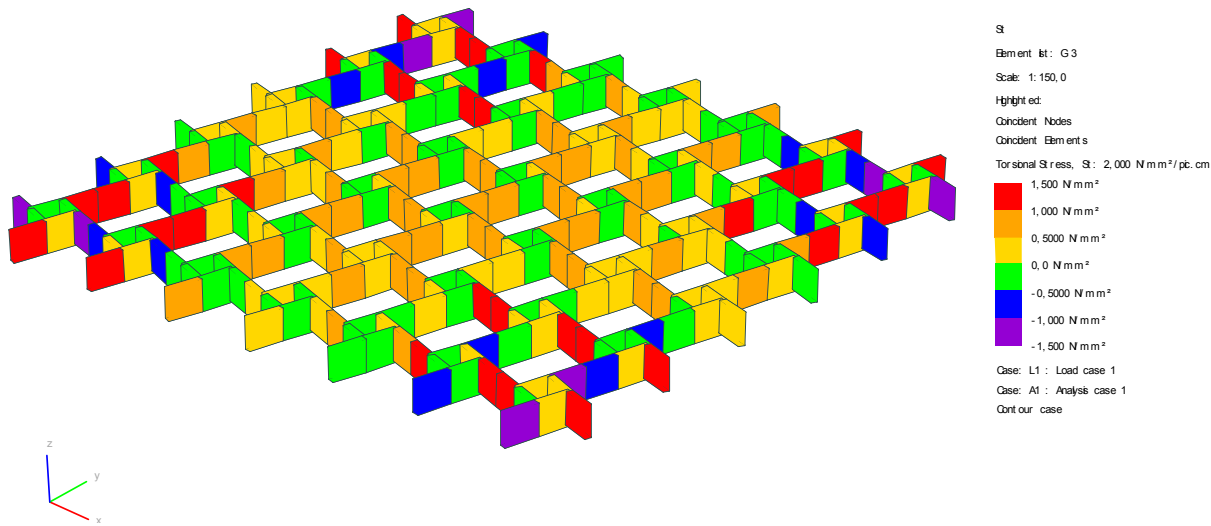


Figure 9.12: Torsional stress distribution T_s

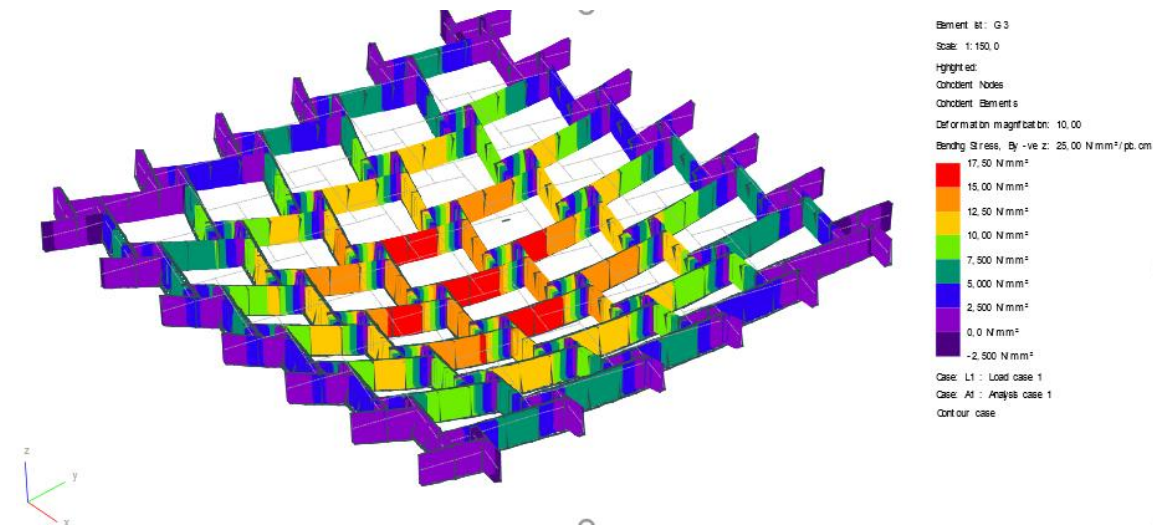


Figure 9.13: Deformed bending stress distribution B_y for a beam dimension of $180 \times 940 \text{ mm}^2$



9.1.6 ULS CHECKS

A torsional moment is acting on the main beams of the RF3 and RF4 structures in addition to the bending moment acting in y-direction. The magnitude of this torsional moment is low in comparison to the bending moment in y-direction. Nevertheless, it should be determined whether the determined structural beam dimensions are able to resist this moment. Furthermore, the beams' capacity against lateral torsional buckling that can occur between two neighboring and connected beams is checked.

LATERAL TORSIONAL BUCKLING RF3

Lateral torsional buckling can only occur between two bracing and adjacent beams who, in this system, always have a center to center distance of $l_{ef} = 2,0m$ (Figure 9.1). The formulation below shows whether the maximum bending stress can be achieved without creating this phenomena:

$$\begin{aligned}\sigma_{m,crit} &= \text{Critical bending stress of a beam bent about its strong axis} \\ &= \frac{0,78 \cdot b^2}{h \cdot l_{ef}} E_{0,9,05} \\ &= \mathbf{227,5 \text{ N/mm}^2}\end{aligned}$$

In which:

$$\begin{aligned}b, h &= \text{Beam width and height} \\ l_{ef} &= \text{Center to center distance of the bracing beams} \\ E_{0,9,05} &= \text{5-percentile value of the modulus of elasticity parallel to the grain}\end{aligned}$$

$$\begin{aligned}\text{In this case:} \\ 220 \times 1000 \text{ mm}^2 \\ 2000 \text{ mm} \\ 9\,400 \text{ N/mm}^2\end{aligned}$$

Thus, the relative slenderness ratio for bending is defined as:

$$\begin{aligned}\lambda_{rel,m} &= \text{Relative slenderness ratio for bending} \\ &= \sqrt{\frac{f_{m,g,k}}{\sigma_{m,crit}}} \\ &= \mathbf{0,32 < 0,75} \quad \rightarrow \quad k_{crit} = 1\end{aligned}$$

In which:

$$f_{m,g,k} = \text{Characteristic bending strength GL24h}$$

$$\begin{aligned}\text{In this case:} \\ 24 \text{ N/mm}^2\end{aligned}$$

Full bending strength can be achieved without risk for buckling

TORSION RF3

The beam can resist the stress induced by torsion when:

$$\begin{aligned}\tau_{tor,d} &= \text{Design shear stress from torsion (see 0)} \\ 3,0 \text{ N/mm}^2 &\leq k_{shape} f_{v,g,d} \\ &\rightarrow \mathbf{3,0 \text{ N/mm}^2 \leq 3,26 \text{ N/mm}^2}\end{aligned}$$

In which:

$$\begin{aligned}k_{shape} &= \text{Factor depending on the shape of the cross-section:} \\ &= \min\left(1 + 0,15 \frac{h}{b}; 2,0\right) \\ &\text{Design shear strength (see 9.1.1):}\end{aligned}$$

$$\begin{aligned}\text{In this case:} \\ 1,68\end{aligned}$$

$$f_{v,g,d} = \frac{f_{v,g,k}}{\gamma_m} k_{mod} k_h k_l$$

$$1,94 \text{ N/mm}^2$$

The determined beam dimension of the RF3 system can resist the stress induced by torsion.

REMARKS STRUCTURAL DESIGN RF3 SYSTEM

See 'Remarks structural design RF4 system'.



LATERAL TORSIONAL BUCKLING RF4

Lateral torsional buckling can only occur between two bracing and adjacent beams who, in this system, always have a center to center distance of $l_{ef} = 2,0m$. The formulation below shows whether the maximum bending stress can be achieved without creating this phenomena:

$$\begin{aligned}\sigma_{m,crit} &= \text{Critical bending stress of a beam bent about its strong axis} \\ &= \frac{0,78 \cdot b^2}{h \cdot l_{ef}} E_{0,9,05} \\ &= \mathbf{126,4 \text{ N/mm}^2}\end{aligned}$$

In which:

$$\begin{aligned}b, h &= \text{Beam width and height} \\ l_{ef} &= \text{Center to center distance of the bracing beams} \\ E_{0,9,05} &= \text{5-percentile value of the modulus of elasticity parallel to the grain}\end{aligned}$$

$$\begin{aligned}\text{In this case:} \\ 180 \times 940 \text{ mm}^2 \\ 2000 \text{ mm} \\ 9\,400 \text{ N/mm}^2\end{aligned}$$

Thus, the relative slenderness ratio for bending is defined as:

$$\begin{aligned}\lambda_{rel,m} &= \text{Relative slenderness ratio for bending} \\ &= \sqrt{\frac{f_{m,g,k}}{\sigma_{m,crit}}} \\ &= \mathbf{0,44 < 0,75} \quad \rightarrow \quad k_{crit} = 1\end{aligned}$$

In which:

$$f_{m,g,k} = \text{Characteristic bending strength GL24h}$$

$$\begin{aligned}\text{In this case:} \\ 24 \text{ N/mm}^2\end{aligned}$$

Full bending strength can be achieved without risk for buckling

TORSION RF4

The beam can resist the stress induced by torsion when:

$$\begin{aligned}\tau_{tor,d} &= \text{Design shear stress from torsion (see 0)} \\ 1,5 \text{ N/mm}^2 &\leq k_{shape} f_{v,g,d} \\ &\rightarrow \mathbf{1,5 \text{ N/mm}^2 \leq 3,18 \text{ N/mm}^2}\end{aligned}$$

In which:

$$\begin{aligned}k_{shape} &= \text{Factor depending on the shape of the cross-section:} \\ &= \min\left(1 + 0,15 \frac{h}{b}; 2,0\right)\end{aligned}$$

$$\begin{aligned}\text{In this case:} \\ 1,64\end{aligned}$$

Design shear strength (see 9.1.1):

$$f_{v,g,d} = \frac{f_{v,g,k}}{\gamma_m} k_{mod} k_h k_l \quad \mathbf{1,94 \text{ N/mm}^2}$$

The determined beam dimension of the RF4 system can resist the stress induced by torsion.

REMARKS STRUCTURAL DESIGN RF4 SYSTEM

- To bear compression perpendicular to the grain at the supports, the size of the supporting areas needs to be designed to satisfy $\sigma_{c,90,d} \leq f_{c,90,g,d}$;
- The shear and perpendicular to the grain capacity of the beams at all individual beam supports depend on the joint design and need to be checked correspondingly;
- This cross section is not subjected to combined bending or normal stresses in the main directions and is therefore not verified in a combined unity check;
- All beam dimensions satisfy the ULS checks.

10 ANNEX 2: EXPLANATION CALCULATION OF BEAM DIMENSIONS AND DETAILING CONFORM EUROCODE 5

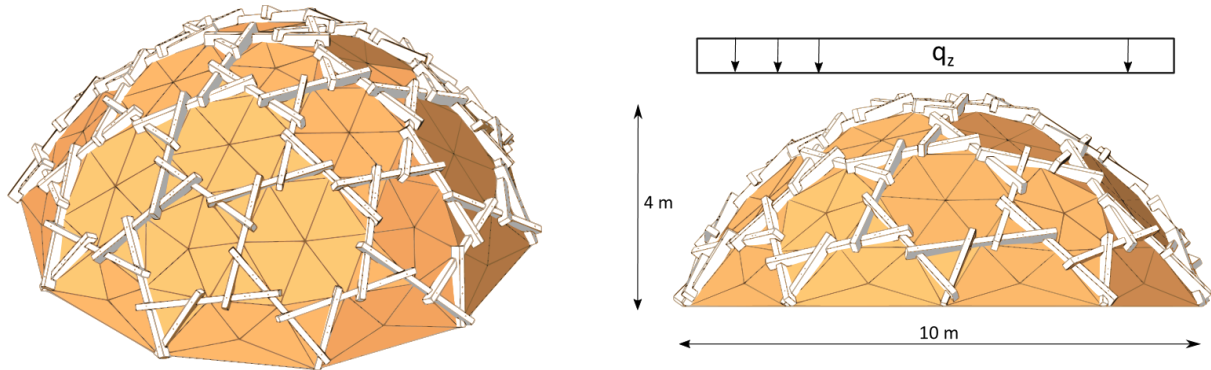


Figure 10.1: Structural design of considered RF

This calculation is the manual elaboration and exploration of a parametrized calculation that is implemented in the tool; ‘The Reciprocal Frame Designer’ (RFD). In this parametric tool, global and local Unity Checks (UC’s), are conducted at every location in the structural design according to EC8. This calculation discusses the maximum forces regarded at one randomly chosen connection location using the discussed boundary conditions, pinned supports, and an uniformly applied load in z-direction ($q_z = 1\text{ kN/m}^2$). The RF design shown above is used to identify all geometric properties.

10.1.1 GSA DATA

The exact values of the used forces in this calculation are displayed on the next page. The figures below can be used to schematically identify the force distribution throughout the RF system.

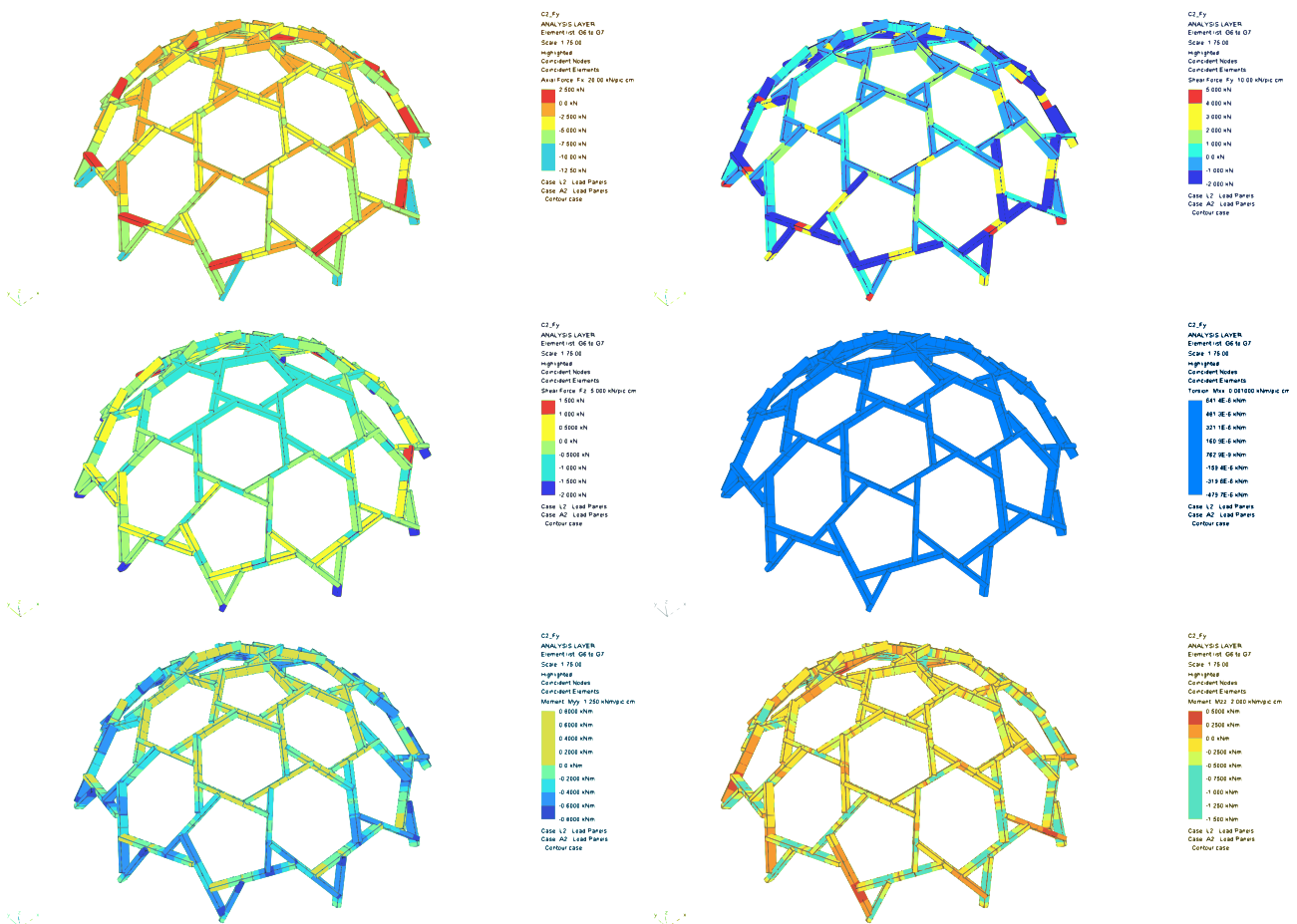


Figure 10.2: Schematic forces from left to right: Fx, Fy, Fz, Mx, My, Mz



10.1.2 DETAILING CLARIFICATION

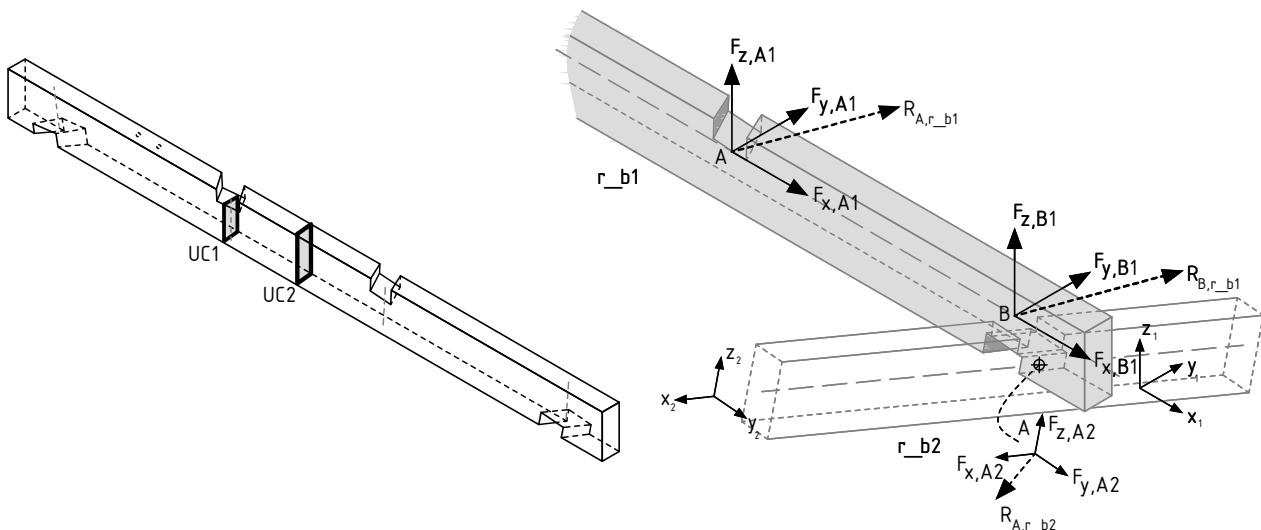


Figure 10.3: Detailing principle with planes (left), local force and axis systems (right)

LOADING

The structural design (Figure 10.1) is loaded by an equally distributed force of 1 kN/m² acting in Z-direction. This force is being transferred to/at the midpoints of each beam resulting in local forces at the connections. At a random location, this results in the following detailing forces (negative F_x = compression, positive F_x = tension).

RF beam 1 (r_{b1})

$$\begin{aligned} F_{x,B1} &= -2,63 \text{ kN} \\ F_{y,B1} &= -0,57 \text{ kN} \\ F_{z,B1} &= -0,86 \text{ kN} \end{aligned}$$

RF beam 2 r_{b2}

$$\begin{aligned} F_{x,A2} &= -1,95 \text{ kN} \\ F_{y,A2} &= 2,04 \text{ kN} \\ F_{z,A2} &= -0,14 \text{ kN} \end{aligned}$$

FORCES AT DETAILING LEVEL

The following minimal and maximal detailing forces can be found in the structure:

RF beam 1 (r_{b1})

| Min. | Max. |
|-----------------------------------|----------------------------------|
| $F_{x,B1,min} = -7,89 \text{ kN}$ | $F_{x,B1,max} = 1,26 \text{ kN}$ |
| $F_{y,B1,min} = -1,75 \text{ kN}$ | $F_{y,B1,max} = 0,51 \text{ kN}$ |
| $F_{z,B1,min} = -0,89 \text{ kN}$ | $F_{z,B1,max} = 1,02 \text{ kN}$ |

RF beam 2 r_{b2}

| Min. | Max. |
|-----------------------------------|-----------------------------------|
| $F_{x,A2,min} = -5,85 \text{ kN}$ | $F_{x,A2,max} = -0,68 \text{ kN}$ |
| $F_{y,A2,min} = -1,61 \text{ kN}$ | $F_{y,A2,max} = 5,56 \text{ kN}$ |
| $F_{z,A2,min} = -2,34 \text{ kN}$ | $F_{z,A2,max} = 0,58 \text{ kN}$ |

FORCES AND BENDING MOMENTS AT BEAM LEVEL

The following extreme forces and bending moments can be found in the structure at plane UC1 and UC2:

| Min. | Max. |
|-------------------------------------|------------------------------------|
| $F_{x,UC1,min} = -10,76 \text{ kN}$ | $F_{x,UC1,max} = -2,38 \text{ kN}$ |
| $F_{x,UC2,min} = -10,76 \text{ kN}$ | $F_{x,UC2,max} = -2,38 \text{ kN}$ |
| $M_{y,UC1,min} = -0,71 \text{ kNm}$ | $M_{y,UC1,max} = 0,40 \text{ kNm}$ |
| $M_{y,UC2,min} = -0,27 \text{ kNm}$ | $M_{y,UC2,max} = 0,60 \text{ kNm}$ |
| $M_{z,UC1,min} = -1,35 \text{ kNm}$ | $M_{z,UC1,max} = 0,42 \text{ kNm}$ |
| $M_{z,UC2,min} = -0,28 \text{ kNm}$ | $M_{z,UC2,max} = 0,28 \text{ kNm}$ |

These forces and bending moments are used in the elaboration to check the beam dimensions. Although almost all structural members are subjected to both compression and bending, they are all considered as beams. This results in a required examination of the following failure mechanisms considered for **GL28C**:



- Lateral torsional **buckling** and **buckling** due to combined axial **compression** and **bending**;
- Combined axial **compression** and **bending stresses** at plane **UC1** and **UC2** (Figure 10.3);
- Combined axial **tension** and **bending stresses** at plane **UC1** and **UC2**;

GEOMETRICAL DATA

To be able to calculate all necessary stresses, the appropriate geometrical properties are identified below. A character clarification can be found at the start of each calculation.

| Beam prop. | | [unit] | |
|------------|----------------------|--------|----|
| e | = Eccentricity beams | 100 | mm |
| w | = Beamwidth | 120 | mm |
| h | = Beamheight | 240 | mm |

| Force prop. | | F_x | $-F_x$ | F_y | $-F_y$ | F_z | $-F_z$ | [unit] |
|-------------|--------------------|-------|--------|-------|--------|-------|--------|----------------------------|
| A_x | = Compression area | 8,8 | 11,9 | 8,9 | 11,8 | 18,2 | - | $\times 10^3 \text{ mm}^2$ |
| h_x | = Lever arm force | 100 | | 100 | | 100 | | mm |
| α | = Angle difference | 12,5 | | 12,5 | | - | | degrees |
| β | = Angle difference | 32,4 | | 32,4 | | - | | degrees |
| γ^* | = Angle difference | - | | - | | - | | degrees |

* $\gamma \approx 0^\circ$

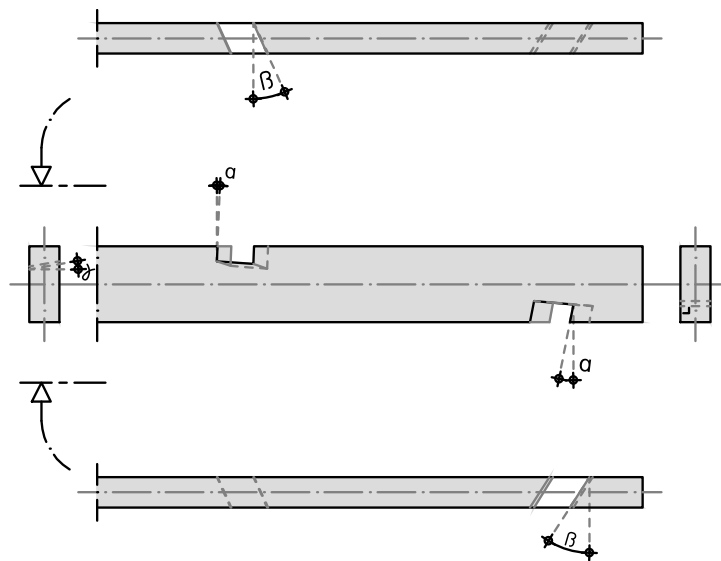


Figure 10.4: Indication of angles



10.1.3 MATERIAL PROPERTIES

The characteristic strength and stiffness properties of the applied timber are conform EN 338 and EN 14080:

| | | GL24h | GL28c | [unit] |
|----------------|---|--------------|--------------|-------------------|
| $f_{m,g,k}$ | = Bending strength | 24 | 28 | N/mm ² |
| $f_{c,0,g,k}$ | = Compression strength | 24 | 26,5 | N/mm ² |
| $f_{c,90,g,k}$ | = Compression strength perp. | 2,5 | 2,5 | N/mm ² |
| $f_{t,0,g,k}$ | = Tension strength | 16,5 | 16,5 | N/mm ² |
| $f_{t,90,g,k}$ | = Tension strength, perp. | 0,5 | 0,5 | N/mm ² |
| $f_{v,g,k}$ | = Shear and torsion strength | 2,5 | 2,5 | N/mm ² |
| $f_{r,g,k}$ | = Rolling shear strength | 1,2 | 1,2 | N/mm ² |
| $E_{0,g,mean}$ | = Modulus of elasticity, parallel | 11 600 | 12 600 | N/mm ² |
| $E_{0,g,05}$ | = 5 percentile value of the modulus of elasticity | 9 600 | 10 400 | N/mm ² |
| $G_{g,mean}$ | = Shear modulus | 720 | 720 | N/mm ² |
| $\rho_{g,k}$ | = Density | 380 | 380 | kg/m ³ |

The design values of the mechanical properties in the Ultimate Limite State (ULS) calculation are determined by:

$$f_d = \frac{f_k}{\gamma_m} k_{mod} k_h k_t$$

= Design value strength =

In which:

| | | |
|------------|--|-----------------------|
| γ_m | = Partial factor for glued laminated timber | In this case: 1,25 |
| k_{mod} | = Modification factor considering load duration and humidity. Climate class: 1 (indoor). Load duration class: Short (wind/snow load on roof) | 0,9 |
| k_h, k_t | = Volume factors depending on element dimensions to be applied to brittle behaving elements tension and/or bending covering possible force distribution. | 1,0 |

This results in the following design values for the strength properties:

| | | GL24h | GL28c | [unit] |
|----------------|------------------------------|--------------|--------------|-------------------|
| $f_{m,g,d}$ | = Bending strength | 17,3 | 20,2 | N/mm ² |
| $f_{c,0,g,d}$ | = Compression strength | 17,3 | 19,1 | N/mm ² |
| $f_{c,90,g,d}$ | = Compression strength perp. | 1,8 | 1,8 | N/mm ² |
| $f_{t,0,g,d}$ | = Tension strength | 11,9 | 11,9 | N/mm ² |
| $f_{t,90,g,d}$ | = Tension strength, perp. | 0,4 | 0,4 | N/mm ² |
| $f_{v,g,d}$ | = Shear and torsion strength | 1,8 | 1,8 | N/mm ² |
| $f_{r,g,d}$ | = Rolling shear strength | 0,9 | 0,9 | N/mm ² |

10.1.4 ULS CHECK BEAMS

The figure below shows the considered planes for the ULS beam checks.

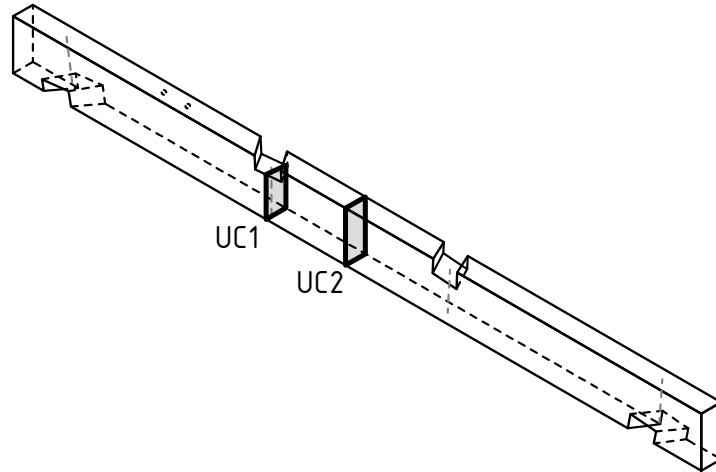


Figure 10.5: Plane locations for maximum stresses and/or lateral torsional buckling

BEAM CAPACITY AT PLANE UC1

The sensitivity of the beam against buckling determines the expression that must be satisfied. In the reviewed situation, connecting beams at plane UC1 provide stability against lateral torsional buckling and normal buckling. This results in a reduced effective beam length.

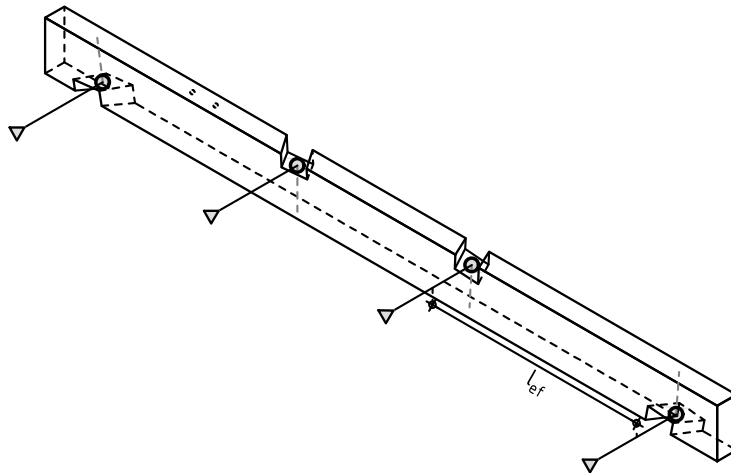


Figure 10.6: Effective length buckling

Lateral torsional buckling can only occur between two bracing and adjacent beams who, in this system, always have a maximum center to center distance of $l_{ef,max} = 1,0m$. The formulation below shows whether the maximum bending stress can be achieved without creating this phenomena:

$$\begin{aligned}
 \sigma_{m,crit} &= \text{Critical bending stress for sawn structural timber and glulam with} \\
 &\quad \text{rectangular cross section from softwood} \\
 &= \frac{0,78 \cdot b^2}{h \cdot l_{ef}} E_{0,05} \\
 &= \mathbf{486,7 \text{ N/mm}^2}
 \end{aligned}$$

In which:

$$\begin{aligned}
 b, h &= \text{Beam width and height} \\
 l_{ef} &= \text{Center to center distance of the bracing beams} \\
 E_{0,05} &= \text{5-percentile value of the modulus of elasticity parallel to the grain}
 \end{aligned}$$

$$\begin{aligned}
 \text{In this case:} \\
 120 \times 240 \text{ mm}^2 \\
 1000 \text{ mm} \\
 10\,400 \text{ N/mm}^2
 \end{aligned}$$



Thus, the relative slenderness ratio for bending is defined as:

$$\begin{aligned}\lambda_{rel,m} &= \text{Relative slenderness ratio for bending} \\ &= \sqrt{f_{m,g,k} / \sigma_{m,crit}} \\ &= \mathbf{0,24 < 0,75} \quad \rightarrow \quad k_{crit} = 1\end{aligned}$$

In which:

$$f_{m,g,k} = \text{Characteristic bending strength GL28C}$$

In this case:

$$28 \text{ N/mm}^2$$

The full bending strength can be achieved without risk for lateral buckling since $\lambda_{rel,m} < 0,75$. The risk for overall buckling is determined below. This is considered at plane UC2 around the beams' weak axis that is in this case the z-axis (buckling around beam width). Buckling at plane UC1 cannot occur due to the bracing beams.

$$\begin{aligned}\lambda_{rel,z,UC1} &= \text{Relative slenderness ratio at plane UC2} \\ &= \frac{\lambda_z}{\pi} \sqrt{\frac{f_{c0,k}}{E_{0,05}}} \\ &= \mathbf{0,23 \leq 0,3}\end{aligned}$$

In which:

$$\lambda_z = \frac{l_e}{i} = \frac{1000}{69,3}$$

In this case:

$$14,4$$

$$l_e = \text{Center to center distance of the bracing beams}$$

$$1000 \text{ mm}$$

$$i = \sqrt{\frac{I_z}{A}} = \sqrt{\frac{1/12 \cdot b h^3}{b h}} = \sqrt{\frac{1/12 \cdot 120 \cdot 240^3}{120 \cdot 240}}$$

$$69,3 \text{ mm}$$

$$f_{c0,k} = \text{Characteristic compression strength GL28C}$$

$$26,5 \text{ N/mm}^2$$

$$E_{0,05} = \text{5 percentile value of the modulus of elasticity GL28C}$$

$$10\,400 \text{ N/mm}^2$$

The full bending strength can be achieved without risk for buckling since $\lambda_{rel} < 0,3$. Consequently, the following expressions do not have to be satisfied since they do not lead to normative values ($k_{crit} = 1, k_{c,y} \wedge k_{c,z} \geq 1$):

$$UC_{c,m,2,1} = \frac{\sigma_{c,0,d}}{k_{c,y} f_{c,0,d}} + \frac{\sigma_{m,y,d}}{f_{m,y,d}} + k_m \frac{\sigma_{m,z,d}}{f_{m,z,d}} \leq 1$$

$$UC_{c,m,3,1} = \frac{\sigma_{c,0,d}}{k_{c,z} f_{c,0,d}} + \left(\frac{k_m \sigma_{m,y,d} + \sigma_{m,z,d}}{k_{crit} f_{m,d}} \right)^2 \leq 1$$

$$UC_{c,m,2,2} = \frac{\sigma_{c,0,d}}{k_{c,z} f_{c,0,d}} + k_m \frac{\sigma_{m,y,d}}{f_{m,y,d}} + \frac{\sigma_{m,z,d}}{f_{m,z,d}} \leq 1$$

$$UC_{c,m,3,2} = \frac{\sigma_{c,0,d}}{k_{c,z} f_{c,0,d}} + \left(\frac{\sigma_{m,y,d} + k_m \sigma_{m,z,d}}{k_{crit} f_{m,d}} \right)^2 \leq 1$$

The beam can resist the stress induced by both axial compression and bending without risk for buckling ($\lambda_{rel} \leq 0,3$) when (NEN-EN 1995-6.3.3):

$$UC_{c,m,1,1} = \left(\frac{\sigma_{c,0,d}}{f_{c,0,d}} \right)^2 + \frac{\sigma_{m,y,d}}{f_{m,y,d}} + k_m \frac{\sigma_{m,z,d}}{f_{m,z,d}} \leq 1$$

$$UC_{c,m,1,2} = \left(\frac{\sigma_{c,0,d}}{f_{c,0,d}} \right)^2 + k_m \frac{\sigma_{m,y,d}}{f_{m,y,d}} + \frac{\sigma_{m,z,d}}{f_{m,z,d}} \leq 1$$

$$UC_{c,m,1,1} \rightarrow \mathbf{0 + 0,03 + 0,14 = 0,17 \leq 1}$$

$$UC_{c,m,1,2} \rightarrow \mathbf{0 + 0,02 + 0,20 = 0,22 \leq 1}$$

In which:

$$k_m = \text{Factor considering re-distribution of bending stresses in a rectangular cross-section for laminated timber}$$

In this case:

$$0,7$$



$$\begin{aligned}
 \sigma_{c,0,d} &= \text{Design compression stress:} \\
 &= \frac{F_{x,UC1}}{A_{UC1}} = \frac{F_{x,UC1}}{w \cdot h_{UC1}} = \frac{10,76 \cdot 10^3}{120 \cdot (240 - 100)} & 0,6 \text{ N/mm}^2 \\
 f_{c,0,d} &= \text{Compression design strength GL28C} & 19,1 \text{ N/mm}^2 \\
 \sigma_{m,y,d} &= \text{Design bending stress in y-direction:} \\
 &= \frac{M_{y,UC1}}{W_{UC1}} = \frac{M_{y,UC1}}{\frac{1}{6} w h_{UC1}^2} = \frac{0,71 \cdot 10^6}{\frac{1}{6} 120 (240 - 100)^2} & 1,8 \text{ N/mm}^2 \\
 f_{m,y,d} &= \text{Bending design strength GL28C} & 20,2 \text{ N/mm}^2 \\
 \sigma_{m,z,d} &= \text{Design bending stress in z-direction:} \\
 &= \frac{M_{z,UC1}}{W_{UC1}} = \frac{M_{z,UC1}}{\frac{1}{6} h_{UC1} w^2} = \frac{1,35 \cdot 10^6}{\frac{1}{6} (240 - 100) 120^2} & 4,1 \text{ N/mm}^2 \\
 f_{m,z,d} &= \text{Bending design strength GL28C} & 20,2 \text{ N/mm}^2
 \end{aligned}$$

The determined beam dimension can resist the stresses induced by compression and bending at plane UC1.

COMBINED AXIAL TENSION AND BENDING STRESSES AT PLANE UC1

In this case, no tension in combination with bending is occurring at plane UC1. However, it does appear next to this plane as can be seen in the detailing forces described under 0. These forces are not normative for the reviewed design as can be seen below because of an extremely small tensile stress but, when tensile stresses will become normative, the following expression needs to be satisfied (NEN-EN 1995-6.2.3):

$$\begin{aligned}
 UC_{t,m,1,1} &= \frac{\sigma_{t,0,d}}{f_{t,0,d}} + \frac{\sigma_{m,y,d}}{f_{m,y,d}} + k_m \frac{\sigma_{m,z,d}}{f_{m,z,d}} \leq 1 \\
 UC_{t,m,1,2} &= \frac{\sigma_{t,0,d}}{f_{t,0,d}} + k_m \frac{\sigma_{m,y,d}}{f_{m,y,d}} + \frac{\sigma_{m,z,d}}{f_{m,z,d}} \leq 1
 \end{aligned}$$

In which:

$$k_m = \text{Factor considering re-distribution of bending stresses in a rectangular cross-section for laminated timber}$$

In this case:

$$0,7$$

Design tensile stress next to plane UC1:

$$\sigma_{c,0,d} = \frac{F_{x,B1}}{A_{UC1}} = \frac{F_{x,B1}}{w \cdot h_{UC1}} = \frac{1,26 \cdot 10^3}{120 \cdot (240 - 100)} & 0,08 \text{ N/mm}^2$$

$$f_{c,0,d} = \text{Tension design strength GL28C} & 19,1 \text{ N/mm}^2$$

COMBINED STRESSES AT PLANE UC2

The same procedure discussed above can be used to determine the UC's for plane UC2. However, the normative stresses are present in plane UC1 because of its plane size and corresponding force/bending moment magnitudes. Therefore, the stresses at plane UC2 are not discussed but, since they can be normative in other designs/situations, they are considered in the RFD.



10.1.5 CHECK OF FORCE EQUILIBRIUM

The designed connection needs to be able to withstand the acting forces to transfer them from one beam to another. The magnitudes of these forces are discussed under 10.1.2.

To ensure equilibrium between the connecting beams, the resultant forces \vec{R} between r_b1 point B, and r_b2 point A need to be equal $\left(\vec{R}_{B,r_b1} = \vec{R}_{A,r_b2} \right)$ which is checked by the general expression:

$$\vec{R} = \sqrt{(F_x^2 + F_y^2 + F_z^2)}$$

In which:

$$\begin{array}{lll} F_x = F_{x,B1} & \checkmark & F_{x,A2} \\ F_y = F_{y,B1} & \checkmark & F_{y,A2} \\ F_z = F_{z,B1} & \checkmark & F_{z,A2} \end{array}$$

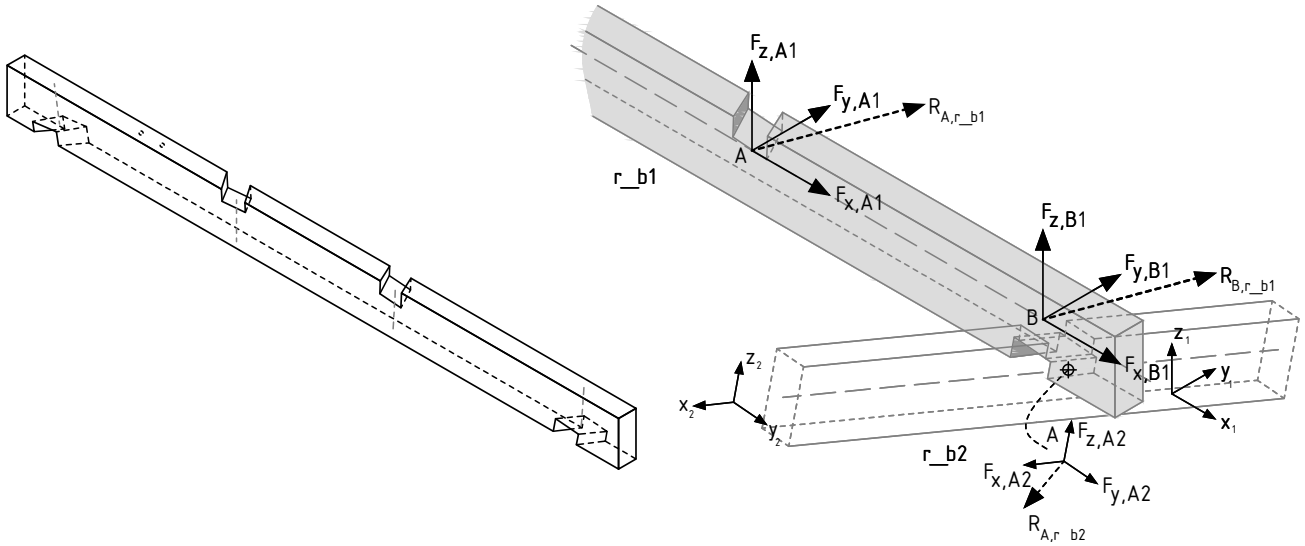


Figure 10.7: Force identification

When regarding the forces described under 10.1.2, this leads to the following resultants:

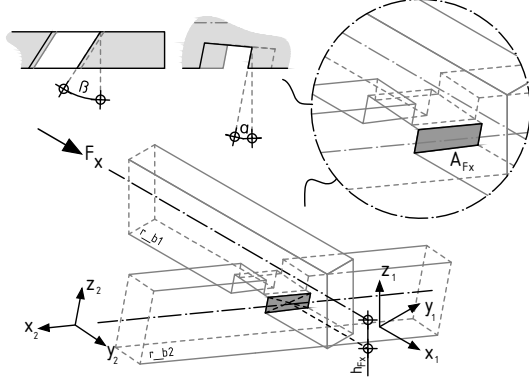
$$\begin{array}{l} \text{RF beam 1 (r_b1)} \\ \left. \begin{array}{l} F_{x,B1} = -2,63 \text{ kN} \\ F_{y,B1} = -0,57 \text{ kN} \\ F_{z,B1} = -0,86 \text{ kN} \end{array} \right\} \rightarrow \vec{R}_{B,r_b1} = \sqrt{(2,63^2 + 0,57^2 + 0,86^2)} = 2,82 \text{ kN} \end{array}$$

$$\begin{array}{l} \text{RF beam 2 r_b2} \\ \left. \begin{array}{l} F_{x,A2} = -1,95 \text{ kN} \\ F_{y,A2} = 2,04 \text{ kN} \\ F_{z,A2} = -0,14 \text{ kN} \end{array} \right\} \rightarrow \vec{R}_{A,r_b2} = \sqrt{(1,95^2 + 2,04^2 + 0,14^2)} = 2,82 \text{ kN} \end{array}$$

There is an equilibrium of forces. The next page shows the required ULS checks at detailing level.

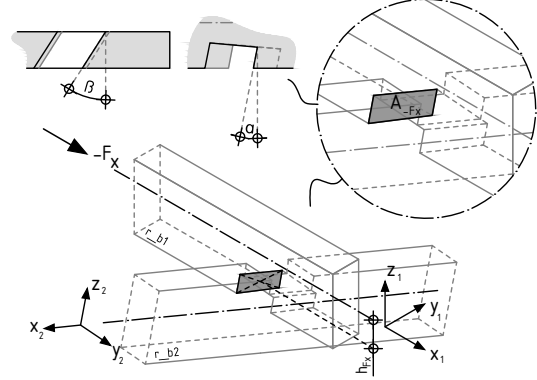
10.1.6 REQUIRED ULS CHECKS AT DETAILING LEVEL

(1) ULS checks force F_x



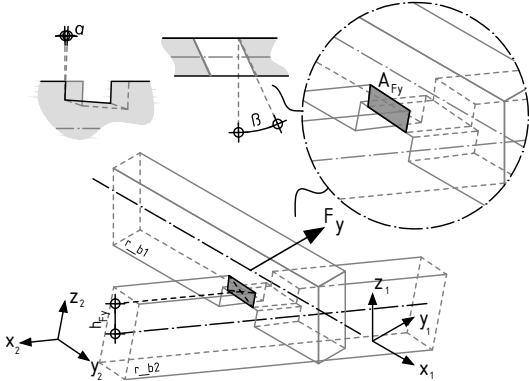
Compression stress by $F_{y,A2}$ at plane A_{Fx} under α and β on **r_b1**
 Compression stress at plane A_{Fx} by $F_{y,A2}$ on **r_b2**
 Tension and shear stress by $F_{x,B1}$ at **plane 2***

(2) ULS checks force $-F_x$



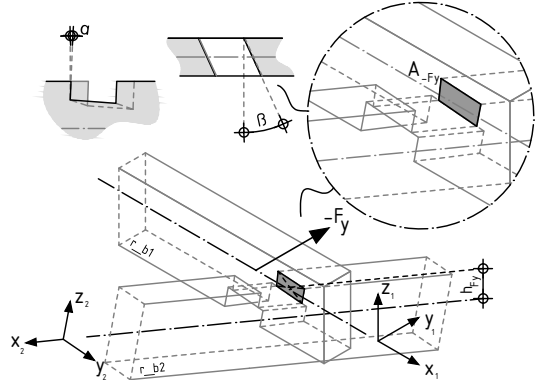
Compression stress by $-F_{y,A2}$ at plane A_{Fx} under α and β on **r_b1**
 Compression stress at plane A_{Fx} by $-F_{y,A2}$ on **r_b2**
 Tension and shear stress by $-F_{x,B1}$ at **plane 2.1***

(3) ULS checks force F_y



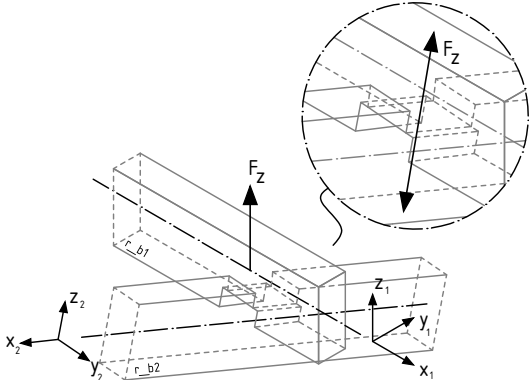
Compression stress by $F_{y,B1}$ at plane A_{Fy} under α and β on **r_b2**
 Compression stress by $F_{y,B1}$ at plane A_{Fy} on **r_b1**
 Tension stress $-F_{x,A2}$ at **plane 2.1***

(4) ULS checks force $-F_y$



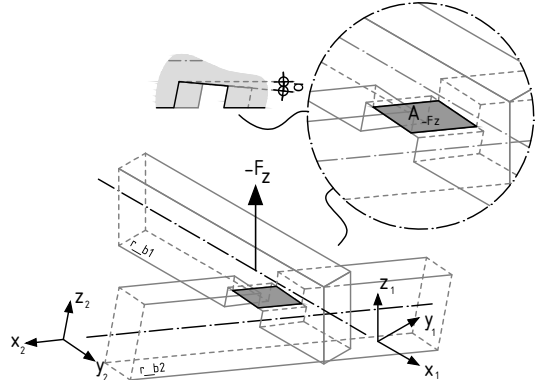
Compression stress by $-F_{y,B1}$ at plane A_{Fy} under α and β on **r_b2**
 Compression stress by $-F_{y,B1}$ at plane A_{Fy} on **r_b1**
 Tension stress $F_{x,A2}$ at **plane 2.1***

(5) ULS checks force F_z

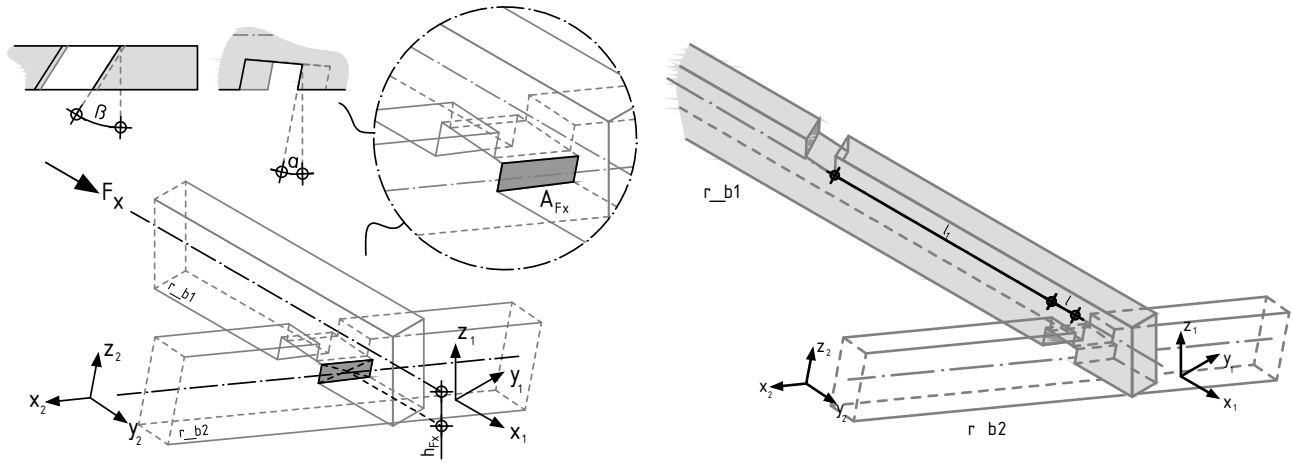


Tension stress by **max.**($F_{z,B1}$, $F_{z,A2}$) acting on the dowel
 Screw: axial withdrawal capacity, head pull-through capacity, tensile capacity
 Bolt: washer pull-through capacity, tensile capacity

(6) ULS checks force $-F_z$



Compression stress by **max.**($-F_{z,B1}$, $-F_{z,A2}$) at plane A_{Fz} under α
 Shear stress by $-F_{z,B1}$ at plane 1

ULS CHECK F_xFigure 10.8: Force plane F_x and length l₁10.1.7 MAXIMUM COMPRESSION STRESS CHECK AT PLANE A_{Fx} ON BEAM R_B1

The force F_x is transferred by compression stresses under angle α and β to the grain resulting in force F_{y,A2} that acts perpendicular to plane A_{Fx}.

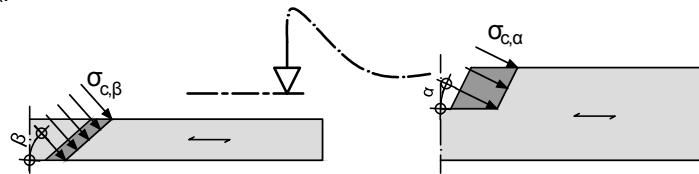


Figure 10.9: Compression stress under an angle to the grain

The acting compression stress must satisfy the following expressions:

$$\sigma_{c,\alpha,d} \leq \frac{f_{c,0,d}}{k_{c,90} f_{c,90,d}} \sin^2 \alpha + \cos^2 \alpha \quad \rightarrow \quad 0,47 \text{ N/mm}^2 \leq 14,3 \text{ N/mm}^2$$

$$\sigma_{c,\beta,d} \leq \frac{f_{c,0,d}}{k_{c,90} f_{c,90,d}} \sin^2 \beta + \cos^2 \beta \quad \rightarrow \quad 0,47 \text{ N/mm}^2 \leq 7,5 \text{ N/mm}^2$$

$$\sigma_{c,\alpha,d} = \sigma_{c,\beta,d} = \text{Compression stress perp. to plane}$$

$$= \frac{F_{y,A2}}{A_{Fx}} = \frac{5,56 \cdot 10^3}{11,9 \cdot 10^3} = 0,47 \text{ N/mm}^2$$

In which:

- $f_{c,0,d}$ = Design compression strength GL28C
- $f_{c,90,d}$ = Design compression strength perp. GL28C
- $k_{c,90}$ = Factor considering load configuration and compressive deformation dependend on length l₁ (Figure 10.8)

$$= 0,6 \text{ m} \leq l_1 \leq 1,0 \text{ m} \quad \left\{ \begin{array}{l} l_1 \geq 2h = 2 \cdot 0,24 = 0,48 \\ l_1 \leq 400 \text{ mm} \forall \beta \\ w_b / \sin(\beta_{\min}) = w_b / \sin(30) = 240 \text{ mm} \end{array} \right\} \rightarrow k_{c,90} = 1,75$$

$$\alpha = \text{Angle to the grain}$$

$$\beta = \text{Angle to the grain}$$

In this case:

$$17,3 \text{ N/mm}^2$$

$$1,8 \text{ N/mm}^2$$

$$1,75$$

$$12,5^\circ$$

$$32,4^\circ$$



MAXIMUM COMPRESSION STRESS PERPENDICULAR AT PLANE A_{Fx} ON BEAM R_B2

The maximum compression stress acting on plane A_{Fx} perpendicular the grain of beam r_b2, must satisfy the following expression:

$$\begin{aligned}\sigma_{c,90,d} &\leq k_{c,90} f_{c,90,d} \rightarrow 0,47 \text{ N/mm}^2 \leq 3,15 \text{ N/mm}^2 \\ \sigma_{c,90,d} &= \text{Compression stress perp. to beam r_b1} \\ &= \frac{F_{y,A2}}{A_{Fx}} = \frac{5,56 \cdot 10^3}{11,9 \cdot 10^3} = 0,47 \text{ N/mm}^2\end{aligned}$$

In which:

$$\begin{aligned}f_{c,90,d} &= \text{Design compression strength perp. GL28C} \\ k_{c,90} &= \text{Factor considering load configuration and compressive deformation} \\ &\quad \text{dependent on length } l_1 \text{ (Figure 10.8)}\end{aligned}$$

In this case:

$$1,8 \text{ N/mm}^2$$

$$1,75$$

MAXIMUM TENSION STRESS CHECK AT PLANE 2 (P2)

The eccentricity between the beams' neutral axis and acting force F_x will cause a bending moment that results in compression and tension perpendicular to the grain. Additionally, shear arising at this point needs to be considered.

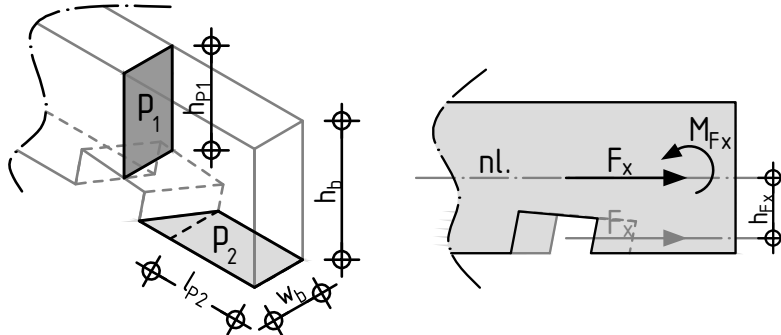


Figure 10.10: Plane 1, 2, and eccentricity h_{Fx}

The combination of acting shear and bending need to satisfy the following expression:

$$\frac{\sigma_{t,90,d}}{f_{t,90,g,d}} + \frac{\tau_d}{f_{v,d}} \leq 1 \rightarrow 1,7 \leq 1$$

In which:

$$\begin{aligned}\sigma_{t,90,d} &= \text{Tensile stress perp. at plane 2, beam r_b1} \\ &= \frac{6M_{Fx}}{bh^2} = \frac{6F_{x,B1}h_{Fx}}{w_b l_{P2}^2} = \frac{6 \cdot 1,26 \cdot 0,1 \cdot 10^6}{120 \cdot 100^2}\end{aligned}$$

$$f_{t,90,g,d} = \text{Tension strength perp.} \quad 0,4 \text{ N/mm}^2$$

$$\begin{aligned}\tau_d &= \text{Shear stress at plane 2, beam r_b1} \quad 0,16 \text{ N/mm}^2 \\ &= \frac{1,5V}{bh_{ef}} = \frac{1,5F_{x,B1}}{w_b l_{P2}} = \frac{1,5 \cdot 1,26 \cdot 10^3}{120 \cdot 100}\end{aligned}$$

$$f_{v,d} = \text{Shear strength GL28C} \quad 1,8 \text{ N/mm}^2$$

Conclusion: the length l_{P2} need to be longer, or screws must be added. Without using screws, the minimal length of l_{P2} can be determined by:

$$l_{P2,min} = \sqrt{\frac{6F_{x,B1}h_{Fx}}{w_b f_{t,90,d}}} + \frac{1,5F_{x,B1}}{w_b f_{v,d}} = \sqrt{\frac{6 \cdot 1,26 \cdot 0,1 \cdot 10^6}{120 \cdot 0,4}} + \frac{1,5 \cdot 1,26 \cdot 10^3}{120 \cdot 1,8} = 135 \text{ mm}$$



If we choose not to lengthen l_{p2} to the minimal required length, self-drilling screw(s) must be applied. Self-drilling screws can almost always be applied without the use of pre-drilled holes. This direct instalment, together with their special shape, results in a greater withdrawal strength compared to traditional screws. With respect to this connection, the screw adds redundancy to the connection and will ensure a peak stress capacity that could be preferable during the implementation of the structure.

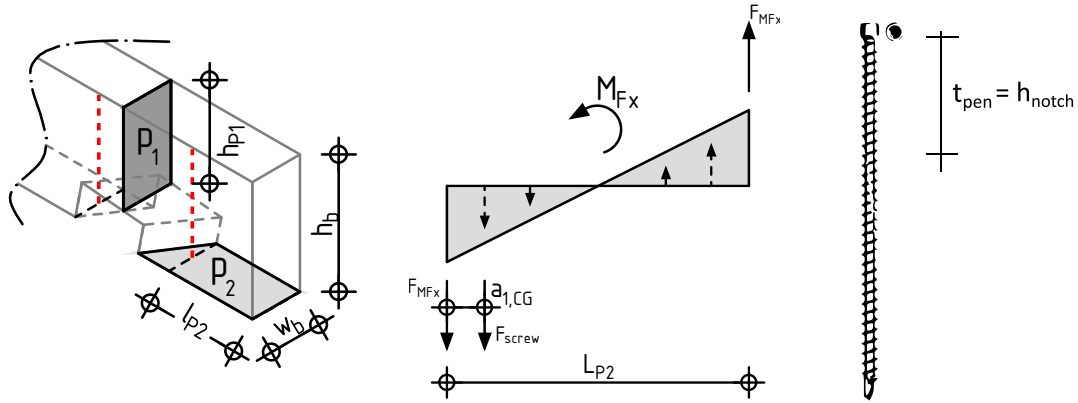


Figure 10.11: Screw locations in red (left), stress plane, and a full threaded screw

The screws reinforce the beam over their full length and are therefore full threaded. A screw length of 195 mm is enough to gap the overall notch height but, it results in a required diameter of $d = 6,5$ mm that is required due to applied torsion at instalment. The capacity of the screw is determined below in which the mechanical properties are taken from the technical Fischer assesement^[27].

Regarding axial load, the minimal edge distance of the screw is given by:

$$a_{1,CG} = a_{2,CG} = \min(4d) = 4 \cdot 6,5 = 26 \text{ mm}$$

This distance results in a maximal tensile force of:

$$F_{screw} = \frac{F_{MFx}}{\frac{L_{p2}}{2}} \left(\frac{L_{p2}}{2} - a_{2,CG} \right) = \left(\frac{M_{Fx}}{L_{p2}} \cdot \frac{L_{p2}}{2} \right) \left(\frac{L_{p2}}{2} - a_{2,CG} \right) = \frac{2M_{Fx}}{L_{p2}} \left(\frac{L_{p2}}{2} - a_{2,CG} \right)$$

$$F_{screw} = \frac{2 \cdot 1,26 \cdot 0,1 \cdot 10^6}{100^2} \left(\frac{100}{2} - 26 \right) \cdot 10^{-3} = 0,6 \text{ kN}$$

The acting tensile force F_{screw} must satisfy the following failure mechanisms:

$$F_{screw} \leq F_{ax,Rd} = \min \left\{ \begin{array}{l} n_{ef} F_{t,k} / \gamma_m \\ n_{ef} f_{ax,k} d_{pen} / \gamma_m \\ n_{ef} f_{head,k} d_h^2 / \gamma_m \end{array} \right. \leq F_{ax,Rd} = \min \left\{ \begin{array}{l} 8,5 \text{ kN} \\ 4,8 \text{ kN} \end{array} \right. \rightarrow 0,6 \text{ kN} \leq 4,8 \text{ kN}$$

In which:

| | | |
|-------------|---|---|
| $F_{ax,Rd}$ | = | Design value of axial withdrawal capacity of the fastener |
| n_{ef} | = | Effective number of fasteners perp. to grain $n_{ef} = n$ |
| γ_m | = | Partial factor for glued laminated timber |
| $F_{t,k}$ | = | Characteristic tensile strength of the fastener ($d = 6$ mm) |

In this case:

| |
|---------|
| 8,5 kN |
| 1 |
| 1,25 |
| 10,7 kN |



| | | | |
|--------------|---|--|------------------------|
| $f_{ax,k}$ | = | Charasteristic withdrawal strenght of the fastener | 11,6 N/mm ² |
| d | = | Outer thread diameter | 6 mm |
| t_{pen} | = | Penetration depth = approximate height notch | 80 mm |
| $f_{head,k}$ | = | Characteristic pull-through parameter | 1,8 N/mm ² |
| d_h | = | Head diameter of connector* | - |

*Does not have to be considered since full threaded.

Conclusion: the minimal length of l_{p2} need to be 135 milimeter or screws must be added. For this particular design, the length l_{p2} is enlarged to 140 milimeter in combination with adding screws at the designated locations.

10.1.8 ULS CHECK -FX

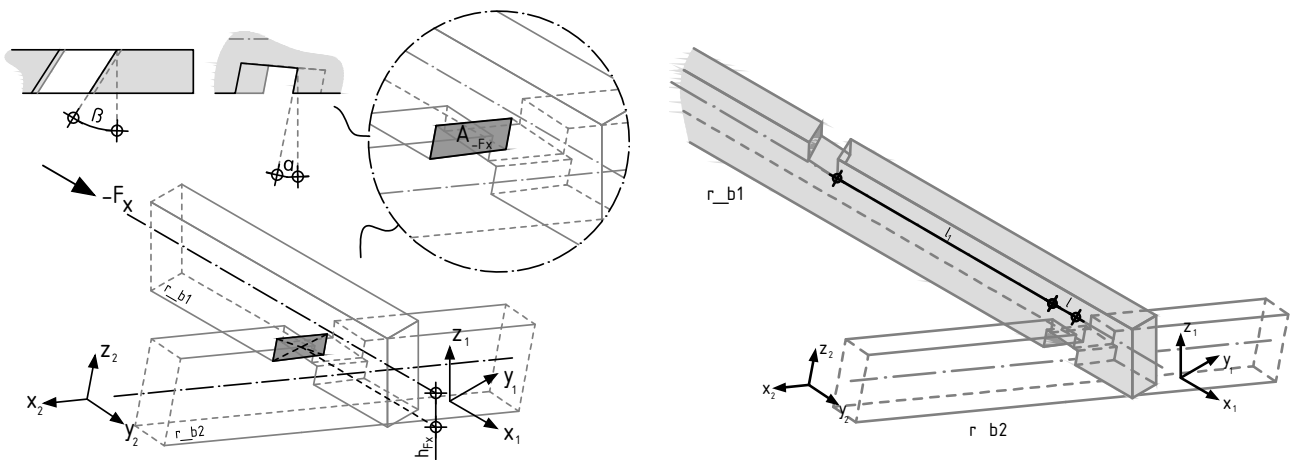


Figure 10.12: Force plane -Fx and length l_1

MAXIMUM COMPRESSION STRESS PERPENDICULAR AT PLANE A_{Fx} ON BEAM R_{B2}

The calculation discussing the ULS check of +Fx, shows that the compression stress perpendicular to plane A_{Fx} is normative over the compression stress that acts under an angle to beam r_{b1} . Therefore, the compression under an angle is not calculated since $\alpha \wedge \beta \nabla \leq 90^\circ$.

The maximum compression stress acting on plane A_{Fx} perpendicular the grain of beam r_{b2} must satisfy the following expression (as showed in 0):

$$\sigma_{c,90,d} \leq k_{c,90} f_{c,90,d}$$

The force $F_{y,A2}$ is governing over force $-F_{y,A2}$ making it unnecessary to check $-F_{y,A2}$.

MAXIMUM TENSION STRESS AT PLANE 2.1 (P2.1)

The eccentricity between the beams' neutral axis and acting force $-F_x$ will cause a bending moment that results in compression and tension perpendicular to the grain . Additionally, shear arising at this point needs to be considered.

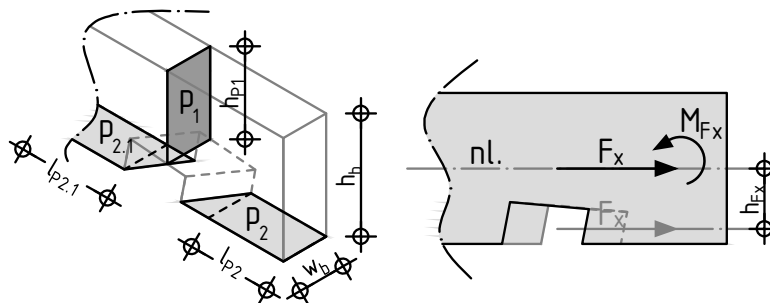


Figure 10.13: Plane 1, 2, 2.1, and eccentricity h_{Fx}



The combination of acting shear and bending need to satisfy the following expression in which the minimal length of $l_{P2.1}$ throughout the whole structure is one meter (Figure 10.13):

$$\frac{\sigma_{t,90,d}}{f_{t,90,g,d}} + \frac{\tau_d}{f_{v,d}} \leq 1 \quad \rightarrow \quad 0,16 \leq 1$$

In which:

$\sigma_{t,90,d}$ = Tensile stress perp. at plane 2, beam r_b1

In this case:

0,04 N/mm²

$$= \frac{6M_{Fx}}{bh^2} = \frac{-6F_{x,B1}h_{Fx}}{w_b l_{P2.1}^2} = \frac{6 \cdot 7,89 \cdot 0,1 \cdot 10^6}{120 \cdot 1000^2}$$

$f_{t,90,g,d}$ = Tension strength perp.

0,4 N/mm²

τ_d = Shear stress at plane 2, beam r_b1

0,1 N/mm²

$$= \frac{1,5V}{bh_{ef}} = \frac{-1,5F_{x,B1}}{w_b l_{P2}} = \frac{1,5 \cdot 7,89 \cdot 10^3}{120 \cdot 1000}$$

$f_{v,d}$ = Shear strength

1,8 N/mm²

Conclusion: the length $l_{P2.1}$ does need to be longer. However, a screw is added to add redundancy and extra strength during implementation (Figure 10.11).

10.1.9 ULS CHECK $\pm F_y$

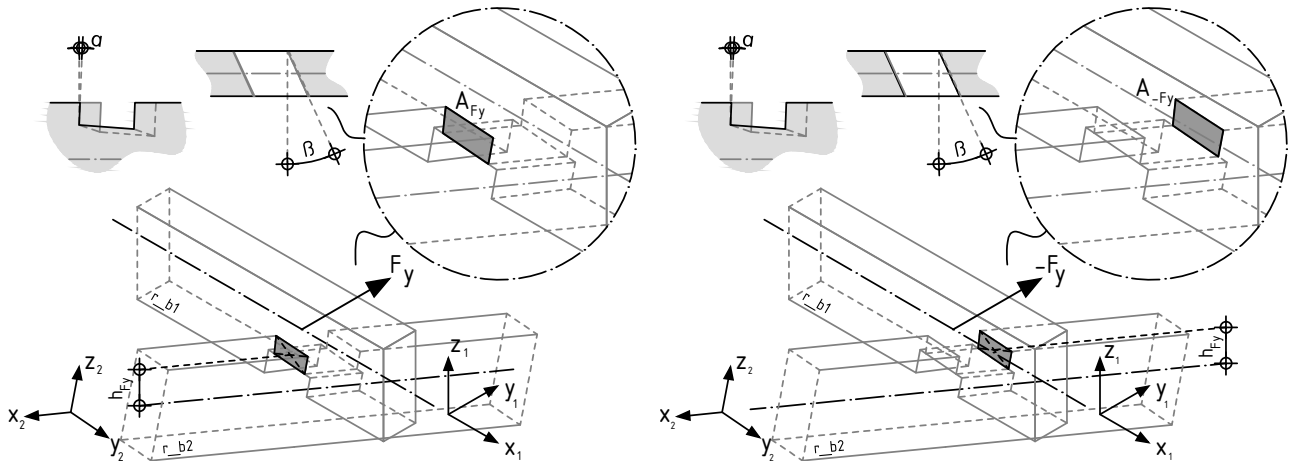


Figure 10.14: Force plane $\pm F_y$ and length l_1

The minimal and maximal local forces in the beam (see 0), show that the forces F_x are normative over F_y . Therefore, and because of geometrical similarities between the planes, the maximum allowable stresses determined under 0 and 10.1.8 also apply to $\pm F_y$. Correspondingly they do not have to be checked.

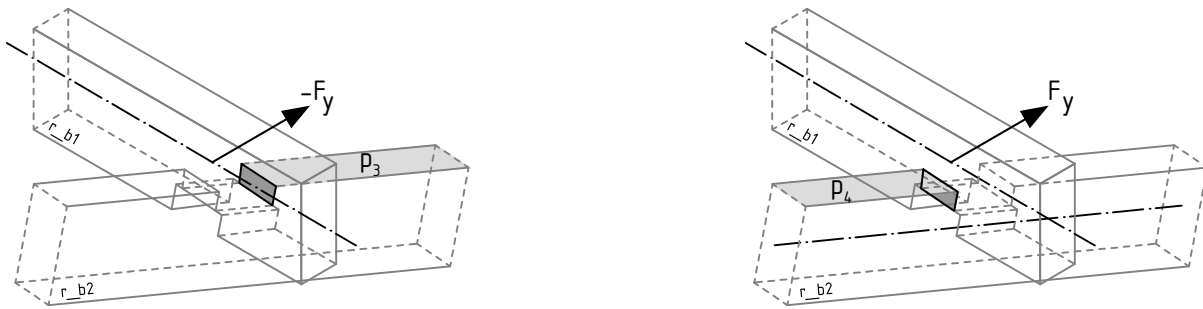


Figure 10.15: Plane 3 and plane 4

When the minimal plane length calculated as 135 millimeter is satisfied throughout the structure in planes P3 and P4, no screws have to be added. This accounts for every location except the planes at the supports. However, due to the reasons regarding redundancy and implementation, full threaded screws are added to all beams at the locations explained below.

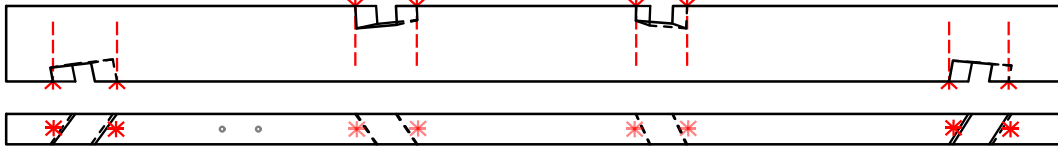


Figure 10.16: Full threaded screw locations indicated in red

10.1.10 ULS CHECK FZ

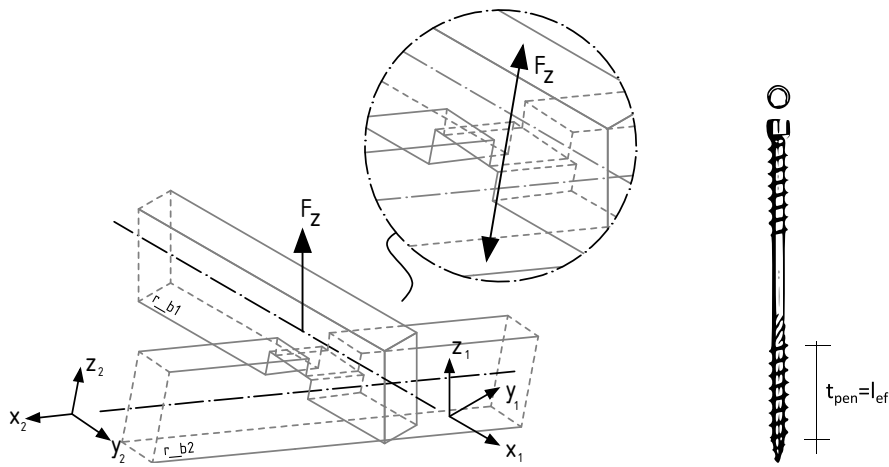


Figure 10.17: Tensile force Fz and implemented screw type

At some locations in the structural design of an RF, tensile forces at the connection can occur. Since this force cannot be withstood directly by the system, it must be transferred by a dowel type connection in the form of a special type of self-drilling screw that is displayed above. The varying installation speed of this double-threaded screw created by the thread geometry, insures that beams are drawn towards each other enabling force transferring by the designated planes. When using bolts, re-tightening may be needed due to shrinkage which is not necessary when using this screw. The acting tensile force F_{screw} must satisfy the following failure mechanisms:

$$F_{screw} \leq F_{ax,Rd} = \min \left\{ \begin{array}{l} n_{ef} F_{t,k} / \gamma_m \\ n_{ef} f_{ax,k} d t_{pen} / \gamma_m \\ n_{ef} f_{head,k} d_h^2 / \gamma_m^* \end{array} \right.$$

$$\leq F_{ax,Rd} = \min(5,6 \text{ kN}; 10,8 \text{ kN}) \rightarrow 1,2 \text{ kN} \leq 5,6 \text{ kN}$$

In which:

| | | |
|-------------|---|--|
| $F_{ax,Rd}$ | = | Design value of axial withdrawal capacity of the fastener |
| n_{ef} | = | Effective number of fasteners perp. to grain $n_{ef} = n$ |
| γ_m | = | Partial factor for glued laminated timber |
| $F_{t,k}$ | = | Characteristic tensile strength of the fastener (d = 6 mm) |
| $f_{ax,k}$ | = | Charasteristic withdrawal strenght of the fastener |
| d | = | Outer thread diameter |
| t_{pen} | = | Penetration depth |

In this case:

| |
|------------------------|
| 8,5 kN |
| 1 |
| 1,25 |
| 10,7 kN |
| 11,6 N/mm ² |
| 6 mm |
| 100 mm |

*Does not have to be considered since full threaded near head.



10.1.11 ULS CHECK -Fz

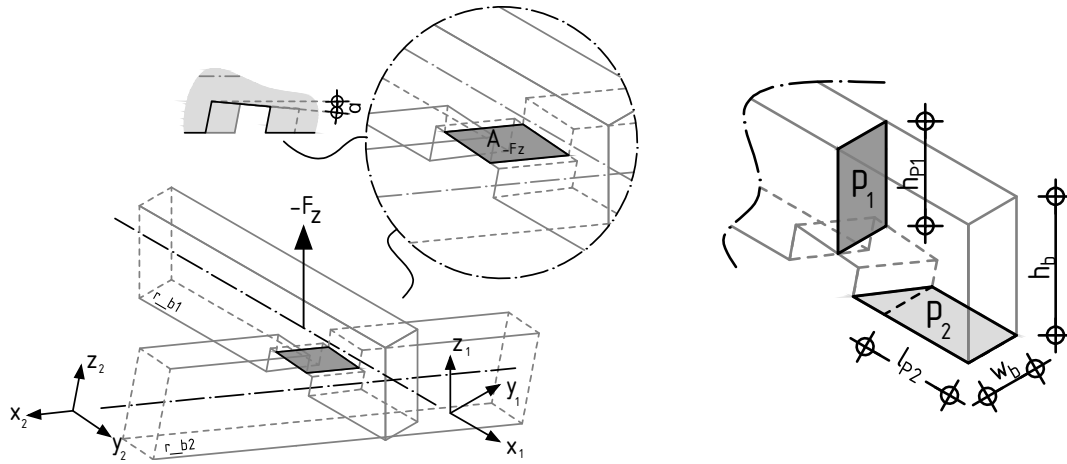


Figure 10.18: Force plane -Fz and plane P1

The compression force $-F_z$ results in compression stress under angle α in plane A_{-Fz} and shear stress in plane 1 (P1).

MAXIMUM COMPRESSION STRESS PERPENDICULAR AT PLANE A_{-Fz} ON BEAM R_{B1} AND R_{B2} CAUSED BY FORCE $-F_z$

The acting compression stress must satisfy the following expression:

$$\sigma_{c,\alpha,d} \leq \frac{f_{c,0,d}}{\frac{f_{c,0,d}}{k_{c,90}f_{c,90,d}} \sin^2 \alpha + \cos^2 \alpha} \rightarrow 0,13 \text{ N/mm}^2 \leq 14,3 \text{ N/mm}^2$$

$$\sigma_{c,\alpha,d} = \text{Compression stress perp. to plane}$$

$$= \frac{-F_{z,A2,\min}}{A_{Fx}} = \frac{2,34 \cdot 10^3}{18,2 \cdot 10^3} = 0,13 \text{ N/mm}^2$$

In which:

$$\begin{aligned} f_{c,0,d} &= \text{Design compression strength} \\ f_{c,90,d} &= \text{Design compression strength perp.} \\ k_{c,90} &= \text{Factor considering load configuration and compressive deformation} \\ &= \text{dependent on length } l_1 \text{ (Figure 10.8)} \\ &= 0,6 \text{ m} \leq l_1 \leq 1,0 \text{ m} \quad \left\{ \begin{array}{l} l_1 \geq 2h = 2 \cdot 0,24 = 0,48 \\ l_1 \leq 400 \text{ mm } \forall \beta \\ w_b / \sin(\beta_{\min}) = w_b / \sin(30) = 240 \text{ mm} \end{array} \right\} \rightarrow k_{c,90} = 1,75 \end{aligned}$$

$$\alpha = \text{Angle to the grain} \quad 12,5^\circ$$

$$\begin{aligned} \text{In this case:} \\ 17,3 \text{ N/mm}^2 \\ 1,8 \text{ N/mm}^2 \\ 1,75 \end{aligned}$$

The compression stress can easily be taken by the structure but, could become normative by changing the overall RF design.

MAXIMUM SHEAR STRESS PERPENDICULAR AT PLANE $P1$ ON BEAM R_{B2}

For this calculation it is assumed that the beam has sufficient shear capacity ($V_{Ed} < V_{Rd}$) when considering the full height. This however, cannot be guaranteed for the notched area where the shear force and stress is the largest thus normative. Therefore, the following expression should be verified:

$$\tau_d \leq k_v f_{v,d} \rightarrow 0,09 \text{ N/mm}^2 \leq 0,8 \text{ N/mm}^2$$

$$= \text{Shear stress at plane 1 by } -F_z$$

$$= \frac{1,5 F_z}{w_b h_{P1}} = \frac{1,5 \cdot \max(F_{z,A2,\max}; F_{z,B1,\max})}{w_b h_{P1}} = \frac{1,5 \cdot 1,02 \cdot 10^3}{120 \cdot (240 - 100)} = 0,09 \text{ N/mm}^2$$



In which:

w_b = Beam width
 h_{P1} = Effective height h_{ef} of plane 1

In this case:

120 mm
 140 mm

And $k_v f_{v,d}$;

k_v = Reduction factor for the allowable shear stress $f_{v,d}$

In this case:

0,44

$$= \min \left\{ \frac{1}{k_n \left(1 + \frac{1,1i^{1,5}}{\sqrt{h}} \right)}, \frac{1}{\sqrt{h} \left(\sqrt{\alpha(1-\alpha)} + 0,8 \frac{x}{h} \sqrt{\frac{1}{\alpha} - \alpha^2} \right)} \right\}$$

$$= \min \left\{ \frac{1}{6,5}, \frac{1}{\sqrt{240} \left(\sqrt{0,58(1-0,58)} + 0,8 \frac{120}{240} \sqrt{\frac{1}{0,58} - 0,58^2} \right)} \right\}$$

$$= \min \left\{ \frac{1}{6,5}, \frac{1}{14,9} \right\} = 0,44$$

k_n = Sheathing material factor; 4,5 for LVL, 5 for solid timber, and 6,5 for glued laminated timber 6,5
 i = Notch inclination 0
 h = Total beam height 240 mm
 x = Distance between supporting force and notch corner 120 mm
 α = $\frac{h_{ef}}{h}$ 0,58

$f_{v,d}$ = Shear strength 1,8 N/mm²

This shows that the beam has sufficient shear capacity at the notches and it is not necessary to add reinforcing screws. These however, are added as explained under 10.1.9 and create a larger shear capacity.

10.1.12 SLS CHECKS

The degree to which the RFs' structural design is statically indefinite makes a manual calculation of the deformation impossible. However, it can be calculated in GSA using a decreased (shear)modulus of elasticity in combination with the characteristic value of the considered load. Additionally, connection settlement due to the fabrication tolerances must be determined by varying the scale factor explained under the form-finding chapter.

The time dependent Youngs Modulus of the GL28C timber is determined by:

$$E_{mean,fin} = \frac{E_{mean}}{1 + \psi_2 k_{def}}$$

In which:

E_{mean} = Mean modulus of elasticity, parallel (GL28C)
 ψ_2 = Quasi permanent load combination factor
 k_{def} = Factor accounting moisture effects on deformation (GL28C)

In this case:

12 600 N/mm²
 [project specific]
 [project specific]

Requirements with respect to deformation are not obligated and project specific but, advised is to take the maximum deformation of the structure should least satisfy $w_2 \leq l_{span}/250$.



11 APPENDIX 1: HOW TO USE THE RECIPROCAL FRAME DESIGNER

The Reciprocal Frame Designer



Author: Tom Godthelp

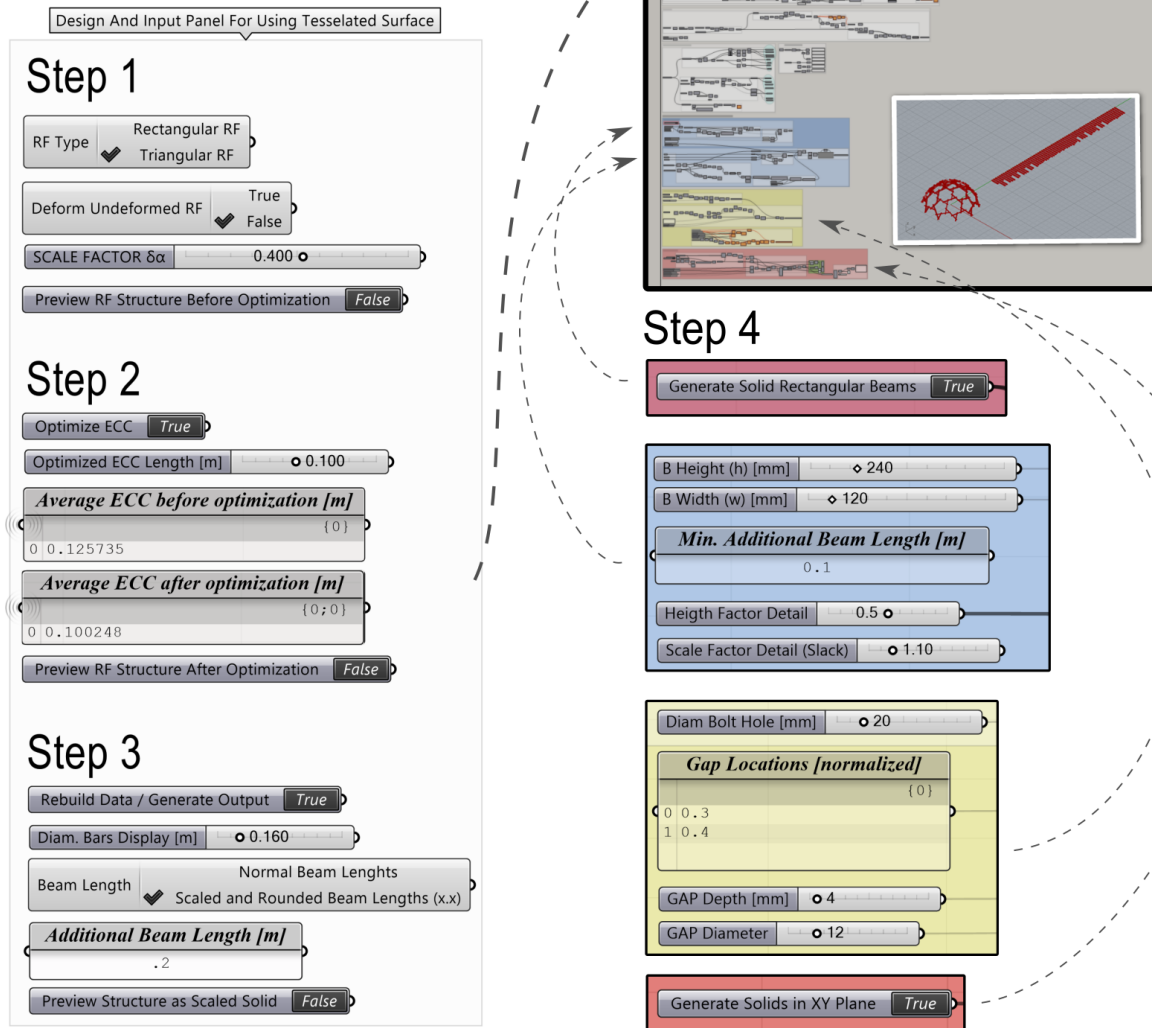


Figure 11.1: Main parameters divided per step on how to use the RFD

Figure 11.1 shows the geometrical design process of an RF in chronological order and divided per step. The structural input, required for mechanical analysis, is not added in this respect. However, the figure does show that data toggles are added at each step to reduce computational time during the form finding process: as written under 6.3.2, the computational time increases with every step. Step 1 to 3 allows direct interaction and represents among others:

- Step 1: defining the scale factor, RF-unit type, and creation of eccentricities if not created by basic geometry;
- Step 2: optimization of the eccentricities to the preferred length;
- Step 3: rebuilding the data and scaling the beam length towards preferred protrusion size (see 5.2.2);
- Step 4: creating the solid beam geometry with corresponding detailing and placement indication based on chapter 5. Furthermore, the 'unfolded' beams can be generated for design to production;
- Always set units to meters in Rhino.

12 APPENDIX 2: IMPLEMENTATION OF THE RFD IN AN ACTUAL PROJECT

During the course of this project, the RFD has been applied in an actual and experimental project that yet has to be built. This project is established in a collaboration between architects from ORIO, and structural designer Arjan Habraken from SID Studio and the TU/e. The design evolved from the rotation of one main RF design that is based on a trimmed elliptical mesh. Hence, the structure is elevated by means of a concrete structure to a certain extend to be able to reach the preferred height. In addition, the structural design is trimmed at places that have been designed as entrance or window by the collaborating architects. The structure is scheduled to be built in the summer of 2019 by using carpenter joints and unbarked round timbers.

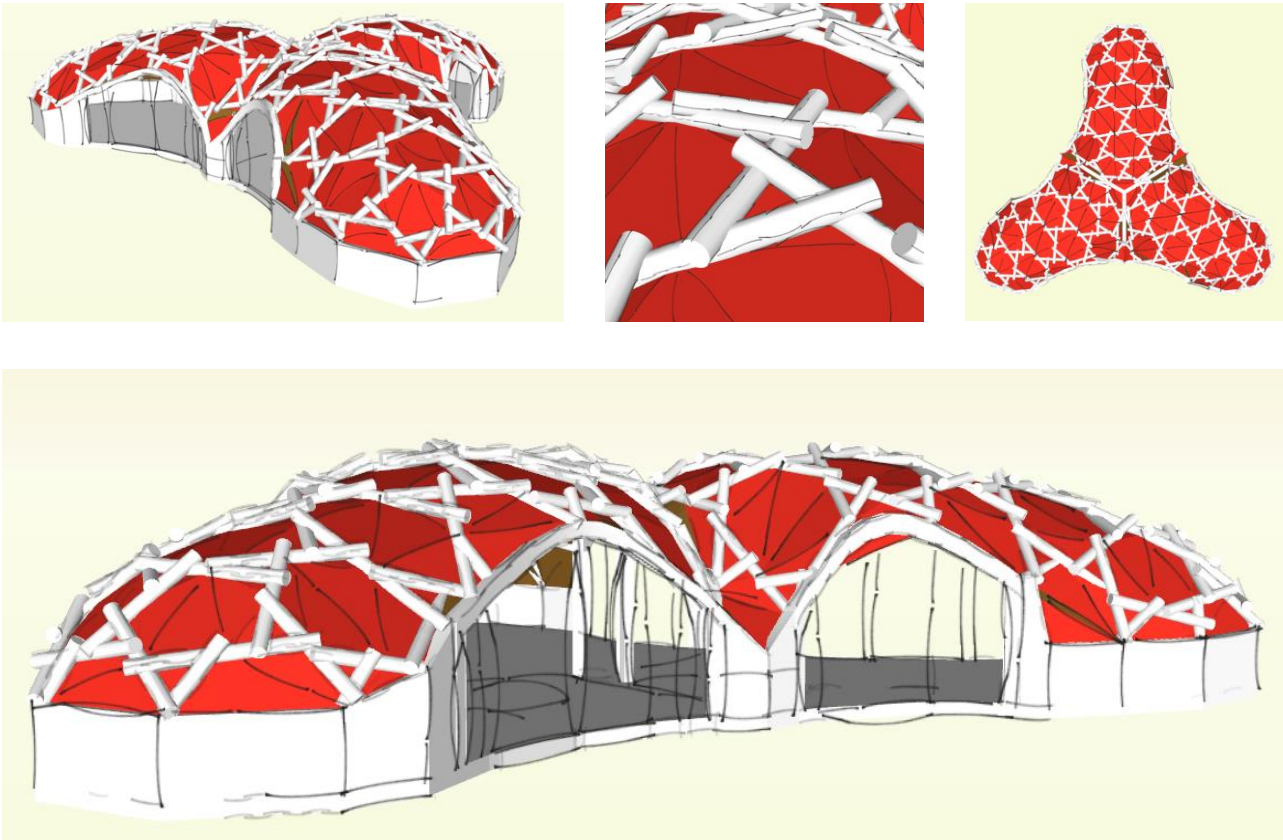


Figure 12.1: Artist impression of the RF scheduled to be built in 2019

THE END